

Dina Riis Kallman

Optimizing biomass formation of riboflavin producing *C. glutamicum* strains growing on SSL sugars using Model Predictive Control

Master's thesis in Chemical Engineering and Biotechnology

Supervisor: Prof. Nadav Bar

June 2020

Dina Riis Kallman

Optimizing biomass formation of riboflavin producing *C. glutamicum* strains growing on SSL sugars using Model Predictive Control

Master's thesis in Chemical Engineering and Biotechnology
Supervisor: Prof. Nadav Bar
June 2020

Norwegian University of Science and Technology
Faculty of Natural Sciences
Department of Biotechnology and Food Science



Kunnskap for en bedre verden

Preface

This master's thesis was submitted as a conclusion of the five year study programme, Chemical Engineering and Biotechnology at NTNU in the spring of 2020. The work is a continuation of a specialization project carried out in the fall of 2019 within the Process Systems Engineering Group at the Department of Chemical Engineering.

I wish to thank my supervisor Professor Nadav Bar for allowing me to be a part of this project, and for his guidance.

Additionally, I want to express my sincerest gratitude to Dr. Fernando Pérez-García for helping me through all the laboratory experiments, and always answering my questions.

A very special thanks to Haakon Eng Holck for all the guidance regarding modeling, and for helping me build the Model Predictive Control. I appreciate all the good discussions we have had.

Although 2020 has been a special year, with limited access to the NTNU campus due to the COVID-19 virus, I am grateful for my supervisors being available and helpful through digital platforms during this spring.

Finally, I am grateful for all the support of my family and friends through the years at NTNU.

Summary

Riboflavin, or vitamin B₂ is essential for the intermediary metabolism for all plant and animal cells. Riboflavin is important in health, food and animal feed industry [1]. *Corynebacterium glutamicum* has been widely used for the industrial production of amino acids and other chemicals [2]. In this study, modified strains of the *C. glutamicum* produced riboflavin using Spent sulfite liquor (SSL) as carbon source. SSL is a residual stream from lignocellulosic biomass treatment. The sugar content of the SSL used included glucose, mannose and xylose [3].

In modern approaches to fermentation control, a mathematical model of the reaction and reactor environment is required [4]. An advanced control technique that can be used for difficult multi variable control problems is model predictive control (MPC) [5]. The MPC algorithm can predict future output values based on measured and predicted input values.

Three genetically modified strains of *C. glutamicum* were modeled regarding consumption of SSL sugars, biomass formation, and riboflavin production. The models were further used in the construction of an MPC algorithm. The aim was to investigate if a combination of strains could increase the biomass formation. Simulations indicated that a combination of *C. glutamicum* strains could improve the biomass yield, and hence the riboflavin yield. The results showed that especially the *C. glutamicum* strain genetically modified to degrade xylose played a crucial role for increasing biomass yield when consuming SSL. However, simulations additionally showed that high production rates of biomass and riboflavin could be obtained by using only one of the strains.

The research done within this thesis provides the basis for optimal exploitation of residual sugar streams, with the long term goal of connecting an optimal and controlled fermentation system to bio-refinery processes. Using a waste stream such as SSL to create new added value chains, contributes to the circular bioeconomy.

Sammendrag

Riboflavin, eller vitamin B₂ er et essensielt mellomledd for alle plante- og dyreceller. Det er industrielt viktig innen helse, mat og i dyrefôrindustrien [1]. *Corynebacterium glutamicum* har blitt mye brukt i industriell produksjon av aminosyrer og andre kjemikalier [2]. I dette studiet har modifiserte stammer av bakterien produsert riboflavin, ved bruk av spent sulfite liquor (SSL) som karbonkilde. SSL er en residualstrøm fra behandling av lignocellulose biomasse. Sukkerinnholdet av SSL brukt inkluderer glukose, mannose og xylose [3].

I moderne tilnærminger til fermenteringskontroll kreves det en matematisk modell av reaksjons- og reaktormiljøet [4]. En avansert kontrollteknikk som kan brukes til vanskelige kontrollproblemer med flere variabler er Model Predictive Control (MPC) [5]. MPC kan forutsi fremtidige outputverdier basert på målte og predikerte inputverdier.

Tre genmodifiserte stammer av *C. glutamicum* ble modellert med tanke på forbruk av SSL-sukker, biomassedannelse og riboflavinproduksjon. Modellene ble videre brukt til å konstruere en MPC algoritme. Målet var å se om biomasseveksten ville øke ved å kombinere stammene. Simuleringer indikerte at en kombinasjon av *C. glutamicum*-stammer kan forbedre biomasseutbyttet, og dermed riboflavinutbyttet. Resultatene viste at spesielt *C. glutamicum*-stammen genetisk modifisert for å nedbryte xylose spilte en avgjørende rolle for å øke utbyttet av biomasse ved bruk av SSL som karbonkilde. Likevel viste simuleringer i tillegg at høye produksjonsrater av biomasse og riboflavin kunne oppnås kun ved bruk av én *C. glutamicum* stamme.

Forskningen gjennomført i denne oppgaven har gitt et grunnlag for optimal utnyttelse av sukker-avfallsstrømmer, med det langsiktige målet om å koble et optimalt og kontrollert fermenteringssystem til bioraffineriprosesser. Ved å bruke en avfallsstrøm som SSL for å skape nye verdikjeder, bidrar dette til den sirkulære bioøkonomien.

Table of Contents

Preface	i
Summary	iii
Sammendrag	iv
Table of Contents	v
List of abbreviations	viii
List of Tables	ix
List of Figures	xi
1 Introduction and background	1
1.1 Aim of the study	2
1.2 Structure of the report	2
2 Theory	4
2.1 Riboflavin	4
2.1.1 Properties of riboflavin	4
2.1.2 Production of riboflavin	5
2.2 <i>Corynebacterium glutamicum</i>	6
2.2.1 Sugars utilization by <i>C. glutamicum</i>	7
2.3 Spent sulfite liquor (SSL)	9
2.4 Modeling of biological processes	9
2.4.1 Enzyme kinetics	10
2.4.2 Cell Growth Kinetics	10
2.4.3 Substrate uptake and product kinetics	12
2.4.4 Continuous-stirred tank reactor	12
2.4.5 Ordinary differential equations	13
2.5 Parameter estimation	13
2.5.1 Nonlinear least squares fitting	14
2.6 Model Predictive Control	14

2.6.1	MPC Strategy	15
2.6.2	Objective function	17
2.6.3	Discretization using direct collocation	19
2.6.4	Moving Horizon Estimation	20
2.6.5	Software	21
3	Materials and method	23
3.1	Work done prior the master's thesis	23
3.1.1	Genetically modified strains of <i>C. glutamicum</i>	23
3.1.2	Fermentation experiments performed	24
3.2	Bioreactors setup and main idea	24
3.3	Modeling of strains	25
3.4	Parameter estimation	26
3.5	MPC formulation	27
3.5.1	Properties of the Optimal Control Problem	30
3.6	Implementation in the laboratory	32
3.6.1	Preparation of preculture and inoculum	33
3.6.2	Bioreactor conditions	34
3.6.3	CSTR setup	35
3.6.4	NUMERA	35
3.6.5	HPLC	35
3.6.6	Running the CSTR experiment using the MPC	36
4	Results	38
4.1	Parameter estimation and model fit	38
4.1.1	RiboGlu	38
4.1.2	RiboMan	40
4.1.3	RiboXyl	43
4.1.4	Estimated parameter values	46
4.2	MPC simulation results	47
4.2.1	Case A: Maximize biomass	47
4.2.2	Case B: Maximize product in F_{out}	55
4.2.3	Case C: Maximize biomass yield	62

4.2.4	Case D: Maximize product yield - linearized approximation	69
4.2.5	Summary of simulation results	76
4.3	MPC simulation results of simplified system	81
4.3.1	Summary of simulation results of simplified system	84
4.4	Comparison of single strains and combination of strains	87
5	Discussion	90
5.1	Modeling and parameter estimation	90
5.2	MPC simulations	91
5.3	Riboflavin biosynthesis genes	93
5.4	Future work	94
6	Conclusion	96
	Appendices	A1
A	Raw data: OD₆₀₀ and HPLC values	A1
B	Calculating cell concentration	A13
C	Stock solutions	A14
D	Parameter estimations including extra terms	A19
E	Previous versions of parameter estimations	A21
F	MPC results using synthetic SSL	A29
G	MPC simulations of simplified system after 80 hours	A41
H	Linearized approximation of Case C	A44

List of Abbreviations

SSL	Spent sulfite liquor
MPC	Model predictive control
FMN	Flavin mononucleotide
ATP	Adenosine triphosphate
FAD	Flavin adenin dinucleotide
ADP	Adenosine diphosphate
DP	Diphosphate
PTS	Phosphoenolpyruvate-dependent sugar phosphotransferase system
PPP	Pentose phosphate pathway
TCA	Tricarboxylic acid cycle
PHB	Polyhydroxybutyrate
CSTR	Continuous-stirred tank reactor
CV	Controlled variables
MV	Manipulated variables
DV	Disturbance variables
OCP	Optimal control problem
EMPC	Economic model predictive control
LP	Linear programming problem
QP	Quadratic problem
NLP	Nonlinear program
NMPC	Nonlinear model predictive control
DAE	Differential algebraic equation
MHE	Moving horizon estimation
OD	Optical density
DO	Dissolved oxygen
HPLC	High pressure liquid chromatography

List of Tables

3.1	Genetically modified strains of <i>C. glutamicum</i>	23
3.2	Overview of experiments performed using modified strains of <i>C. glutamicum</i>	24
3.3	Parameters to be estimated	26
3.4	States of MPC formulation	27
3.5	Inputs of MPC formulation	28
3.6	Sugar composition of SSL and synthetic SSL	28
3.7	OCP properties used for MPC simulations.	30
3.8	States of simplified MPC formulation	33
3.9	Inputs of simplified MPC formulation	33
3.10	Fermentation conditions	34
3.11	Buffer gradient for HPLC measurements of riboflavin	36
4.1	Parameters estimated for RiboGlu, RiboMan and RiboXyl strains	46
4.2	Biomass and riboflavin results of Case A using 0-1 L/h SSL	50
4.3	Biomass and riboflavin results of Case A using 0.1 L/h SSL	53
4.4	Biomass and riboflavin results of Case B using 0-1 L/h SSL	57
4.5	Biomass and riboflavin results of Case B using 0.1 L/h SSL	60
4.6	Biomass and riboflavin results of Case C using 0-1 L/h SSL	64
4.7	Biomass and riboflavin results of Case C using 0.1 L/h SSL	67
4.8	Biomass and riboflavin results of Case D using 0-1 L/h SSL	71
4.9	Biomass and riboflavin results of Case D using 0.1 L/h SSL	74
4.10	Biomass and riboflavin results of simplified system after 24 hours	83
A.1	Raw data: RiboGlu growing on glucose	A1
A.2	Raw data: RiboGlu growing on mannose	A2
A.3	Raw data: RiboGlu growing on synthetic SSL	A4
A.4	Raw data: RiboMan growing on glucose	A5
A.5	Raw data: RiboMan growing on mannose	A6
A.6	Raw data: RiboMan growing on synthetic SSL	A7
A.7	Raw data: RiboXyl growing on glucose	A9
A.8	Raw data: RiboXyl growing on xylose	A10
A.9	Raw data: RiboXyl growing on synthetic SSL	A11

A.10 Standards from HPLC chromatograms used for RiboGlu and RiboMan strains	A12
A.11 Standards from HPLC chromatograms used for RiboXyl strains	A13
C.1 CGXII buffer recipe	A14
C.2 BHI medium recipe	A14
C.3 Carbon source stock solution recipe	A15
C.4 Final feed reactor solution recipe	A15
C.5 Final main reactor solution recipe	A16
C.6 Biotin solution recipe	A16
C.7 Trace elements solution recipe	A17
C.8 Ca-stock solution recipe	A17
C.9 Mg-stock solution recipe	A17
C.10 IPTG stock solution recipe	A17
C.11 Kanamycin stock solution recipe	A18
C.12 Spectinomycin stock solution recipe	A18
D.1 Parameters estimated including m_p	A19
D.2 Parameters estimated including three separate Y_p 's	A20
E.1 Previous version of parameters estimated for RiboGlu strain	A22
E.2 Parameters estimated for RiboMan strain based on updated constraints .	A27
F.1 Biomass and riboflavin results of Case A using 0-1 L/h synthetic SSL . .	A31
F.2 Biomass and riboflavin results of Case B using 0-1 L/h synthetic SSL . .	A34
F.3 Biomass and riboflavin results of Case C using 0-1 L/h synthetic SSL . .	A37
F.4 Biomass and riboflavin results of Case D using 0-1 L/h synthetic SSL . .	A40
G.1 Biomass and riboflavin results of simplified system after 80 hours	A43
H.1 Biomass and riboflavin results of linearized Case C	A46

List of Figures

2.1	Chemical structure of riboflavin	4
2.2	Reactions for biosynthesis of riboflavin by <i>C. glutamicum</i>	6
2.3	Metabolic engineering strategies of <i>C. glutamicum</i>	8
2.4	Batch growth curve	10
2.5	Relationship between μ and s	11
2.6	MPC strategy	15
2.7	Basic structure of MPC systems [12].	16
2.8	Local and global optima	18
2.9	Collocation method	20
2.10	MHE strategy	21
3.1	Flow diagram of combining different strains of <i>C. glutamicum</i>	25
3.2	Simplified flow diagram of feeding RiboGlu strain of <i>C. glutamicum</i> to a main reactor	32
4.1	RiboGlu strain model simulations with glucose as its carbon source . . .	39
4.2	RiboGlu strain model simulations with mannose as its carbon source . .	39
4.3	RiboGlu strain model simulations with synthetic SSL as its carbon source	40
4.4	RiboMan strain model simulations with glucose as its carbon source . . .	41
4.5	RiboMan strain model simulations with mannose as its carbon source . .	41
4.6	RiboMan strain model simulations with synthetic SSL as its carbon source	42
4.7	RiboXyl strain model simulations with glucose as its carbon source . . .	43
4.8	RiboXyl strain model simulations with xylose as its carbon source	44
4.9	RiboXyl strain model simulations with synthetic SSL as its carbon source	45
4.10	MPC simulation results: Inputs of Case A with a SSL flow rate of 0-1 L/h	48
4.11	MPC simulation results: States of Case A with a SSL flow rate of 0-1 L/h	49
4.12	MPC simulation results: Riboflavin results of Case A with a SSL flow rate of 0-1 L/h	50
4.13	MPC simulation results: Inputs of Case A with a SSL flow rate of 0.1 L/h	51
4.14	MPC simulation results: States of Case A with a SSL flow rate of 0.1 L/h	52
4.15	MPC simulation results: Riboflavin results of Case A with a SSL flow rate of 0.1 L/h	53
4.16	MPC simulation results: Inputs of Case B with a SSL flow rate of 0-1 L/h	55

4.17 MPC simulation results: States of Case B with a SSL flow rate of 0-1 L/h	56
4.18 MPC simulation results: Riboflavin results of Case B with a SSL flow rate of 0-1 L/h	57
4.19 MPC simulation results: Inputs of Case B with a SSL flow rate of 0.1 L/h	58
4.20 MPC simulation results: States of Case B with a SSL flow rate of 0.1 L/h	59
4.21 MPC simulation results: Riboflavin results of Case B with a SSL flow rate of 0.1 L/h	60
4.22 MPC simulation results: Inputs of Case C with a SSL flow rate of 0-1 L/h	62
4.23 MPC simulation results: States of Case C with a SSL flow rate of 0-1 L/h	63
4.24 MPC simulation results: Riboflavin results of Case C with a SSL flow rate of 0-1 L/h	64
4.25 MPC simulation results: Inputs of Case C with a SSL flow rate of 0.1 L/h	65
4.26 MPC simulation results: States of Case C with a SSL flow rate of 0.1 L/h	66
4.27 MPC simulation results: Riboflavin results of Case C with a SSL flow rate of 0.1 L/h	67
4.28 MPC simulation results: Inputs of Case D with a SSL flow rate of 0-1 L/h	69
4.29 MPC simulation results: States of Case D with a SSL flow rate of 0-1 L/h	70
4.30 MPC simulation results: Riboflavin results of Case D with a SSL flow rate of 0-1 L/h	71
4.31 MPC simulation results: Inputs of Case D with a SSL flow rate of 0.1 L/h	72
4.32 MPC simulation results: States of Case D with a SSL flow rate of 0.1 L/h	73
4.33 MPC simulation results: Riboflavin results of Case D with a SSL flow rate of 0.1 L/h	74
4.34 Summary of riboflavin results	76
4.35 Summary of biomass results	77
4.36 Summary of biomass used	78
4.37 Summary of sugars used	80
4.38 MPC simulation results: Inputs of simplified system implemented to the laboratory	81
4.39 MPC simulation results: States of simplified system implemented to the laboratory	82

4.40	MPC simulation results: Riboflavin results of simplified system implemented to the laboratory	83
4.41	Comparing riboflavin yields when using one vs multiple strains	84
4.42	Comparing biomass results when using one vs multiple strains	85
4.43	Comparing biomass used when using one vs multiple strains	85
4.44	Comparing synthetic SSL used when using one vs multiple strains	86
4.45	Riboflavin results obtained by single and combined strains	87
4.46	Biomass results obtained by single and combined strains	88
E.1	Previous version of RiboGlu strain model simulations with synthetic SSL as its carbon source	A21
E.2	Summary of riboflavin results based on previous version of RiboGlu parameters	A23
E.3	Summary of biomass results based on previous version of RiboGlu parameters	A24
E.4	Summary of biomass used based on previous version of RiboGlu parameters	A25
E.5	Summary of SSL used based on previous version of RiboGlu parameters .	A26
E.6	RiboMan strain model simulations with synthetic SSL as its carbon source based on updated constraints	A28
F.1	MPC results: Inputs of Case A with a synthetic SSL flow rate of 0-1 L/h	A29
F.2	MPC results: States of Case A with a synthetic SSL flow rate of 0-1 L/h	A30
F.3	MPC results: Riboflavin results of Case A with a synthetic SSL flow rate of 0-1 L/h	A31
F.4	MPC results: Inputs of Case B with a synthetic SSL flow rate of 0-1 L/h	A32
F.5	MPC results: States of Case B with a synthetic SSL flow rate of 0-1 L/h	A33
F.6	MPC results: Riboflavin results of Case B with a synthetic SSL flow rate of 0-1 L/h	A34
F.7	MPC results: Inputs of Case C with a synthetic SSL flow rate of 0-1 L/h	A35
F.8	MPC results: States of Case C with a synthetic SSL flow rate of 0-1 L/h	A36
F.9	MPC results: Riboflavin results of Case C with a synthetic SSL flow rate of 0-1 L/h	A37
F.10	MPC results: Inputs of Case D with a synthetic SSL flow rate of 0-1 L/h	A38
F.11	MPC results: States of Case D with a synthetic SSL flow rate of 0-1 L/h	A39

F.12 MPC results: Riboflavin results of Case D with a synthetic SSL flow rate of 0-1 L/h	A40
G.1 MPC results: Inputs of simplified system implemented to the laboratory .	A41
G.2 MPC results: States of simplified system implemented to the laboratory .	A42
G.3 MPC results: Riboflavin results of simplified system implemented to the laboratory	A43
H.1 MPC simulation results: Inputs of linearized Case C	A44
H.2 MPC simulation results: States of linearized Case C	A45
H.3 MPC simulation results: Riboflavin results of linearized Case C	A46

1 Introduction and background

Riboflavin, or vitamin B₂ is essential for the intermediary metabolism for all plant and animal cells. It is the precursor of flavin mononucleotide (FMN) and flavin adenine dinucleotide (FAD) which are important cofactors in biological reduction-oxidation reactions [6]. Riboflavin has several health properties, such as reducing the risk of vascular diseases and promoting lipid metabolism. This makes riboflavin industrially important in health, food and animal feed industry [1]. Chemical production of riboflavin has been used for decades, but already in year 2000 Stahmann et al. [7], stated that it was in the course of being replaced by microbial processes. The aim was to reduce the costs, waste and energy requirements as well as using renewable resources for production. In 2016 the riboflavin production had shifted from chemical synthesis to fermentation processes exclusively [8].

According to Yuan et al. [9], the core of circular economy is the circular flow of materials and the use of raw materials and energy through multiple phases. Spent sulfite liquor (SSL) is a residual stream from lignocellulosic biomass treatment, that can be used as a carbon source for the production of a chemical of industrial importance, such as riboflavin [10]. A *C. glutamicum* strain overexpressing the sigma factor gene *sigH*, showed in previous studies production of riboflavin from glucose [11]. The specialization project conducted in the fall of 2019, showed that further genetic modifications of the *C. glutamicum* riboflavin producer enabled consumption of SSL sugars [data not yet published]. Using a waste stream to create new added value chains, contributes to the circular economy. The environmental perspective was a personal motivation for performing experiments in the specialization project, and continuing the work of this master's thesis.

In modern approaches to fermentation control, a mathematical model of the reaction and reactor environment is required [4]. For biological processes, constructing model structures can be difficult because of the complexity of cellular processes, and environmental factors affecting the cell culture. Therefore models are usually simplified approximate representations deduced from observation. Bioprocesses usually require a particular pH, temperature, dissolved oxygen tension, feed rate and other variables to maximize the pro-

ductivity of a cell culture. An advanced control technique that can be used for difficult multivariable control problems is model predictive control (MPC) [5]. The idea of MPC is the explicit use of a model to predict the process output at future time instants [12]. MPC has a variety of applications, but it has been particularly used in chemical process industry and refineries [13]. It was originally used for linear plant models, where the constraints on the inputs and outputs were the only type of nonlinearity being addressed. However in the last couple of decades, both publications and industrial applications has addressed the use of MPC with nonlinear models [14–16].

1.1 Aim of the study

In the specialization project conducted prior to this master’s thesis, genetically modified strains of *C. glutamicum* were used in fermentations with sugars present in SSL (glucose, mannose and xylose) as carbon sources, producing riboflavin. It was shown that the riboflavin production could be biomass growth related. The aim for the master’s thesis was to make models for each strain, taking into account the sugar consumption, biomass and product formation obtained from previous experiments. The models with estimated parameters would be used to construct an MPC algorithm. The MPC was developed to investigate if a combination of strains could increase the biomass growth, and hence the riboflavin production. After simulations had been performed the final aim was to implement the MPC to a laboratory experiment.

1.2 Structure of the report

This report is divided into 6 main sections:

1. Introduction and background
2. Theory
3. Materials and method
4. Results
 - This section includes results obtained from parameter estimation and MPC simulations. The main interpretations and discussion is included.
5. Discussion
 - This section includes further discussion, alternative interpretations and future work.
6. Conclusion

2 Theory

The first three subsections of this chapter are obtained from the Specialization project "Riboflavin production from genetically modified strains of *Corynebacterium glutamicum* using sugars present in spent sulfite liquor" [17]. The sections provides background theory about riboflavin, *C. glutamicum* and SSL. Section 2.4 to 2.6 provides theory about modeling of biological processes, parameter estimation and MPC.

2.1 Riboflavin

Riboflavin, or vitamin B₂ is essential for the metabolism of carbohydrates, amino acids and lipids. It also supports cellular antioxidant protection and is found in all plant and animal cells [6]. Riboflavin got its name because it is a derivative of ribose. Its chemical structure is shown in Figure 2.1.

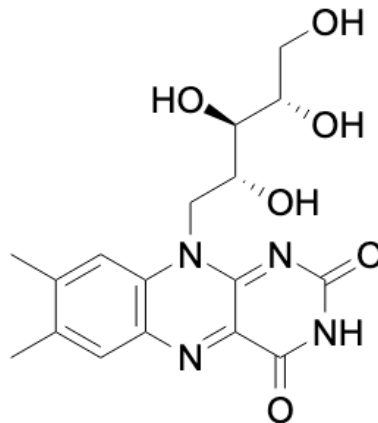


Figure 2.1: Chemical structure of riboflavin [6]

Riboflavin is widely distributed in foods, bound to proteins mainly in the form of FMN and FAD [6].

2.1.1 Properties of riboflavin

Riboflavin may play a role in reducing the risk of vascular diseases, as it is involved in reducing the homocystein metabolism [1]. High levels of homocystein in the blood has been associated with vascular diseases. Riboflavin has the capacity of forming complexes with divalent cations as Fe^{2+} and Zn^{2+} , and can be crucial for the bioavailability of these minerals [1]. A lack of riboflavin can enhance carcinogenesis [6]. There may be several reasons for this, such as diminished antioxidant protection, increased activation of carcinogens and oxidative damage to DNA. A lack of riboflavin may also reduce folate

metabolism, reduce DNA synthesis, repair and methylation. Riboflavin has been shown to have antimalarial effects, and promotes lipid metabolism [6]. Riboflavin deficiency in both humans and animals has therefore critical consequences that affects many tissues. This makes riboflavin an important product in the health, food and animal feed industry. It is naturally present in some foods, but it is also used as an additive, predominantly for fortification in products like cereals, soups, soft drinks, meal replacements, and baby food [18]. Riboflavin is also an authorized naturally derived food colorant, providing a yellow colour [19].

2.1.2 Production of riboflavin

Riboflavin was previously chemically obtained from D-glucose by the Karrer-Tishler process [20]. This is a long process including many steps, and the use of a large amount of organic solvents. The process could obtain an overall riboflavin yield of 60% [21], but already in 2000 Stahmann et al. [7], stated that it was in the course of being replaced by microbial processes. Back then three microorganisms were being used for industrial riboflavin production: the natural overproducers of riboflavin hemiascomycetes *Ashbya gossypii* [22], a filamentous fungus, *Candida famata* [23], as well as the Gram positive bacterium *Bacillus subtilis* [24] that had been genetically modified for the overproduction of riboflavin. The aim of using microbial processes is to reduce the costs, waste and energy requirements as well as using renewable resources for production. In 2016 it was stated that riboflavin was exclusively produced by microbial fermentations, and that all previous chemical synthesis had been replaced [8]. The biosynthetic reaction of riboflavin in *C. glutamicum* is shown in Figure 2.2 [25].

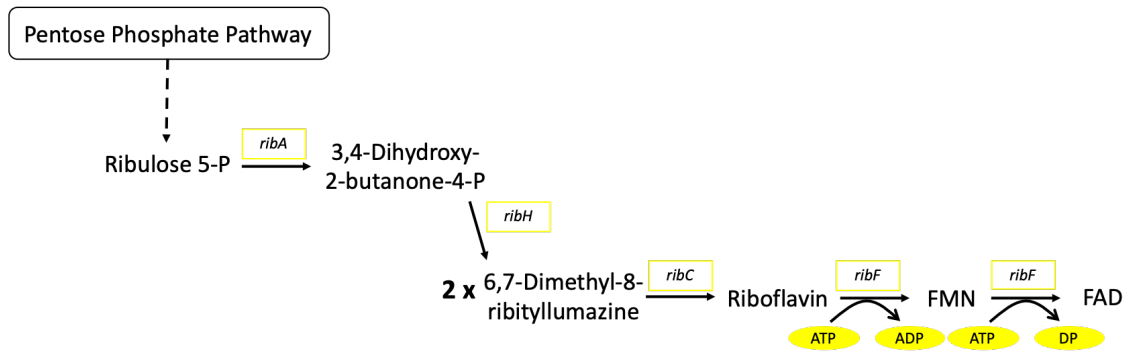


Figure 2.2: Reactions for biosynthesis of riboflavin by *C. glutamicum* [25]. Genes are framed, and energy demand in the reaction of ATP (Adenosine Triphosphate) to ADP (Adenosine Diphosphate), and DP (Diphosphate) is highlighted. The *ribA* gene encodes for 3,4-Dihydroxy-2-butanone-4-phosphatesynthase, *ribH* encodes for 6,7-dimethyl-8-ribityllumazine synthase, *ribC* encodes for riboflavin synthase, and *ribF* encodes for riboflavin kinase and FMN adenylyltransferase.

A. gossypii and *B. subtilis* are still the main microorganisms used for the production of riboflavin, and they have been genetically modified for that purpose. In 2014 Lin et al. [26] included *zwf* and *gnd* genes from *C. glutamicum* in *Escherichia coli* for riboflavin production. They optimized the fermentation conditions and obtained a final concentration of 2708.2 mg/L of riboflavin with a yield of 137.5 mg riboflavin/g glucose when cultivated in shake flasks. Genetically modified *C. glutamicum* strains had already been used for the production of riboflavin from glucose as the sole carbon source, obtaining a titer of 32.4 μM [11] using baffled flasks and 4 % of glucose as carbon source. From the experiments performed in the specialization project a titer of 28.10 μM was obtained during reactor batch cultivation using 2 % glucose as carbon source, yielding 176 micrograms of riboflavin per gram of glucose [17].

2.2 *Corynebacterium glutamicum*

The bacterium *C. glutamicum* is Gram-positive and non-spore-forming. It is non-pathogenic and has been widely used for the industrial production of amino acids, as well as other chemicals [2]. *C. glutamicum* was discovered in 1956 because of its ability to excrete the amino acid L-glutamate, a flavor enhancer [27]. The microorganism is a short rod shaped bacterium with thickened ends, also called "coryneform". *C. glutamicum* has been extensively engineered to enable and optimize consumption of alternative carbon sources while producing added value compounds [28–30].

2.2.1 Sugars utilization by *C. glutamicum*

Studies have revealed that *C. glutamicum* takes up sugars such as sucrose, fructose and glucose via the phosphoenolpyruvate-dependent sugar phosphotransferase system (PTS) [31]. PTS is the first step in the sugar metabolism, and may therefore be one of the targets for improving amino acid production [32]. *C. glutamicum* possesses various sugar uptake systems and it is missing a carbon catabolite repression system. Therefore *C. glutamicum* has the ability to co-metabolize different substrates [33–35]. Because of the cost of feedstocks, several approaches to either increase the substrate spectrum of *C. glutamicum* towards cheaper carbon sources or to improve the utilization of sugars has been investigated [30]. Since *C. glutamicum* co-metabolizes different carbon sources, in contrast to other bacteria such as *E. coli* or *B. subtilis*, an approach for increasing productivity is to do a simultaneous feeding of selected carbon sources [36].

After the uptake of sugars such as glucose, sucrose, and fructose, and phosphorylation through the PTS, the sugar phosphates of *C. glutamicum* catabolizes through the glycolysis, pentose phosphate pathway (PPP) and the Tricarboxylic acid cycle (TCA cycle). Mannose can enter *C. glutamicum* by using the PTS system of glucose and fructose [35]. Xylose is transported into *C. glutamicum* through the permease IolT1 [37]. A schematic representation of the metabolic engineering strategies of *C. glutamicum*, consuming the SSL sugars glucose, mannose and xylose is shown in Figure 2.3 (for more information about SSL, see Section 2.3).

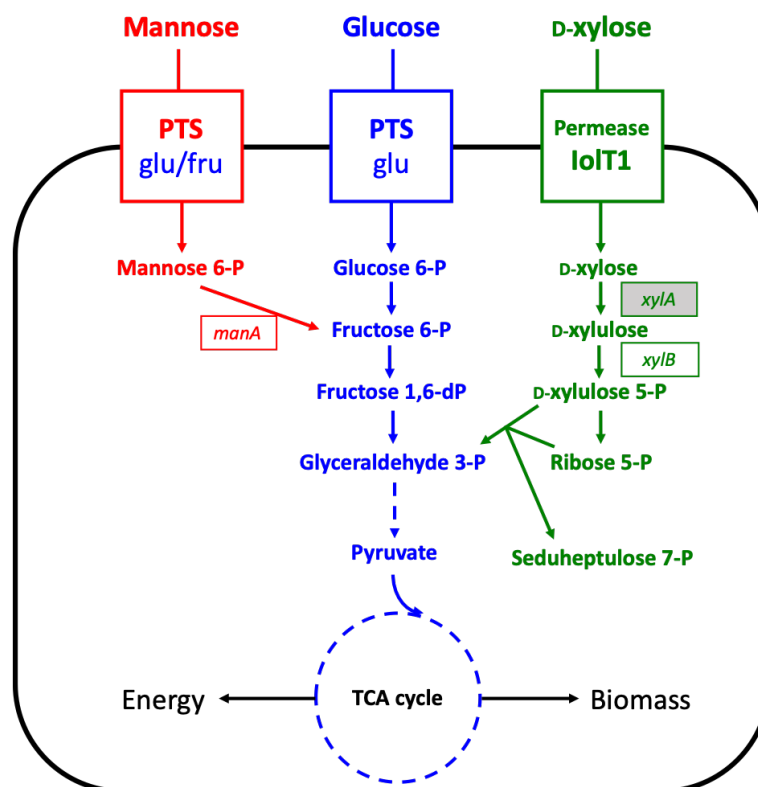


Figure 2.3: Schematic representation of the metabolic engineering strategies of *C. glutamicum*, with the SSL sugars glucose, mannose and D-xylose. The overexpressed genes are framed. The gray shade of *xylA* indicates that the gene is hereologous (from *Xanthomonas campestris*). *manA* and *xylB* are endogenous genes. The genes are encoding xylulokinase, mannose-6-phosphate isomerase and xylose isomerase respectively. Glucose is transported through the membrane by its own PTS, mannose can enter *C. glutamicum* by using the PTS system of glucose and fructose [35]. D-xylose is transported into *C. glutamicum* through the permease IolT1 [37].

2.3 Spent sulfite liquor (SSL)

Spent sulfite liquor (SSL) is a by-product generated in pulp mills. Once the pulp is formed, wood digestion under acidic conditions produces lignin and hemicellulose, which pass through the residual aqueous phase and produce the waste product SSL [38]. SSL is a renewable source containing lignosulfonates, depolymerised hemicelluloses, acids, tannins and furfurals. The SSL has historically been used as a substrate for industrial ethanol production, and has later been used to produce protein biomass (single cell protein) for animal feed by yeasts [10], as well as high-value compounds like polyhydroxybutyrate (PHB) [39], succinic acid [40], and bioethanol [41]. Problems encountered when fermenting SSL include forestry and agricultural residues, high-osmotic strength, low sugar content, inhibitors, and a large proportion of pentose sugars [42]. The sugar content ranges from 3-4%, depending on the source of wood. Pulped softwood produces a majority of hexose sugars, such as glucose and mannose, while pulped hardwood can produce pentose sugars like xylose up to 50% of the sugars.

2.4 Modeling of biological processes

According to Szallasi et al. [43], even relatively small systems of interacting parts can exhibit complex behavior, that are hard to analyze using traditional mathematical and analytical methods. Modeling these systems using iterated computer simulations leads to prediction, control and a better understanding of the systems. Szallasi et al. [43] states that biological systems are inherently complex, and that they must be modeled and studied in this way if we are going to continue to make strides in our understanding of these phenomena. There are several reasons why biological systems should be modeled. One main reason is to test if the model is accurate, and reflecting experimental facts. Another reason could be to analyze the model to understand what parts of the system that contributes to certain properties of interests. A model could furthermore be used to analyze the effect of manipulating experimental conditions without performing costly and complex experiments. The typical strategy for modeling biological processes is the ordinary differential equation (ODE) approach. This approach contains three initial phases: structural model, kinetic rate equations and parametrization of the model. This strategy will be described in this section.

2.4.1 Enzyme kinetics

Many enzymes has common kinetic properties. Once a substrate is added to an enzyme, the reaction reaches steady state rapidly [44]. As the concentration of the substrate increases, the steady state activity of the enzyme increases hyperbolically to reach its maximum rate V_{max} , where all the enzyme has formed a complex with substrate. The volumetric rate of reaction, V_0 can be represented by the Michaelis Menten equation, as shown in Equation (2.1).

$$V_0 = \frac{V_{max}[S]}{K_m + [S]} \quad (2.1)$$

This equation relates the initial rate of reaction to the substrate concentration $[S]$, and V_{max} to through the Michaelis Menten constant K_m . K_m is the substrate concentration at which half of the enzyme's active sites are saturated with substrate [45]. Even though Equation (2.1) is true for many enzymes, the magnitude of V_{max} and K_m can differ from one enzyme to another [44]. When there are multiple substrates, more complex kinetic equations must be applied [45].

2.4.2 Cell Growth Kinetics

When cells grow in batch cultures, different phases of cell growth can be observed, as shown in Figure 2.4.

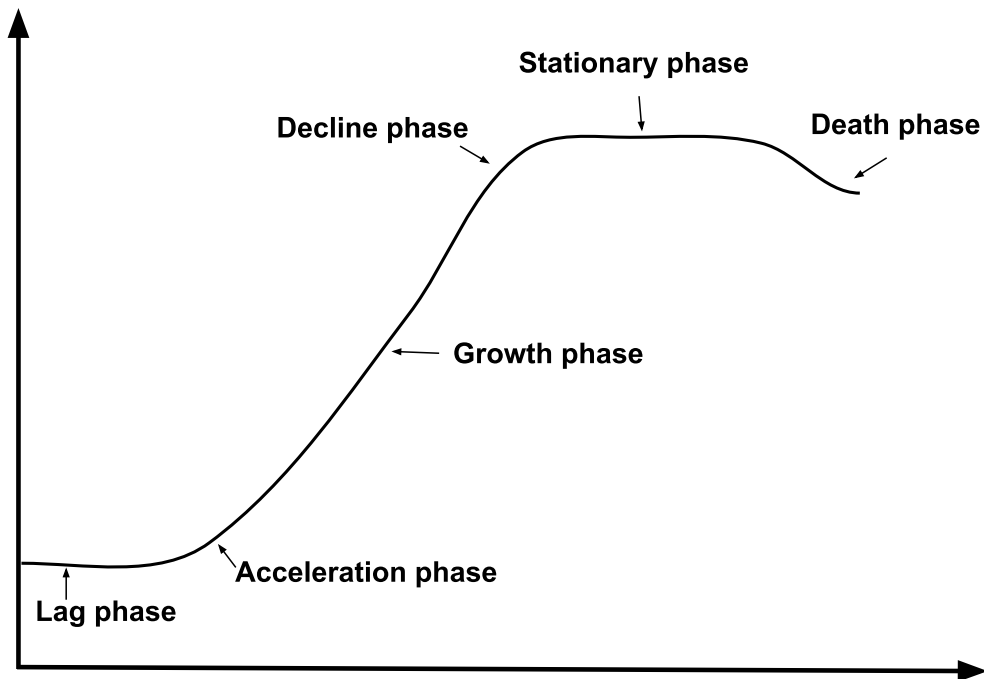


Figure 2.4: Typical batch growth curve, indicating the different phases of cell growth [46].

As cell metabolism depends on the integrated action of diverse enzymes, the cell growth kinetics are often expressed using similar equations as the Michaelis Menten equation [46]. During the growth and decline phases of batch cultures, the cells specific growth rate, μ is depending on the concentration of nutrients in the medium [46]. There is often a carbon or nitrogen source working as a growth limiting substrate, affecting the specific growth rate. During a balanced growth (constant composition of biomass), this can be represented by the Monod equation, as shown in Equation (2.2).

$$\mu = \frac{\mu_{max}[S]}{K_S + [S]} \quad (2.2)$$

Here μ_{max} is the maximum specific growth rate, $[S]$ is the concentration of the growth limiting substrate and K_S is the substrate constant. The values of K_S are typically very small, in the order of mg/L for carbohydrate substrates. K_S is the substrate concentration where the maximum specific growth rate has reached its half value, and can be described graphically by Figure 2.5.

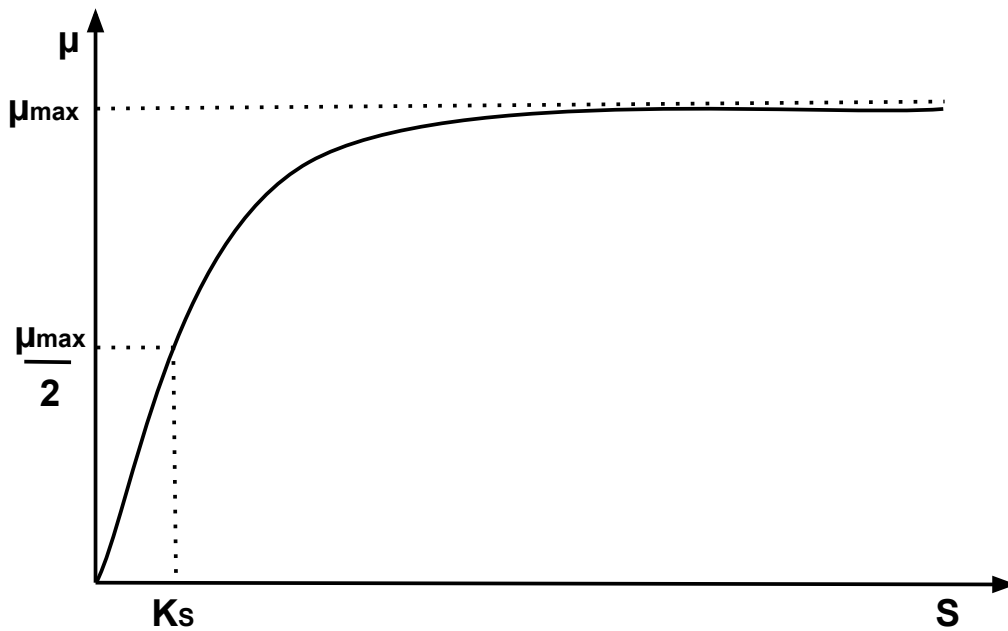


Figure 2.5: Relationship between cells specific growth rate (μ) and the concentration of growth-limiting substrate in cell culture (S). The substrate constant, K_S is the substrate concentration where the maximum specific growth rate has reached its half value [46].

The Monod equation is the most frequently used equation expressing growth rate as a function of substrate concentration. When growth is inhibited by high substrate or product concentrations, extra terms can be added to account for the effects. The rate of cell growth can be described by Equation (2.3) during growth and decline phases.

$$r_X = \mu x \quad (2.3)$$

Here r_X is the volumetric rate of biomass formation, and x is the viable cell concentration.

2.4.3 Substrate uptake and product kinetics

The volumetric rate of substrate uptake (r_S) in the absence of extracellular product synthesis can be described by Equation (2.4) [47].

$$r_S = \frac{r_X}{Y_{XS}} + m_S x \quad (2.4)$$

Here Y_{XS} represents the true yield of biomass from substrate, m_S is the maintenance coefficient. Maintenance activities such as cell motility, adjustment of membrane potential and internal pH occurs by living cells continuously. It requires energy in the form of ATP, and product formation using ATP generating pathways must therefore account for this, as shown in Equation (2.5) [48].

$$r_P = Y_{PX} r_X + m_P x \quad (2.5)$$

Here r_P is the volumetric rate of product formation, Y_{PX} is the theoretical or true yield of product from biomass, m_P is the specific rate of product formation due to maintenance.

2.4.4 Continuous-stirred tank reactor

The Continuous-stirred tank reactor (CSTR) is a type of reactor commonly used in industrial processing. It is usually operated at steady state, and is assumed to be perfectly mixed [49]. Hence there is no time- or position dependence of the temperature, concentration or reaction rate inside the CSTR. Thus the temperature and concentration in the exit stream are modeled as being the same as inside the reactor. The design equation of a CSTR is described in Equation (2.6).

$$V = \frac{F_{j,0} - F_j}{-r_j} \quad (2.6)$$

Here $F_{j,0}$ is the rate of flow of j into the system, F_j is the rate of flow of j out of the system, and r_j is the rate of formation of species j .

2.4.5 Ordinary differential equations

Periodic activities of biological and biochemical systems have been observed through the years [50, 51], and a way to explain the phenomenon is through ODEs [52]. The mathematical model makes a more accurate description of the biological system, as well as making prediction possible. If $J \subseteq \mathbb{R}$, $U \subseteq \mathbb{R}^n$ and $\Lambda \subseteq \mathbb{R}^k$ are open subsets, and $f : J \times U \times \Lambda \rightarrow \mathbb{R}^n$ is continuously differentiable, an ODE can be represented as in Equation (2.7).

$$\dot{x} = f(t, x, \lambda) \quad (2.7)$$

Here the dot denotes differentiation with respect to the independent variable t , the dependent variable x is a vector of state variables and λ is a vector of parameters [53]. When a differential equation is used to model the evolution of a state variable for a physical process, future values of the state variable is usually determined from its initial condition, as shown in Equation (2.8).

$$x(t_0) = x_0 \quad (2.8)$$

If the ODE is defined as in Equation (2.7), and $(t_0, x_0) \in J \times U$, then Equation (2.7) and (2.8) is called an initial value problem. There are many ways to solve ODEs, and the ODE solvers in MATLAB solve initial value problems with a variety of properties [54]. The solver *ode45* solve non-stiff differential equations, integrating them from t_0 to t_f .

2.5 Parameter estimation

Dynamical models of biological processes will usually have unknown parameters such as growth rates, constants and yields as presented in Section 2.4.2 and 2.4.3. While sometimes it is feasible to measure the parameters experimentally (especially the ones with a physical meaning), it may be very hard, expensive, time consuming, or even impossible [55]. Parameter estimation is therefore a key issue in computational and systems biology. According to Lillacci et al. [55], parameter knowledge is crucial to obtain quantitative or qualitative information from models. In parameter estimation, the experimental data is used to constrain the unknown parameters [56]. The process usually involves searching through various values of the unknown parameters, solving the system with a given set of values of them, before adjusting the parameter values trying to improve their fit to the experimental data. Several optimization techniques can be used for the purpose, but in this report nonlinear least squares fitting was used.

2.5.1 Nonlinear least squares fitting

Nonlinear least squares problems have objective functions on the form shown in Equation (2.9) [57].

$$\min_{x \in \mathbb{R}^n} f(x) = \frac{1}{2} R(x)^T R(x) = \frac{1}{2} \sum_{i=1}^m r_i(x)^2 \quad (2.9)$$

Where $m > n$, The vector $R : (\mathbb{R}^n \rightarrow \mathbb{R}^m)$ is nonlinear in x , and is called the residual. The nonlinear least squares problem usually arises from data-fitting applications, where the goal is to fit the data $t_i, y_i, i = 1, \dots, m$, with a model $m(x, t)$ that is nonlinear in x . In such cases, $r_i(x) = m(x, t_i) - y_i$, and x will be chosen so that the sum of the squares of the residuals ($r_i(x)$'s) is minimized. The MATLAB Optimization Toolbox software includes the function *lsqnonlin* [58], a function solving nonlinear least-squares problems. The function

$$x = \text{lsqnonlin}(\text{fun}, x0, lb, ub, options)$$

minimizes with the optimizations options specified in *options*. It additionally defines a set of lower (*lb*) and upper (*ub*) bounds on the design variables in x , so that the solution is always in the range $lb \leq x \leq ub$.

2.6 Model Predictive Control

MPC is an advanced control technique important for solving difficult multi variable control problems [5]. If there is a reasonably accurate dynamic model of a process with multiple inputs and outputs, the model together with current measurements can be used to predict future output values or controlled variables (CVs). The appropriate input changes in the input variables or manipulated variables (MVs) can be calculated based on predictions and measurements. Disturbance variables (DVs) can also be taken into account, and can affect the CVs. The MPC can be used for controlling a great variety of processes, from processes with relatively simple dynamics, to more complex ones, including systems with long delay times [12].

2.6.1 MPC Strategy

The MPC strategy can be described by Figure 2.6.

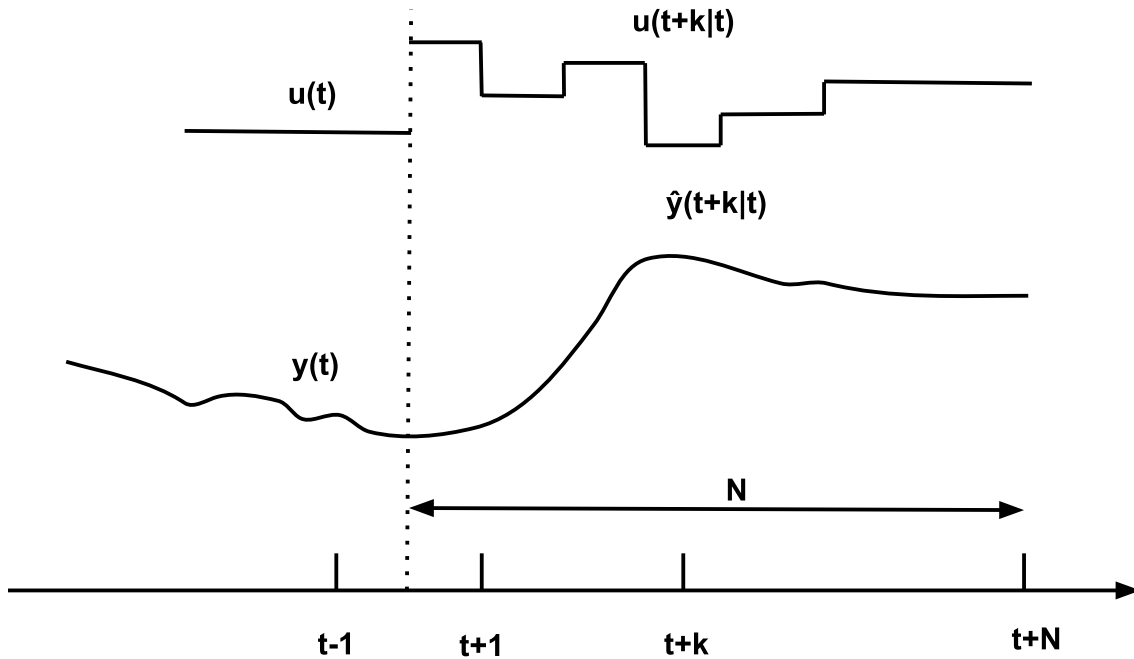


Figure 2.6: MPC strategy. $u(t)$ and $y(t)$ are previous inputs and outputs respectively, while $u(t+k|t)$ and $\hat{y}(t+k|t)$ are the predicted inputs and outputs respectively (for $k = 1, \dots, N$). N is the prediction horizon [12].

Future outputs within the prediction horizon, N , are predicted at each time instant, t . The predicted outputs $\hat{y}(t+k|t)$ for $k = 1, \dots, N$ are depending on the known values up to instant t , and on the future control signals $u(t+k|t)$, for $k = 0, \dots, N-1$. These signals will be sent to the system and calculated by optimizing a criterion to keep the process as close as possible to the reference trajectory. If the criterion is quadratic, the model is linear and there are no constraints, an explicit solution can be obtained. If not, an iterative optimization method must be used. MPC relies on the receding horizon concept: At time t , the optimal control sequence is found over a finite horizon of N control intervals [59]. Even though the optimal sequence of N steps are found, only the first element will be applied - the first optimal control movement $u(t|t)$ [12]. At time $t+1$, new state estimates are calculated, and the optimization is repeated to keep all the sequences up to date. In this way, feedback is utilized to update the optimization over the time horizon selected, and thereby predicting the future system outputs. The basic structure of how the MPC system works is shown in Figure 2.7.

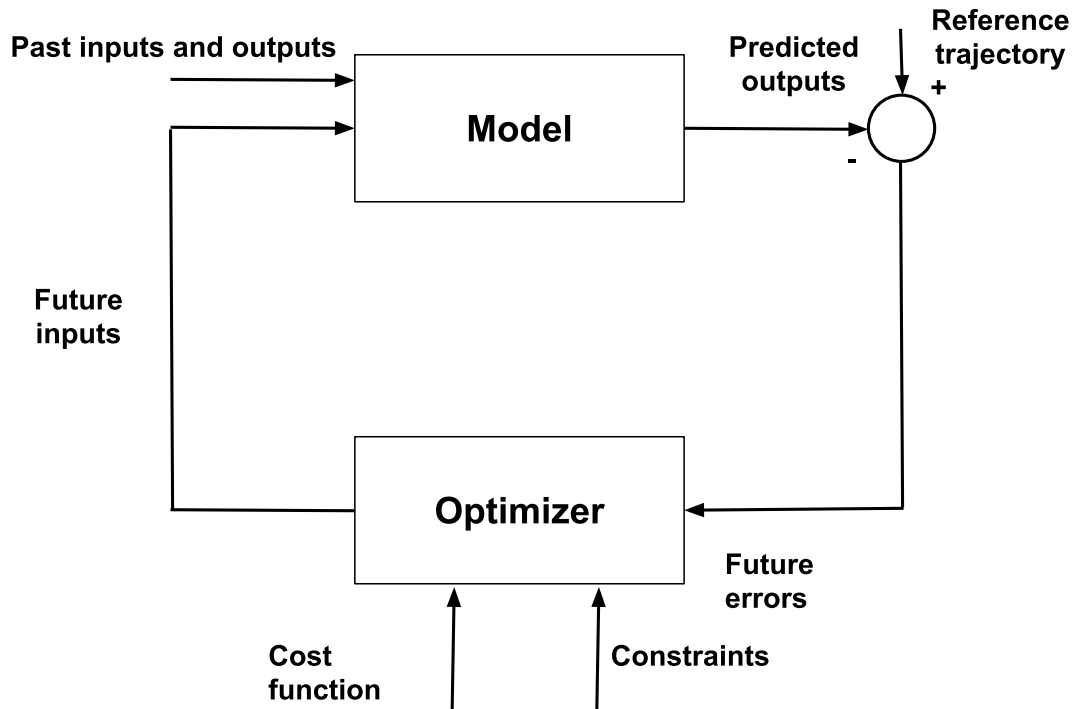


Figure 2.7: Basic structure of MPC systems [12].

The process model is predicting the future values of the output variables (CVs), based on past and current values. The residuals or errors are served as feedback to the optimizer. Constraints on both input and output variables are additionally served to the optimizer. These can include upper and lower limits, such as maximum pump rate, pressure or minimum temperature in a reactor. The optimal future control actions are calculated by the optimizer considering both these constraints as well as the cost function. This is called the Optimal Control Problem (OCP). The model must capture the process dynamics to precisely predict the future outputs. The size of the OCP being solved by the optimizer (see Figure 2.7) depends on the amount of variables, and the amount of control intervals in the prediction horizon. The optimal solutions or future inputs may change regularly due to changes of conditions in the process, access and cost of raw materials or energy.

2.6.2 Objective function

The optimization problem is formulated as an objective function to be minimized or maximized. The general form of the optimization problem is described by Equation (2.10).

$$\min_u J(x(t), u(t)) \quad (2.10a)$$

subject to

$$g_i(x(t), u(t)) = 0 \quad i = 1, \dots, m \quad (2.10b)$$

$$h_j(x(t), u(t)) \leq 0 \quad j = 1, \dots, p \quad (2.10c)$$

$$x_{min} \leq x \leq x_{max} \quad (2.10d)$$

$$u_{min} \leq u \leq u_{max} \quad (2.10e)$$

The objective function $J(x(t), u(t))$ is a function of the states x and the inputs u for each control interval in the entire prediction horizon. The function must satisfy a set of constraints, g_i and h_j , which represents equality and inequality constraints respectively. x and u are constrained by lower (x_{min} , u_{min}) and upper (x_{max} , u_{max}) bounds. The traditional way to formulate the MPC is by having J be a quadratic performance index [60]. This is a measure of the predicted deviation of the inputs and states from their predefined set-points, forcing the process to the optimal steady-state. However, in this thesis, an economic MPC (EMPC) has been implemented. EMPC formulates the objective function directly as the metric desired to optimize. This avoids the need for offline optimization and improves performance for processes where optimal operation does not necessarily correspond to a predefined set of set-points. The optimal solution corresponds to a local or global optimum. Local and global optima can be illustrated as shown in Figure 2.8.

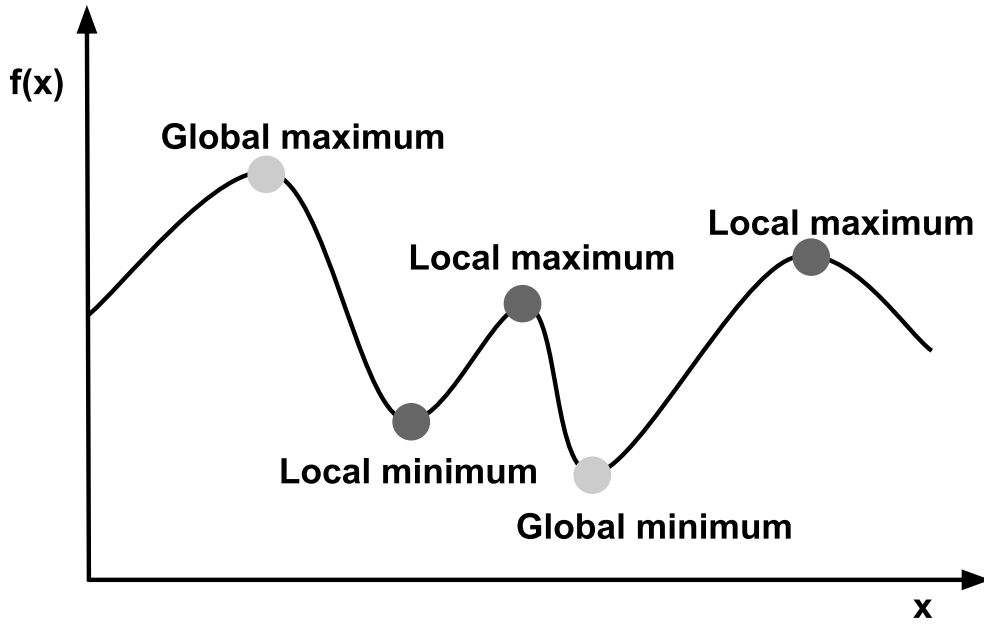


Figure 2.8: Illustration of local and global optima for the objective function $f(x)$ as a function of variable x (light shaded dots = local, darker shaded dots = global optima). [61].

Definition 2.1 and 2.2 defines global and local optima [61].

Definition 2.1 Let $x = (x_1, x_2, \dots, x_n)$ be a feasible solution to a minimization problem $f(x)$. x is then:

- a) A global minimum if $f(x) \leq f(y)$ for any feasible point $y = (y_1, y_2, \dots, y_n)$
- b) A local minimum if $f(x) \leq f(y)$ for any feasible point $y = (y_1, y_2, \dots, y_n)$ sufficiently close to x .

Definition 2.2 Let $x = (x_1, x_2, \dots, x_n)$ be a feasible solution to a maximization problem $f(x)$. x is then:

- a) A global maximum if $f(x) \geq f(y)$ for any feasible point $y = (y_1, y_2, \dots, y_n)$
- b) A local maximum if $f(x) \geq f(y)$ for any feasible point $y = (y_1, y_2, \dots, y_n)$ sufficiently close to x .

If the solution found is a global optimum, it is the best possible solution. If the optimization problem is convex, any optimal solution is the global solution according to Theorem 2.1 [61].

Theorem 2.1 (Local = global in convex optimization) *Let $f : C \rightarrow \mathbb{R}$ be a convex function defined on the convex set C . Let $x^* \in C$ be a local minimum of f over C . Then x^* is a global minimum of f over C .*

Optimization problems are classified depending on their objective function and constraints. If the objective function and all the constraints are linear functions of the decision variables, the problem is a linear programming problem (LP), which is easy to solve [62]. If the objective function is quadratic, with linear constraints, the problem is a quadratic problem (QP). The QP may be convex, and easy to solve, or non-convex and more difficult to solve. The hardest problems to solve are the nonlinear programs (NLPs), where the constraints and the objective function might be nonlinear. The problems solved in this thesis were nonlinear, and can therefore be called a nonlinear MPC (NMPC).

2.6.3 Discretization using direct collocation

There are various approaches used to solve optimal control problems. The direct way to solve them is discretizing dimensional optimal control problems to NLP problems, and then establish the optimality conditions [63]. There are different discretization techniques, but in this thesis the technique chosen was collocation. Collocation methods are used to transcribe differential dynamic constraints to a set of algebraic constraints [64]. The idea is to choose a polynomial up to a certain degree, with a number of points (collocation points) within the time domain, where the polynomials are required to satisfy the equations of motion at the collocation points. The aim is to choose parameters and basis functions giving the residuals at the collocation points the value zero [65]. Collocation points are selected as roots of shifted Gauss-Legendre, Gauss-Radau or Gauss-Labatto polynomials. The three methods has decreasing errors respectively [66]. Instead of doing collocation of the whole prediction horizon, the horizon can be divided into finite elements, where collocation can be performed on each element, as shown in Figure 2.9.

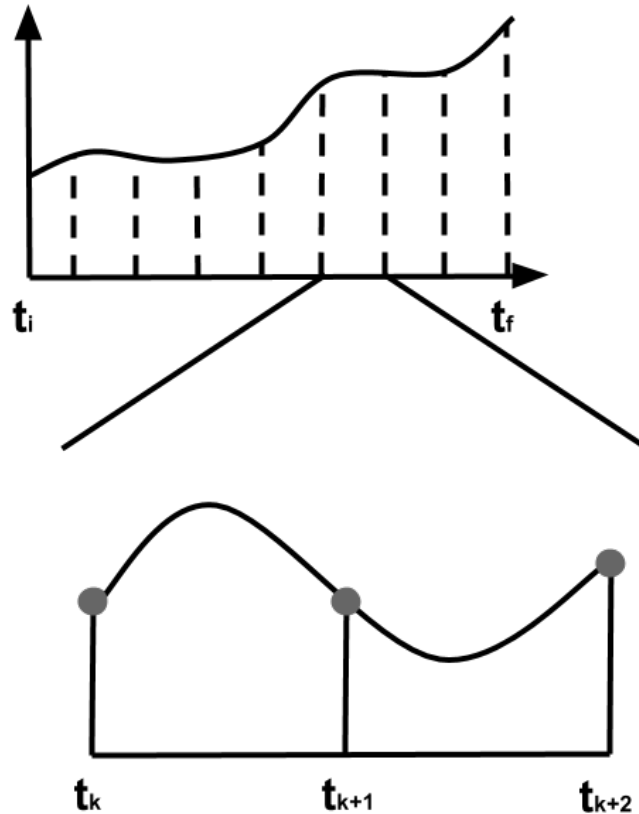


Figure 2.9: Collocation method, with time horizon $T = t_f$, number of steps (or finite elements) in the time horizon $N = 8$, and number of collocation points per step $d = 3$ [64].

The use of collocation on finite elements, leaves the discretization A-stable, high order and able to handle non-smooth events at element boundaries [66]. The approach leads to a discretization that is equivalent to Runge-Kutta methods. The discretization does not rely on embedded differential algebraic equation (DAE) solvers, but the entire problem is addressed at the level of the NLP solver. This leads to first and second derivatives being available through the optimization modeling system, where both structure and sparsity can be exploited. However the drawback is that an efficient large-scale NLP solver is required to take full advantage of the approach.

2.6.4 Moving Horizon Estimation

Once an MPC is implemented in reality, not all states are given. In a bioreactor for instance, not all concentrations can be measured directly. To know where the process is at all times, states must be estimated based on output measurements. The Kalman filter is usually the optimal state estimator for unconstrained, linear systems, where measurements are noisy [67]. However many physical systems behaves in a nonlinear matter, and

have states subject to constraints, making the Kalman filter non-applicable. A technique formulating state estimation in a probabilistic setting is the moving horizon estimation (MHE). The MHE strategy is reformulating the estimation problem as a quadratic program using a moving fixed-size estimation window [68]. In 1992 Ramamurthi et al. [69] investigated the moving horizon estimation as an extension of MPC. Instead of predicting ahead, like an MPC, the MHE looks back at input-output data over a finite horizon [70]. It tries finding an estimated state trajectory which is consistent with an assumed model, fitting the experimental data. The MHE strategy can be described by Figure 2.10.

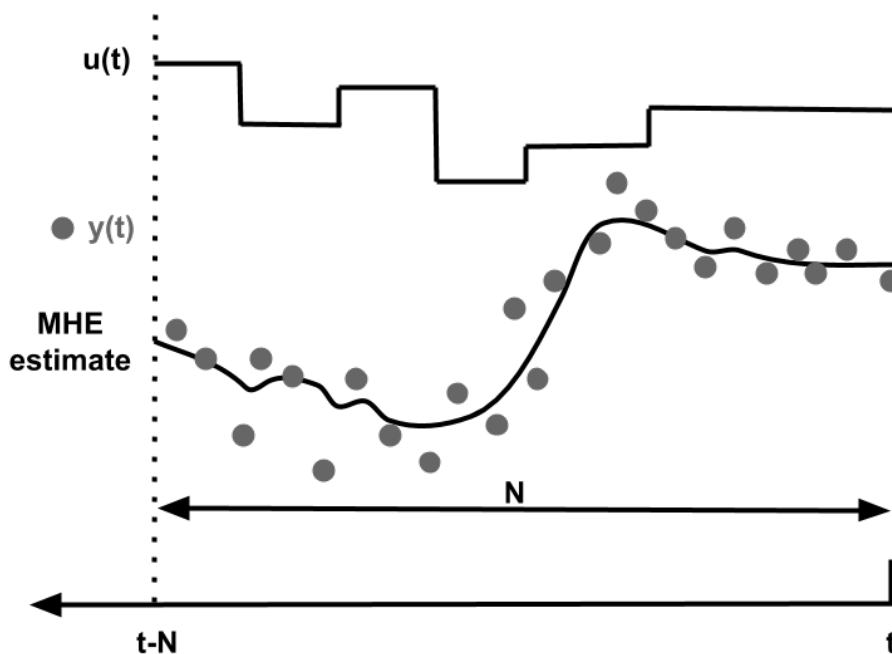


Figure 2.10: MHE strategy. $u(t)$ and $y(t)$ are previous inputs and outputs respectively. Given this information, the MHE computes the accumulation state estimate being communicated to the MPC. N is the estimation horizon [71].

2.6.5 Software

CasADi is an open-source tool for nonlinear optimization and algorithmic differentiation, and was the software used for this thesis. The tool includes a rich set of differentiable operations, including implicit functions, integrators and external code [72]. This enables coding of a variety of optimal control formulations.

3 Materials and method

3.1 Work done prior the master's thesis

The following subsections are obtained from the Specialization project "Riboflavin production from genetically modified strains of *Corynebacterium glutamicum* using sugars present in spent sulfite liquor", as well as further experiments performed by Dr. Fernando Pérez-García. The methods used for the implementation of the MPC in the laboratory (Section 3.6) were also based on the methods used previously in the specialization project, in order to obtain comparable results.

3.1.1 Genetically modified strains of *C. glutamicum*

In the experiments performed, the strains used are presented in Table 3.1, and were constructed at the Department of Genetics of Prokaryotes at Bielefeld University (Germany).

Table 3.1: Genetically modified strains of *C. glutamicum* used for fermentation experiments with the aim of producing riboflavin using sugars present in SSL.

Name	Strain
RiboGlu	<i>C. glutamicum</i> -(pEKEx3- <i>sigH</i>)(pSH1)
RiboMan	<i>C. glutamicum</i> -(pEKEx3- <i>sigH</i>)(pSH1- <i>manA</i>)
RiboXyl	<i>C. glutamicum</i> -(pEKEx3- <i>sigH</i>)(pSH1- <i>xylAB</i>)

All the strains use pEKEx3 [73] as a *E. coli*/*C. glutamicum* shuttle vector with the inducible promoter P_{tac} for the overexpression of *sigH* gene via IPTG induction. Sigma factors are targets to modify transcription regulation in bacteria and to influence production capacities [11]. An overexpression of *sigH* leads to an increased expression of riboflavin biosynthesis genes.

The strains in Table 3.1 use pSH1 [74] as a *E. coli*/*C. glutamicum* shuttle vector with a constitutive promoter P_{tuf} for the overexpression of *manA* or *xylAB* genes, enabling the utilization of mannose or xylose as carbon sources respectively.

3.1.2 Fermentation experiments performed

For the experiments performed in the specialization project, the fermentations started as a batch phase, followed by one feeding phase with a feeding rate of 3.5 mL/min. Further work during this master's thesis however, only includes the data obtained from the batch phases of the experiments.

The experiments were performed combining different *C. glutamicum* strains with different carbon sources (Table 3.2).

Table 3.2: An overview of the 9 different fermentation experiments using modified strains of *C. glutamicum* (see Table 3.1 for modification details) with various carbon sources. *Synthetic SSL had a composition of 20 g/L glucose + 20 g/L mannose + 20 g/L xylose.

Strain	Carbon source	Carbon source	Carbon source
	1. experiment	2. experiment	3. experiment
RiboGlu	Glucose (20g/L)	Mannose (20 g/L)	Synthetic SSL*
RiboMan	Glucose (20g/L)	Mannose (20 g/L)	Synthetic SSL*
RiboXyl	Glucose (20g/L)	Xylose (20 g/L)	Synthetic SSL*

3.2 Bioreactors setup and main idea

The idea of this master's thesis was to construct an MPC algorithm, combining the different strains to a main reactor, and to optimize the biomass growth. The main reactor would then be a CSTR operated at steady state. The idea is graphically explained in Figure 3.1.

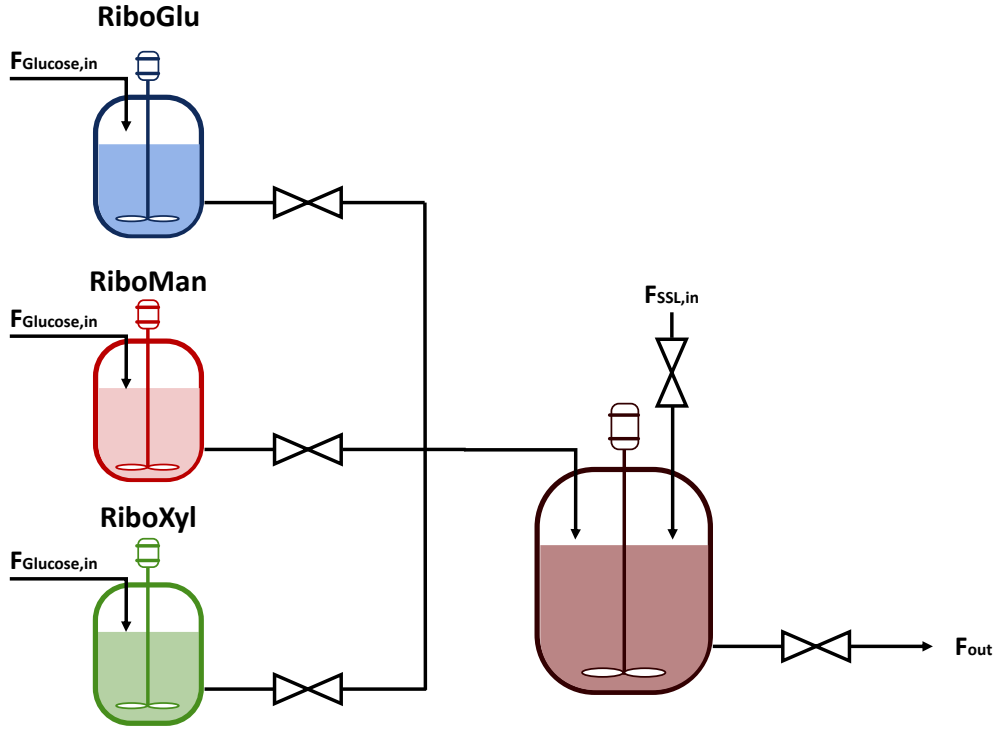


Figure 3.1: Flow diagram of combining different strains of *C. glutamicum* (see Table 3.1 for modification details) to a main CSTR reactor. $F_{RiboGlu,in}$, $F_{RiboMan,in}$ and $F_{RiboXyl,in}$ are feeds of RiboGlu, RiboMan and RiboXyl respectively. $F_{SSL,in}$ is the feed of SSL into the main reactor, and F_{out} is the product stream out of the reactor. $F_{Glucose,in}$ is the feed of glucose to the feed-reactors.

As shown in Figure 3.1, three reactors with the strains RiboGlu, RiboMan and RiboXyl will feed the main CSTR reactor with feeds $F_{RiboGlu,in}$, $F_{RiboMan,in}$ and $F_{RiboXyl,in}$ respectively. A fourth feed into the main reactor is the flow of SSL into the reactor ($F_{SSL,in}$). F_{out} is the out-stream or the product stream. The idea of the three feeding reactors was to perform batch experiments until stationary phase of biomass was reached, aiming to obtain similar concentrations of biomass in the three reactors. The three strains would use glucose as their carbon source. To prevent cells from dying, small amounts of glucose would be added after stationary phase had been reached ($F_{Glucose,in}$).

3.3 Modeling of strains

By using the equations described in Section 2.4.2 and 2.4.3, models for each of the three strains were made. ODE's for biomass concentration (X), sugar concentration (Glu , Man and Xyl), and product concentration (P) were formulated as shown in Equation (3.1).

$$\dot{X} = r_x \quad (3.1a)$$

$$\dot{Glu} = r_{s1} \quad (3.1b)$$

$$\dot{Man} = r_{s2} \quad (3.1c)$$

$$\dot{Xyl} = r_{s3} \quad (3.1d)$$

$$\dot{P} = r_p \quad (3.1e)$$

3.4 Parameter estimation

Once models of the different strains were made, MATLAB was used to estimate the unknown parameters. The MATLAB solver *ode45* was used to solve the ODE's, and the MATLAB function *lsqnonlin* fitted the estimated data to the experimental data. The parameters estimated are listed in Table 3.3.

Table 3.3: Overview of parameters estimated. $i = 1, 2, 3$ and represents the three sugars glucose, mannose and xylose respectively. 10 parameters were estimated for each strain described in Table 3.1.

Parameter	Unit	Description	Lower constraint	Upper constraint
$\mu_{max,i}$	h^{-1}	Maximum specific growth rate	0	5
$K_{S,i}$	g/L	Monod substrate constant	0	1000
$Y_{XS,i}$	g/g	Yield of biomass from substrate	-1	0
Y_{PX}	g/g	Yield of product from substrate	0	1

Different constraints and initial guesses were tested to find the optimal model fit with the experimental data. It was observed that initial guesses especially affected the outcome of the estimated parameters. As the rate of substrate uptake, r_s in Equation (2.4) is expressed as a positive expression in the model used, $Y_{XS,i}$ was constrained to have a negative value. The rate of substrate uptake can also be described as:

$$r_s = -\frac{r_X}{Y_{XS}}$$

providing positive values of Y_{XS} [75]. In both cases, the true yield of biomass from substrate is a positive value.

The constraints chosen were based on previous results from research done on *C. glutamicum* [76, 77], but were extended if the parameter results reached the exact constraints. As the aim of this study was to increase the biomass formation, the importance of the model describing the biomass formation was higher, compared to the description of sugar consumption and product formation. Hence the biomass part was weighted 10 times more, to improve the biomass fit to the experimental data.

3.5 MPC formulation

The MPC algorithm of the main reactor showed in Figure 3.1 was formulated using the parameters estimated for each strain, combined with the equations described in Section 2.4.2 and 2.4.3. The states and inputs used are presented in Table 3.4 and 3.5 respectively.

Table 3.4: States used for MPC formulation of system described in Figure 3.1, with constraints and start values.

States	Unit	Lower constraint	Upper constraint	Start value
RiboGlu	g/L	0	infinity	0
RiboMan	g/L	0	infinity	0
RiboXyl	g/L	0	infinity	0
Glucose	g/L	0	infinity	20
Mannose	g/L	0	infinity	20
Xylose	g/L	0	infinity	20
Riboflavin	μM	0	infinity	0
$V_{\text{main reactor}}$	L	0.7	1	0.7
$V_{\text{RiboGlu reactor}}$	L	0.7	1	1
$V_{\text{RiboMan reactor}}$	L	0.7	1	1
$V_{\text{RiboXyl reactor}}$	L	0.7	1	1

Table 3.5: Inputs used for MPC formulation of system described in Figure 3.1, with constraints and start values. *Simulations were also run constraining $F_{SSL,in}$ to have a constant stream of 0.1 L/h.

Inputs	Unit	Lower constraint	Upper constraint	Start value
$F_{RiboGlu,in}$	L/h	0	1	0
$F_{RiboMan,in}$	L/h	0	1	0
$F_{RiboXyl,in}$	L/h	0	1	0
$F_{SSL,in}$ *	L/h	0	1	0
F_{out}	L/h	0	1	0

The constraints were chosen to be feasible in the laboratory. Although the working volume of the Labfors reactors is 2.5 L, the maximum volume chosen was set to 1 L to have room for potential foam formation. The minimum volume was set to 0.7 L, enabling the probes measuring OD, DO and pH to touch the liquid phase. The external pumps available in the laboratory had a maximum capacity of 2.5 L/h, but the inputs were constrained to a maximum of 1 L/h, as the maximum volume of the reactors were set to 1 L. The sugar composition of the SSL and synthetic SSL used for the simulations are given in Table 3.6.

Table 3.6: Sugar concentration of glucose, mannose and xylose in SSL (based on real SSL composition [data not yet published]) and synthetic SSL used for MPC simulations.

Sugar	C_{SSL} [g/L]	C_{synSSL} [g/L]
Glucose	36	20
Mannose	110	20
Xylose	45	20

The dilutions of the different substrates or sugars, S were described using Equation (3.2).

$$\begin{aligned}
 D_S = & \frac{F_{SSL,in} \cdot ([SSL_{S,in}] - [S])}{V} + \frac{F_{RiboGlu,in} \cdot ([RiboGlu_{S,in}] - [S])}{V} \\
 & + \frac{F_{RiboMan,in} \cdot ([RiboMan_{S,in}] - [S])}{V} + \frac{F_{RiboXyl,in} \cdot ([RiboXyl_{S,in}] - [S])}{V}
 \end{aligned} \tag{3.2}$$

Here D_S are the dilution terms of the sugars S (Glucose, Mannose and Xylose). $F_{SSL,in}$ is the stream of SSL into the reactor, $[SSL_{S,in}]$ is the concentration of sugar S in the SSL stream, $[S]$ is the concentration of sugar S in the reactor, and V is the liquid volume in the reactor. $F_{RiboGlu,in}$, $F_{RiboMan,in}$ and $F_{RiboXyl,in}$ are the flows of the RiboGlu, RiboMan and RiboXyl strains respectively into the main reactor. $[RiboGlu_{S,in}]$, $[RiboMan_{S,in}]$ and $[RiboXyl_{S,in}]$ are the concentrations of sugar S in the feed reactors of RiboGlu, RiboMan and RiboXyl respectively. The latter concentrations are assumed to be zero due to full consumption of sugars once stationary phase is reached.

The dilutions of the biomass terms were described using Equation (3.3).

$$D_i = \frac{F_{SSL,in} \cdot (-[X_i])}{V} + \frac{F_{RiboGlu,in} \cdot ([RiboGlu_{X_i}] - [X_i])}{V} + \frac{F_{RiboMan,in} \cdot ([RiboMan_{X_i}] - [X_i])}{V} + \frac{F_{RiboXyl,in} \cdot ([RiboXyl_{X_i}] - [X_i])}{V} \quad (3.3)$$

Here D_i is the dilution of the strain i . $[X_i]$ is the biomass concentration of strain i in the main reactor. $[RiboGlu_{X_i}]$, $[RiboMan_{X_i}]$, and $[RiboXyl_{X_i}]$ are the biomass concentrations of strain i in the feeding reactors of RiboGlu, RiboMan and RiboXyl respectively.

The dilutions of the product term was described using Equation (3.4).

$$D_P = \frac{F_{SSL,in} \cdot (-[P])}{V} + \frac{F_{RiboGlu,in} \cdot ([RiboGlu_P] - [P])}{V} + \frac{F_{RiboMan,in} \cdot ([RiboMan_P] - [P])}{V} + \frac{F_{RiboXyl,in} \cdot ([RiboXyl_P] - [P])}{V} \quad (3.4)$$

Here D_P is the dilution of the product. $[P]$ is the product concentration in the main reactor. $[RiboGlu_P]$, $[RiboMan_P]$, and $[RiboXyl_P]$ are the product concentrations in the feeding reactors of RiboGlu, RiboMan and RiboXyl respectively. To see how much P was generated in the main reactor, these values were set to zero.

The final 11 ODEs used for the states in the MPC algorithm are described by Equation (3.5).

$$\dot{X}_{RiboGlu} = r_x RiboGlu + D_{RiboGlu} \quad (3.5a)$$

$$\dot{X}_{RiboMan} = r_x RiboMan + D_{RiboMan} \quad (3.5b)$$

$$\dot{X}_{RiboXyl} = r_x RiboXyl + D_{RiboXyl} \quad (3.5c)$$

$$\dot{Glu} = r_{s1} RiboGlu + r_{s1} RiboMan + r_{s1} RiboXyl + D_{Glu} \quad (3.5d)$$

$$\dot{Man} = r_{s2} RiboGlu + r_{s2} RiboMan + r_{s2} RiboXyl + D_{Man} \quad (3.5e)$$

$$\dot{Xyl} = r_{s3} RiboGlu + r_{s3} RiboMan + r_{s3} RiboXyl + D_{Xyl} \quad (3.5f)$$

$$\dot{P} = r_p RiboGlu + r_p RiboMan + r_p RiboXyl + D_P \quad (3.5g)$$

$$\dot{V} = F_{RiboGlu,in} + F_{RiboMan,in} + F_{RiboXyl,in} + F_{SSL,in} - F_{out} \quad (3.5h)$$

$$\dot{V}_{RiboGlu} = -F_{RiboGlu,in} \quad (3.5i)$$

$$\dot{V}_{RiboMan} = -F_{RiboMan,in} \quad (3.5j)$$

$$\dot{V}_{RiboXyl} = -F_{RiboXyl,in} \quad (3.5k)$$

3.5.1 Properties of the Optimal Control Problem

The MPC simulations were tested using various time horizons, control intervals and collocation points, but the final properties used for the cases presented in this thesis are summarized in Table 3.7.

Table 3.7: OCP properties used for MPC simulations.

Symbol	Value	Description
d	3	Number of collocation points per control interval
T	20	Time horizon
N	50	Number of control intervals in T

The recommended practice is to choose these optimal control problem (OCP) properties early in the controller design, and to keep them constant while tuning other controller parameters [78]. The OCP properties used were chosen based on a trade-off between the performance and the computational effort used. Generally larger numbers of time intervals leads to shorter lengths of the control intervals and lower discretization errors

[79]. However the dimension of the resulting NLP problem will need more computational effort to solve. A smaller number of intervals gives an inaccurate state trajectory. Shorter control intervals gives more rapid updates of both states and inputs, improving the accuracy of the state estimation, and the responsiveness of the MPC. The time horizon and control interval (T/N) chosen could have been longer or shorter as well, but this horizon caught the dynamics of the system in a good way. The objective function is the sum of the stage cost at each time step, and can be defined by Equation (3.6).

$$J = \sum_i^N l(x_i, u_i) \quad (3.6)$$

Here l is the stage cost for control interval i . Various stage costs (l) were tested, but the simulation results described in this thesis are based on the stage costs described in Equation (3.7) to (3.10). The MPC algorithm automatically minimizes l , consequently to maximize terms of l , a negative sign was required.

Case A: Maximize biomass

$$l = -X_{RiboGlu} - X_{RiboMan} - X_{RiboXyl} \quad (3.7)$$

Case B: Maximize product in F_{out}

$$l = -P \cdot F_{out} \quad (3.8)$$

Case C: Maximize biomass yield[†]

$$l = -\frac{X_{RiboGlu} \cdot F_{out}}{[SSL] \cdot F_{SSL,in} + 0.1} - \frac{X_{RiboMan} \cdot F_{out}}{[SSL] \cdot F_{SSL,in} + 0.1} - \frac{X_{RiboXyl} \cdot F_{out}}{[SSL] \cdot F_{SSL,in} + 0.1} \quad (3.9)$$

Case D: Maximize product yield - linearized approximation[‡]

$$l = -P \cdot F_{out} + F_{SSL,in} \cdot (Glu + Man + Xyl) \quad (3.10)$$

[†]0.1 was added in the denominator to avoid the value zero, and the MPC not to run

[‡]Due to high computational effort solving the product yield, a linear approximation was done

3.6 Implementation in the laboratory

Due to limitations of access to the NTNU campus the spring of 2020, the physical experiments testing the MPC algorithm had to be simplified, and the number of planned experiments were reduced to one. This led to a simplification of the idea described in Figure 3.1. The aim of this experiment was firstly to compare the performance of the MPC on the real system with that of the simulations. The simpler model can be described by Figure 3.2, and only includes one feeding reactor containing the RiboGlu strain.

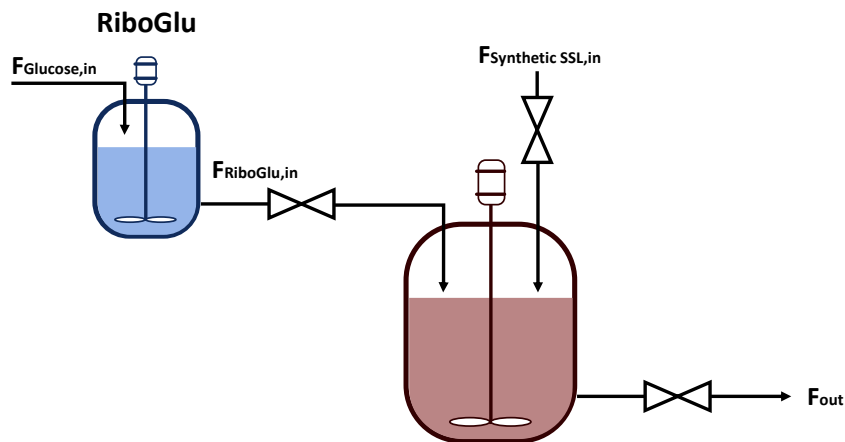


Figure 3.2: Simplified version of the idea presented in Figure 3.1. The figure shows a flow diagram of feeding the RiboGlu strain of *C. glutamicum* (see Table 3.1 for modification details) to a main CSTR reactor. $F_{RiboGlu,in}$ is the feed of RiboGlu. $F_{Synthetic\ SSL,in}$ is the feed of synthetic SSL into the main reactor, and F_{out} is the product stream out of the reactor. $F_{Glucose,in}$ is the feed of glucose.

The fermentation of the RiboGlu strain was performed using glucose as its carbon source. The minimal medium CGXII was used for the main cultivation of the RiboGlu strain, while the complex medium BHI supplemented with 0.5% of sugar was used for the cell preculture. Recipes of the medium and stock solutions are attached in Appendix Section C. The sugar composition of the synthetic SSL used for the simulations are given in Table 3.6. The properties of the optimal control problem (OCP) used for the MPC algorithm implemented to the laboratory are given in Table 3.7. The states and inputs used are presented in Table 3.8 and 3.9 respectively.

Table 3.8: States used for MPC formulation of system described in Figure 3.2, with constraints and start values.

States	Unit	Lower constraint	Upper constraint	Start value
RiboGlu	g/L	0	infinity	0
Glucose	g/L	0	infinity	20
Mannose	g/L	0	infinity	20
Xylose	g/L	0	infinity	20
Riboflavin	μ M	0	infinity	0
$V_{\text{main reactor}}$	L	0.7	1	0.7
$V_{\text{RiboGlu reactor}}$	L	0.7	1	1

Table 3.9: Inputs used for MPC formulation of system described in Figure 3.2, with constraints and start values.

Inputs	Unit	Lower constraint	Upper constraint	Start value
$F_{\text{RiboGlu},in}$	L/h	0	1	0
$F_{\text{Synthetic SSL},in}$	L/h	0	1	0
F_{out}	L/h	0	1	0

MPC simulations of the simplified system were done using simplifications of all the Cases (A-D). Case C was chosen as the stage cost to test experimentally, as it included more input steps. Since the aim of the implementation in the lab firstly was to compare the performance of the MPC on the real system with that of the simulations, a case including more inputs was assumed to show more clearly any deviation from the simulations. The simplified stage cost of Case C, using only the RiboGlu strain is presented in Equation (3.11).

$$l = \frac{-X_{\text{RiboGlu}} \cdot F_{out}}{F_{\text{Synthetic SSL},in} \cdot [\text{Synthetic SSL}] + 0.1} \quad (3.11)$$

In this case synthetic SSL was used (composition is presented in Table 3.6). Simulation results using this stage cost are presented in Section 4.3.

3.6.1 Preparation of preculture and inoculum

A fresh agar plate was streaked with the RiboGlu strain. The plate was kept at 30°C overnight. Colonies from the plate were added to at least 200 mL of the complex media BHI supplemented with glucose 0.5 %, the antibiotics Kanamycin and Spectomycin

(Recipes are attached in Appendix Section C.4) were added in the final concentrations of 25 $\mu\text{g}/\text{mL}$ and 100 $\mu\text{g}/\text{mL}$ respectively. The flask preculture grew overnight at 30°C and 200 rpm. The next day OD_{600} of the preculture was measured using a spectrophotometer at 600 nm. The amount of cells needed for inoculation of the reactor with $\text{OD}_{600} = 1$ was calculated using Equation Equation (3.12), where C_1 and C_2 are the concentrations, V_1 and V_2 are the associated volumes.

$$C_1V_1 = C_2V_2 \quad (3.12)$$

The needed volume was collected in falcon tubes, and centrifuged at 5000 rpm for 10 minutes at room temperature. The supernatants were discarded, and the cells were resuspended in CGXII buffer (without carbon source) as cell's washing step. The cells were again centrifuged with the same conditions, before the supernatants were discarded again. The resulting cell pellet was resuspended in 50mL of CGXII buffer and used as the inoculum for the reactor.

3.6.2 Bioreactor conditions

The fermentation was performed in a fed-batch 3.6 L bioreactor from Labfors, with a maximum working volume of 2.5 L. The bioreactor included probes for measuring optical density (OD), dissolved oxygen (DO), pH and temperature. It also had a sampler tube, antifoam tube, rotor/stirrer and metal baffles. The fermentation method was prepared as showed in Table 3.10.

Table 3.10: Fermentation conditions for production of riboflavin using RiboGlu strain of *C. glutamicum*.

Condition	T [°C]	pH	DO [%]	Stirrer speed [rpm]	Air supply [NL]
Value	30 ± 0.5	7 ± 0.1	30	200	2

The DO was automatically controlled by the stirring speed to keep it at 30%. The pH was adjusted automatically by addition of acid (phosphoric acid 10%) and base (potassium hydroxide 4 M), while the addition of antifoam (Antifoam 204, Sigma) was done manually when needed.

3.6.3 CSTR setup

The feed-reactor outlet tube ($F_{RiboGlu,in}$) was connected to the main reactor under sterile conditions, and an external pump was connected in order to control the feed input. The $F_{Synthetic\ SSL,in}$ tube, and the F_{out} tube were connected to external pumps as well. In order to collect samples automatically from this reactor, the NUMERA systems from Secure-Cells was connected to the main reactor. Ideally NUMERA would be directly connected to the High-Performance Liquid Chromatography (HPLC), but due to technical inconveniences the samples were transferred manually (See Section 3.6.4 and 3.6.5 for details about NUMERA and HPLC).

3.6.4 NUMERA

NUMERA is an automated sampling and sample processing system for on-line analytics in up- and down-stream bioprocesses. It enables high-frequency sampling of small volumes precisely. In combination with the software Lucullus PIMS it covers the workflow from process planning, automated sample processing, data recording to online data analysis and process control [80]. NUMERA can collect, dilute (up to 1:25), filter and store samples (at 4°C) automatically. The samples were manually transferred to the HPLC. In the specialization project, the samples were unfiltered by NUMERA and OD_{600} was measured manually using spectrophotometer. Subsequently supernatants were collected and used for HPLC measurements. However in this experiment, filtering by NUMERA was included in order to make the samples immediately prepared for the HPLC. By using the OD probe for measuring biomass concentrations, the delay of manual measurements would be reduced. The OD data would have been given directly to the MPC.

3.6.5 HPLC

High-performance liquid chromatography or HPLC is a type of liquid chromatography where a sample with liquid or an appropriately dissolved solid sample is forced through a column by liquid at high pressure [81]. The column is packed with a stationary phase to facilitate separation, before the sample is pumped into a detector. The detector monitors concentrations of the separated components, and its signal response provides a "fingerprint" of its chemical composition. If standards of the components are available, and the components of the sample are known and sufficiently resolved, quantitative information can be obtained. Depending on what compound that will be measured, there are used different columns and detectors. Two columns and detectors were used for the ex-

periments. Sugars were analyzed by HPLC using a Macherey-Nagel NUCLEOGEL®Pb column (300 x 7.8 mm) [82]. The mobile phase was deionized water with a flow rate of 0.4 ml/min at 80°C. The compounds were detected using ERC RefratoMax 520 refractive index detector. The sugar analysis can be fed directly to the MPC. Riboflavin was subsequently analyzed by HPLC using a Macherey-Nagel NUCLEODUR®C₈ Gravity column (125 x 2.0 mm) [11]. The mobile phase consisted of two buffers (Buffer A: 20mM CH₃COONa, Buffer B: 20mM CH₃COONa, 100% CH₃CN and 100% CH₃OH in a ratio of 1:2:2 respectively). An overview over the buffer gradient is shown in Table 3.11.

Table 3.11: Buffer gradient for HPLC measurements of riboflavin.

Time	Flow [ml/min]	% Buffer A	% Buffer B
0.0	0.450	100	0
17.0	0.450	40	60
18.0	0.450	0	100
18.1	0.800	0	100
24.0	0.800	0	100
24.1	0.450	100	0
28.0	0.450	100	0

Riboflavin is a fluorescent compound, and does not need to be derivatized as is the case with amino acids [82]. The fluorescence from riboflavin was monitored with a Ultimate 3000 RS Fluorescence Detector (Dionex). The riboflavin spectra has a maximum excitation wavelength of 450 nm and a maximum emission wavelength of 535 nm. The Chromeleon software was used to analyze samples and standards chromatograms.

3.6.6 Running the CSTR experiment using the MPC

Due to a technical error regarding the data type of the external pump measurements, changes in reactor volumes were undetected. This led to an immediate feed of the $F_{RiboGlu,in}$, emptying the RiboGlu reactor. The experiment was therefore terminated. Due to limited access to the laboratory because of the COVID-19 virus and time constraints, the experiment could not be repeated during the Master's project. Once the simple version of the MPC is working, the experiments combining the strains as shown in Figure 3.1 can be performed.

4 Results

This section is divided into four subsections. Section 4.1 presents the results of parameter estimation and model fit, Section 4.2 presents the MPC simulation results of Case A-D, Section 4.3 presents the MPC simulation results of the simplified system, and finally Section 4.4 presents a comparison of using single strains and a combination of strains. Each section includes a discussion and the main interpretations of the results. The discussion chapter in Section 5 includes further discussion, alternative interpretations of the results and future work.

4.1 Parameter estimation and model fit

The parameters estimated for the three strains presented in Table 3.1, were based on experiments performed during the specialization project of the fall 2019. The final values of the parameters estimated are summarized in Section 4.1.4. The following sections presents the model estimations with the parameters, compared to the experimental data obtained. Experimental raw data is attached in Appendix Section A. The models estimated for the RiboGlu, RiboMan and RiboXyl strains depicted in Figure 4.1 to 4.9 generally describe the biomass formation and sugar consumption well. However behavior of riboflavin production, generally does not match the experimental data obtained, except for when growing on synthetic SSL. As seen in Equation (2.5), the kinetic expressions used shows that volumetric rate of product formation is proportional to the volumetric rate of biomass formation (Equation (2.3)). Experimentally, this proportionality was mainly not achieved.

4.1.1 RiboGlu

Three different experiments using the carbon sources glucose, mannose and synthetic SSL were the basis of the parameter estimation of the RiboGlu strain. Figure 4.1 to 4.3 shows model simulations with parameters given in Table 4.1, together with the experimental data.

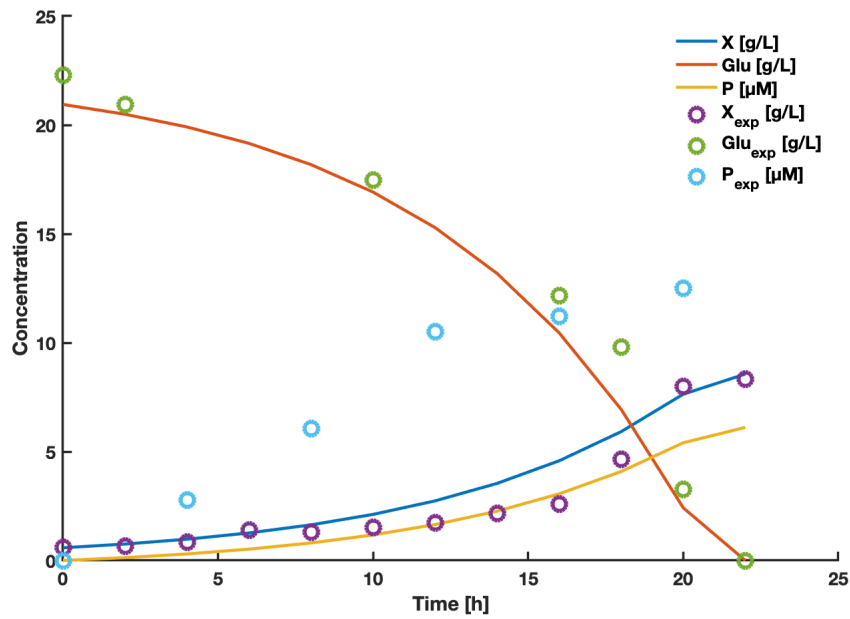


Figure 4.1: RiboGlu strain model simulations with glucose as its carbon source. Circles represents experimental data, while solid lines represents the data fitted using estimated parameters. X and Glu represents biomass and glucose concentrations respectively in g/L, P represents product concentration of riboflavin in μM .

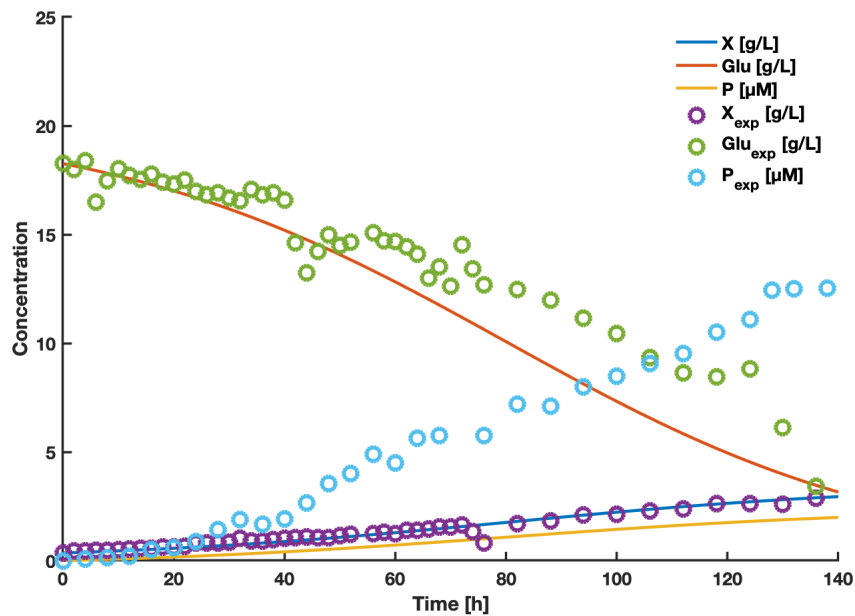


Figure 4.2: RiboGlu strain model simulations with mannose as its carbon source. Circles represents experimental data, while solid lines represents the data fitted using estimated parameters. X and Man represents biomass and mannose concentrations respectively in g/L, P represents product concentration of riboflavin in μM .

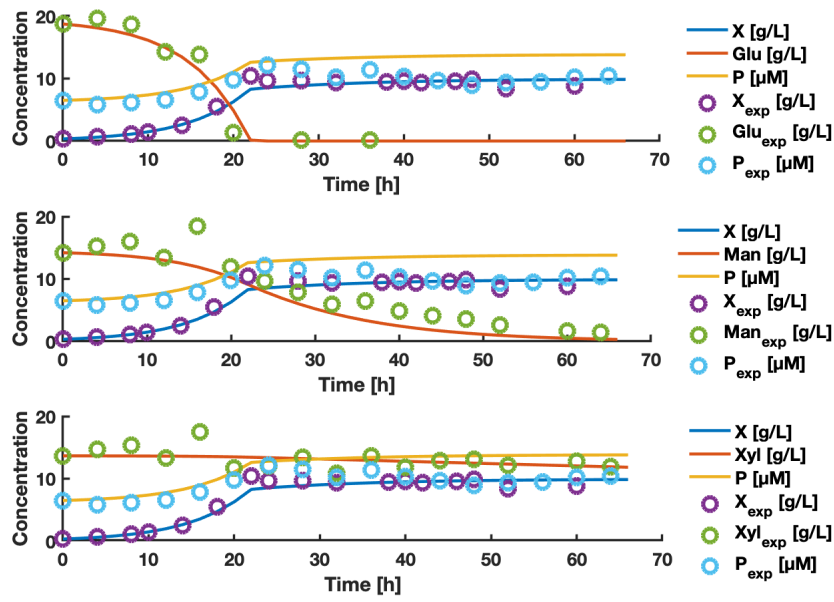


Figure 4.3: RiboGlu strain model simulations with synthetic SSL as its carbon source. Circles represents experimental data, while solid lines represents the data fitted using estimated parameters. X, Glu, Man, and Xyl represents biomass, glucose, mannose and xylose concentrations respectively in g/L, P represents product concentration of riboflavin in μM .

As explained in Section 3.4, the initial guesses of parameters affected the outcome of the estimated parameters, and hence the model fit. An old version of the parameter estimation of RiboGlu strain can be seen in Appendix Section E.1. The new parameter estimations were performed, which lead to an improvement of the RiboGlu model regarding xylose consumption. A change of initial guesses lead to a 20-fold increase of the $K_{S,3}$, and a 40-fold decrease of $\mu_{max,3}$. This improved the data fit of xylose greatly, as seen in Figure 4.3 (compared to Figure E.1).

4.1.2 RiboMan

Three different experiments using the carbon sources glucose, mannose and synthetic SSL were the basis of the parameter estimation of the RiboMan strain. Figure 4.4 to 4.6 shows model simulations with parameters given in Table 4.1, together with the experimental data.

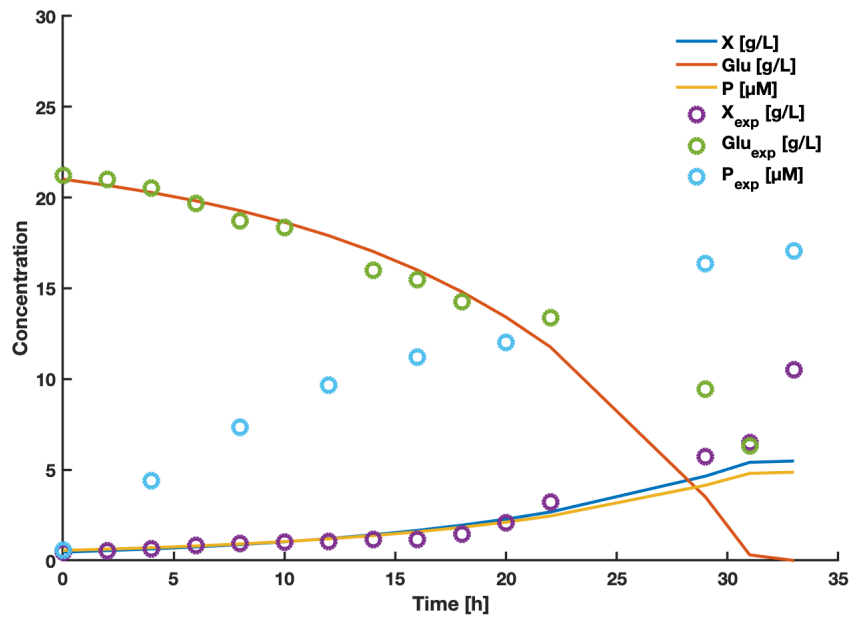


Figure 4.4: RiboMan strain model simulations with glucose as its carbon source. Circles represents experimental data, while solid lines represents the data fitted using estimated parameters. X and Glu represents biomass and glucose concentrations respectively in g/L, P represents product concentration of riboflavin in μ M.

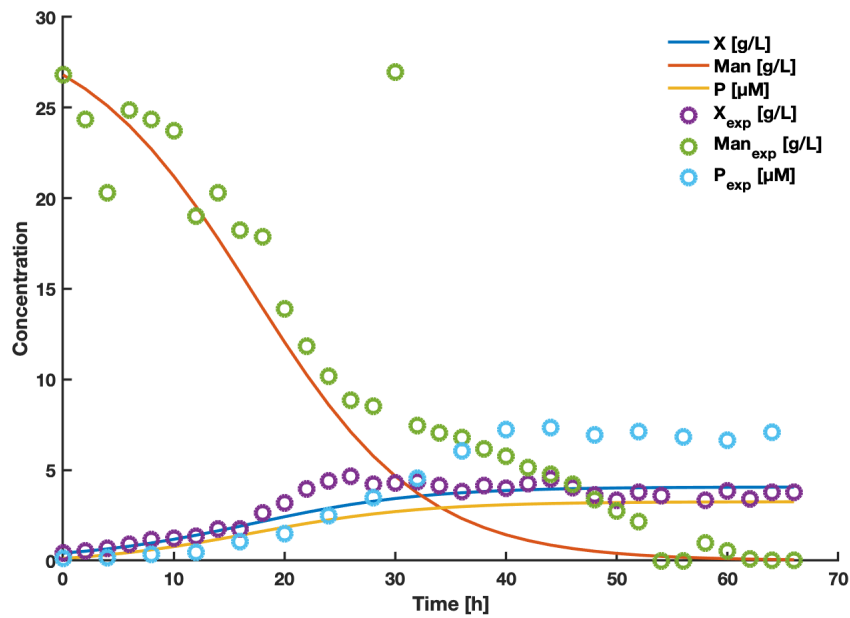


Figure 4.5: RiboMan strain model simulations with mannose as its carbon source. Circles represents experimental data, while solid lines represents the data fitted using estimated parameters. X and Man represents biomass and mannose concentrations respectively in g/L, P represents product concentration of riboflavin in μ M.

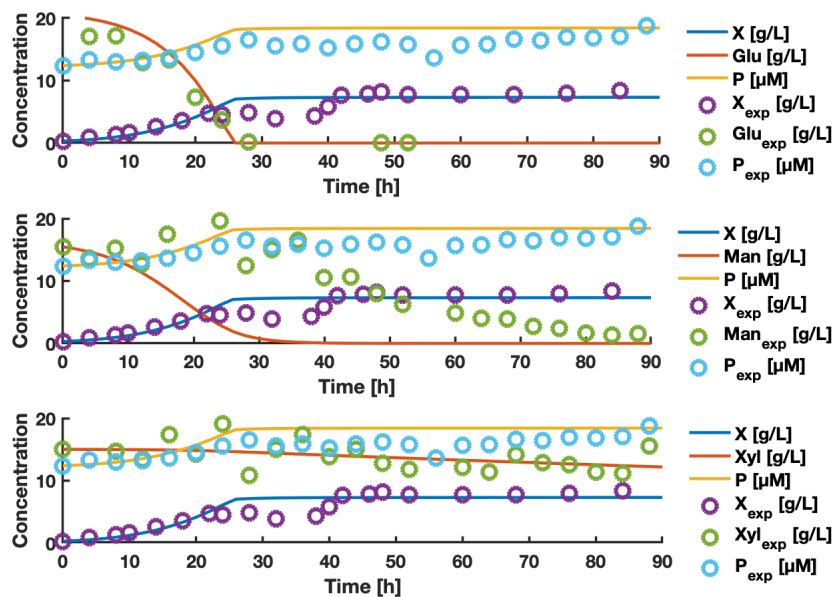


Figure 4.6: RiboMan strain model simulations with synthetic SSL as its carbon source. Circles represents experimental data, while solid lines represents the data fitted using estimated parameters. X, Glu, Man, and Xyl represents biomass, glucose, mannose and xylose concentrations respectively in g/L, P represents product concentration of riboflavin in μM .

It can be observed from Figure 4.6 that the model of RiboMan strain growing on SSL deviates when describing the consumption of mannose. The model shows that mannose is completely consumed after 30 hours, while experimental data shows that it is never completely consumed during a batch of 92 hours. This deviation is probably due to substrate inhibition, where glucose is the preferred carbon source as it is consumed faster (See Figure 4.4 and Figure 4.5). This can cause problems for the accuracy of the MPC algorithm, regarding the feed of the RiboMan strain into the main reactor, and hence other inputs. Especially considering the high concentration of mannose in the real SSL available (see Table 3.6 for composition). Different initial guesses and constraints were tested trying to improve the RiboMan model as well. As an increase of $K_{S,3}$ and decrease of $\mu_{max,3}$ of the RiboGlu model improved the xylose model fit significantly, a lower constraint of 800 for $K_{S,2}$, and a higher constraint of 1 for $\mu_{max,2}$ were assumed to improve the parameters, and hence the model fit of RiboMan expressing a slower consumption of mannose. The results obtained however, did not improve the model fit, as seen in Figure E.6. The parameters estimated with the new constraints reached the exact constraint values.

4.1.3 RiboXyl

Three different experiments using the carbon sources glucose, xylose and synthetic SSL were the basis of the parameter estimation of the RiboXyl strain. Figure 4.7 to 4.9 shows model simulations with parameters given in Table 4.1, together with the experimental data.

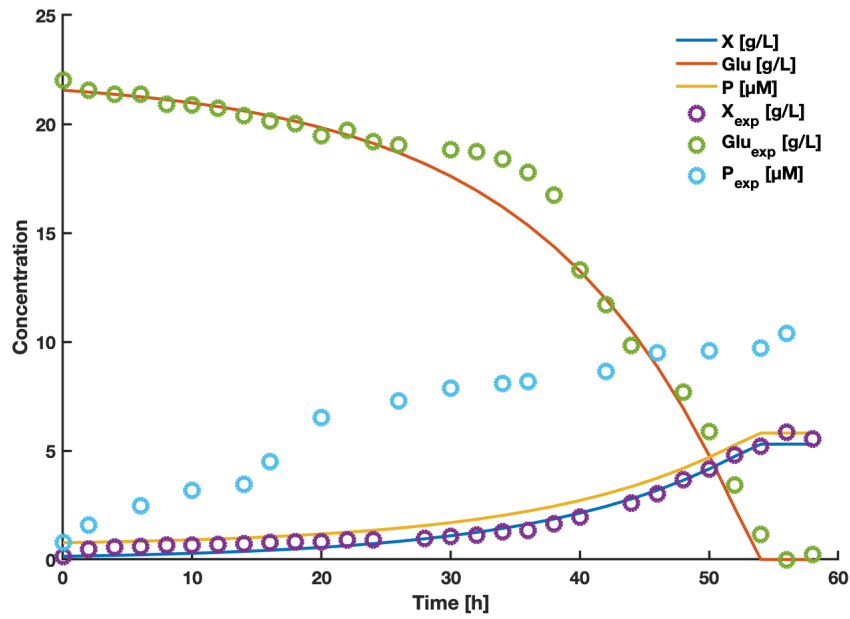


Figure 4.7: RiboXyl strain model simulations with glucose as its carbon source. Circles represents experimental data, while solid lines represents the data fitted using estimated parameters. X and Glu represents biomass and glucose concentrations respectively in g/L, P represents product concentration of riboflavin in μ M.

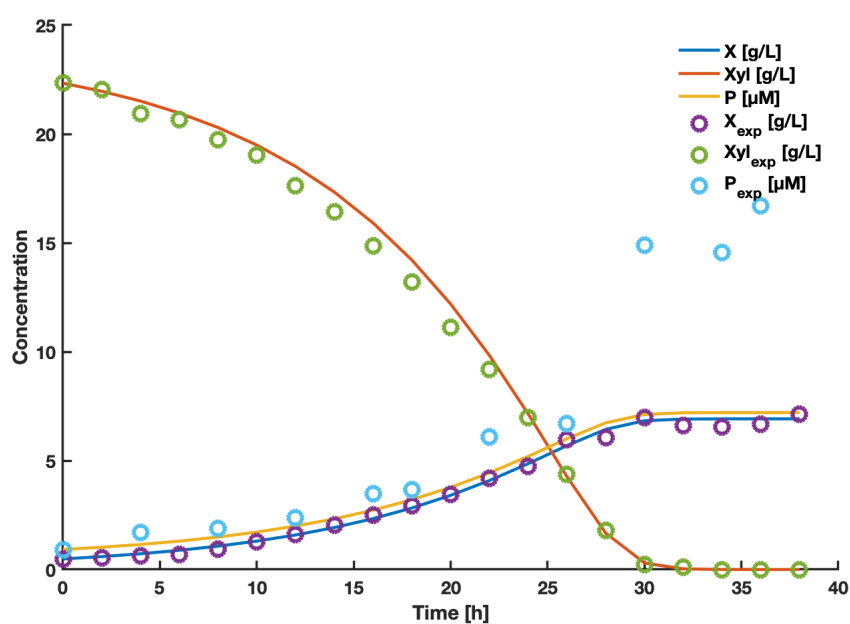


Figure 4.8: RiboXyl strain model simulations with xylose as its carbon source. Circles represents experimental data, while solid lines represents the data fitted using estimated parameters. X and Xyl represents biomass and xylose concentrations respectively in g/L, P represents product concentration of riboflavin in μM .

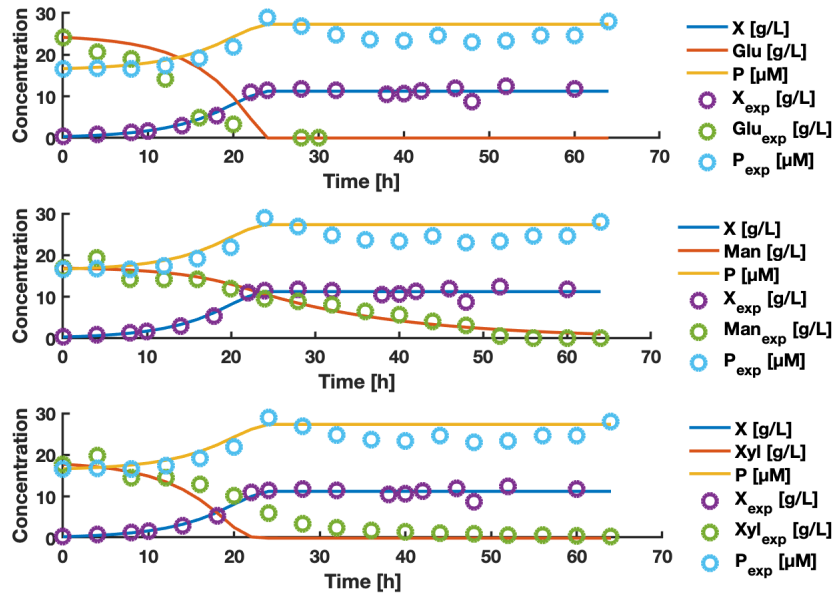


Figure 4.9: RiboXyl strain model simulations with synthetic SSL as its carbon source. Circles represents experimental data, while solid lines represents the data fitted using estimated parameters. X, Glu, Man, and Xyl represents biomass, glucose, mannose and xylose concentrations respectively in g/L, P represents product concentration of riboflavin in μM .

The RiboXyl strain is the only strain consuming xylose, as can be seen in Figure 4.9 (compared to Figure 4.3 and 4.6). The decrease in xylose concentration for the other cases is due to dilution from the addition of acid, base and antifoam.

4.1.3.1 Product formation of *C. glutamicum* growing on synthetic SSL

Figure 4.3, 4.6 and 4.9 shows the models of the RiboGlu, RiboMan, and RiboXyl strains respectively when growing on synthetic SSL. In all the cases, the description of product formation seems to fit the experimental data. These were the only cases where the experimental data actually showed that the product formation of riboflavin was proportional to the biomass formation. It can be observed that the concentrations of P_{exp} are positive at time=0. This may also be a reason for the good fit with the model, and contributing to its proportionality towards the biomass formation. However this feature is probably due to a delay of sample measurements, or cross contamination between samples if the HPLC washing steps were too short. As the aim of this master's thesis was to see if a combination of strains could increase the biomass formation while being fed SSL, it was assumed that the models, and parameters estimated for *C. glutamicum* strains growing

on synthetic SSL were of highest importance.

4.1.4 Estimated parameter values

The parameters estimated for modeling biomass formation of the three strains (presented in Table 3.1), sugar consumption and product formation are presented in Table 4.1.

Table 4.1: Parameters estimated for the three strains presented in Table 3.1. Estimations were based on experiments performed during the specialization project. Raw data is attached in Appendix Section A. Description of the parameters is presented in Table 3.3.

Parameter	RiboGlu	RiboMan	RiboXyl	Lower constraint	Upper constraint
$\mu_{max,1}$	0.1290	0.0798	0.0675	0	5
$\mu_{max,2}$	0.7299	4.1547	0.0003	0	5
$\mu_{max,3}$	0.0013	0.0033	0.1082	0	5
$K_{s,1}$	0.0523	0.0678	0.0905	0	1000
$K_{s,2}$	523.9684	946.95	653.7131	0	1000
$K_{s,3}$	834.3772	943.5982	2.0783	0	1000
$Y_{xs,1}$	-0.3806	-0.2389	-0.2396	-1	0
$Y_{xs,2}$	-0.1716	-0.1361	-0.0001	-1	0
$Y_{xs,3}$	-0.0050	-0.0088	-0.2876	-1	0
Y_{px}	0.7663	0.8584	0.9751	0	1

The different behavior of mannose and RiboMan strain may also be observed through the parameter results in Table 4.1. For all the strains, $K_{S,2}$ - the substrate constant of mannose is high. Generally the K_S -values obtained are higher than typical values in the order mg/L for carbohydrate substrates, as stated by Doran [46]. As K_S is the substrate concentration where the maximum specific growth rate has reached its half value, it makes sense that high $K_{S,2}$ values are obtained, as the *C. glutamicum* growth using mannose as its carbon source is slower. The fact that all strains has lower $K_{S,1}$ values also makes sense, as this is the substrate constant of glucose. Glucose is one of the native carbon sources of *C. glutamicum*, and widely used in research and industrial fermentations [2, 28]. Typically the use of glucose as carbon source provides competitive production yields [29, 83].

4.2 MPC simulation results

The following sections presents the results of the MPC simulations. In all the cases, the OCP had the time horizon, number of control intervals and number of collocation points outlined in Table 3.7. The constraints used are presented in Table 3.4 and 3.5. The cases presented in this section uses real SSL, while simulation results obtained by using a variable feed stream of synthetic SSL are attached in Appendix Section F (composition is described in Table 3.6).

Each section in this chapter contains the graphical simulation results of inputs, states and riboflavin production, followed by the biomass and riboflavin produced by the two versions of the case after 80 hours. After all the graphical results of the case has been presented, a discussion comparing the simulation results of the case is presented. Finally Section 4.2.5 summarizes, and compares the key results obtained from the different cases A-D, including key results obtained by using synthetic SSL.

4.2.1 Case A: Maximize biomass

From the simulations using the objective function of maximizing biomass concentration (Equation (3.7)), the system was simulated under two different conditions when using real SSL: one with a variable feed stream and one with a fixed feed stream. This provided different results regarding biomass and product yields. The MPC simulation results of Case A can be graphically described by Figure 4.10 to 4.15. Results obtained using a variable feed stream of synthetic SSL, are attached in Appendix Section F.1. A comparison of the versions is presented in Subsection 4.2.1.3.

4.2.1.1 SSL with flow rate of 0-1 L/h

Figure 4.10, 4.11 and 4.12 shows the inputs, states and riboflavin results respectively obtained from MPC simulations using the objective function of Case A (Equation (3.7)) with a varying SSL flow rate in the range 0-1 L/h.

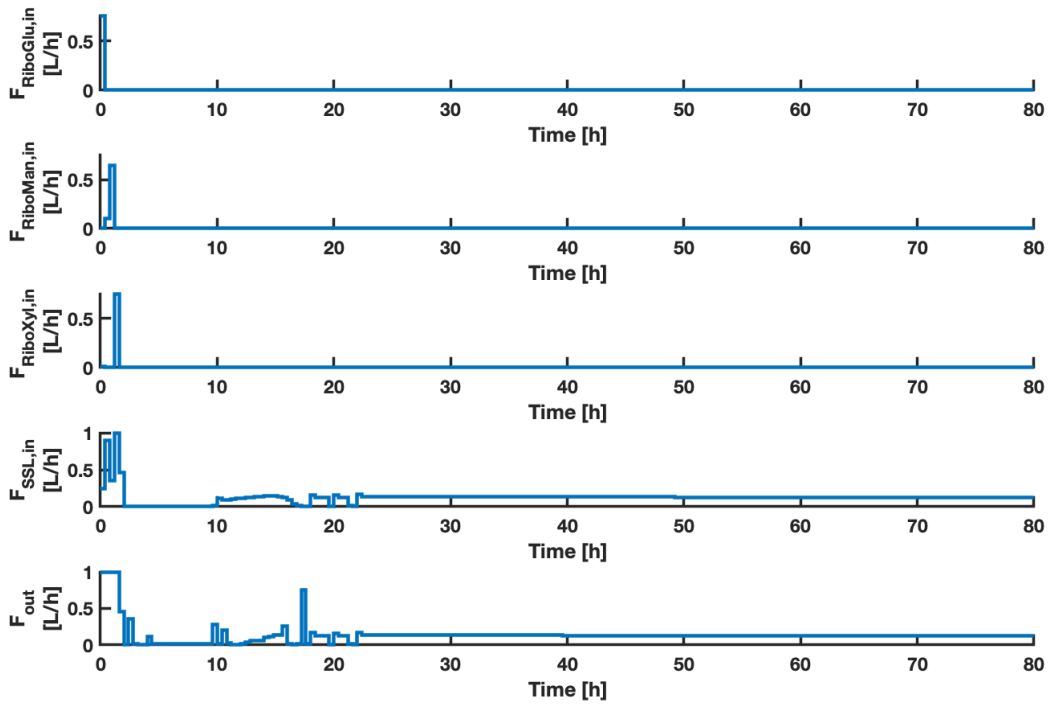


Figure 4.10: The plots shows the inputs $F_{RiboGlu,in}$, $F_{RiboMan,in}$, $F_{RiboXyl,in}$, $F_{SSL,in}$ and F_{out} as a function of time. The MPC inputs were calculated using the objective function of Case A (described in Equation (3.7)). The $F_{SSL,in}$ had a lower constraint of 0 and an upper constraint of 1 L/h.

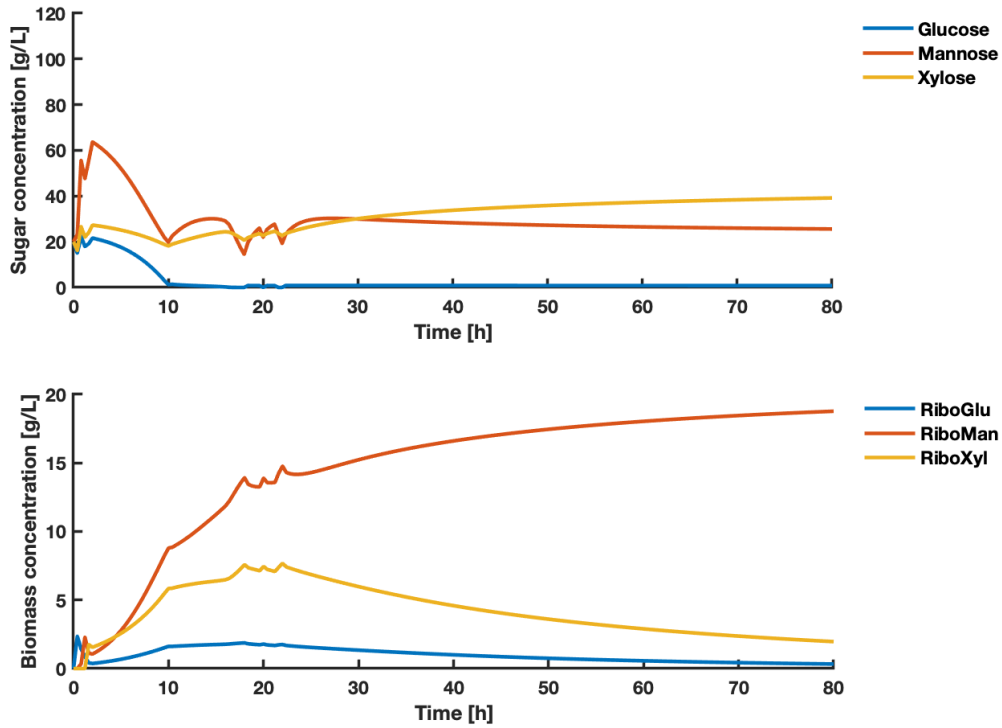


Figure 4.11: The upper plot shows the concentrations of the states glucose, mannose, xylose as a function of time. The lower plot shows the concentrations of states RiboGlu, RiboMan and RiboXyl as a function of time. The states are a result of the inputs shown in Figure 4.10 using the objective function of Case A (described in Equation (3.7)). The $F_{SSL,in}$ had a lower constraint of 0 and an upper constraint of 1 L/h.

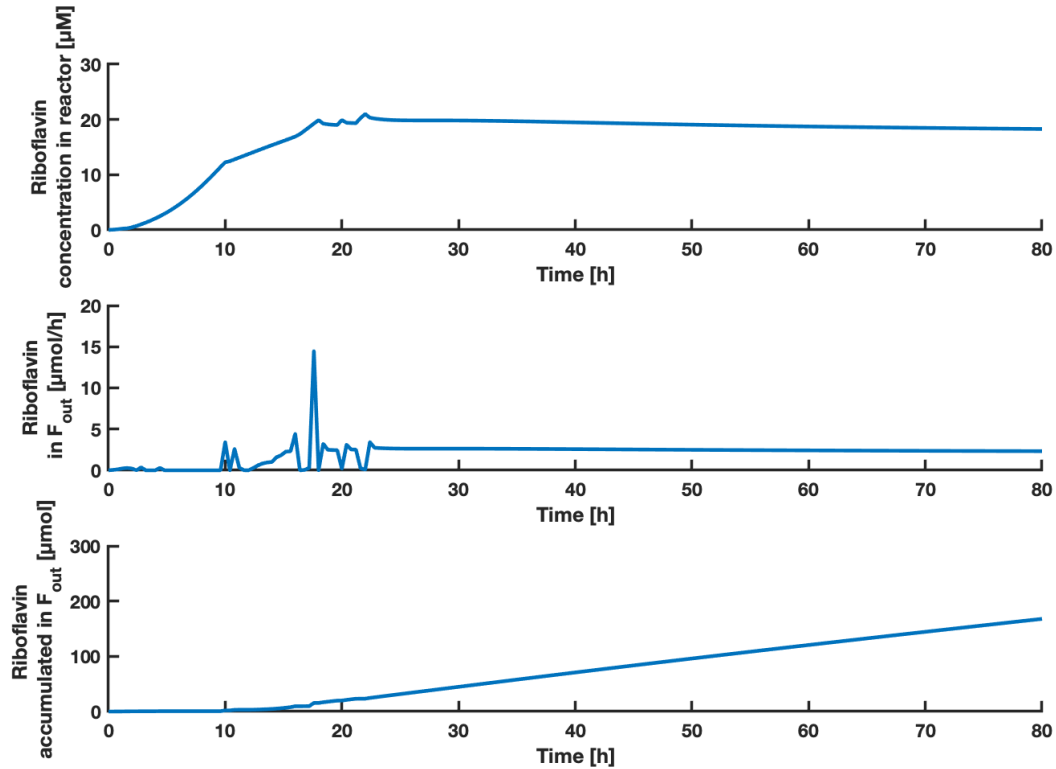


Figure 4.12: The upper plot shows the concentration of riboflavin as a function of time. The middle plot shows the amount of riboflavin in the F_{out} stream as a function of time. The lower plot shows the accumulated amount of riboflavin in the F_{out} stream as a function of time. The predicted states of riboflavin concentration in the reactor are a result of the inputs shown in Figure 4.10 using the objective function of Case A (described in Equation (3.7)). The $F_{SSL,in}$ had a lower constraint of 0 and an upper constraint of 1 L/h.

For Case A with a SSL stream of 0-1 L/h, the MPC predicted accumulated amounts of biomass, riboflavin and associated yields as shown in Table 4.2.

Table 4.2: The table shows the accumulated amounts of RiboGlu, RiboMan and RiboXyl strains, with associated biomass yield, X . The accumulated amount of the product riboflavin P , and the associated yield is shown. The values were calculated based on simulation results for Case A using 0-1 L/h SSL.

RiboGlu [g]	RiboMan [g]	RiboXyl [g]	X yield [g/g SSL]	P [µmol]	P yield [µg/g SSL]
11.40	161.5	41.50	0.1044	197.5	36.19

4.2.1.2 SSL with flow rate of 0.1 L/h

Figure 4.13, 4.14 and 4.15 shows the inputs, states and riboflavin results respectively obtained from MPC simulations using the objective function of Case A (Equation (3.7)) with a constant SSL flow rate of 0.1 L/h.

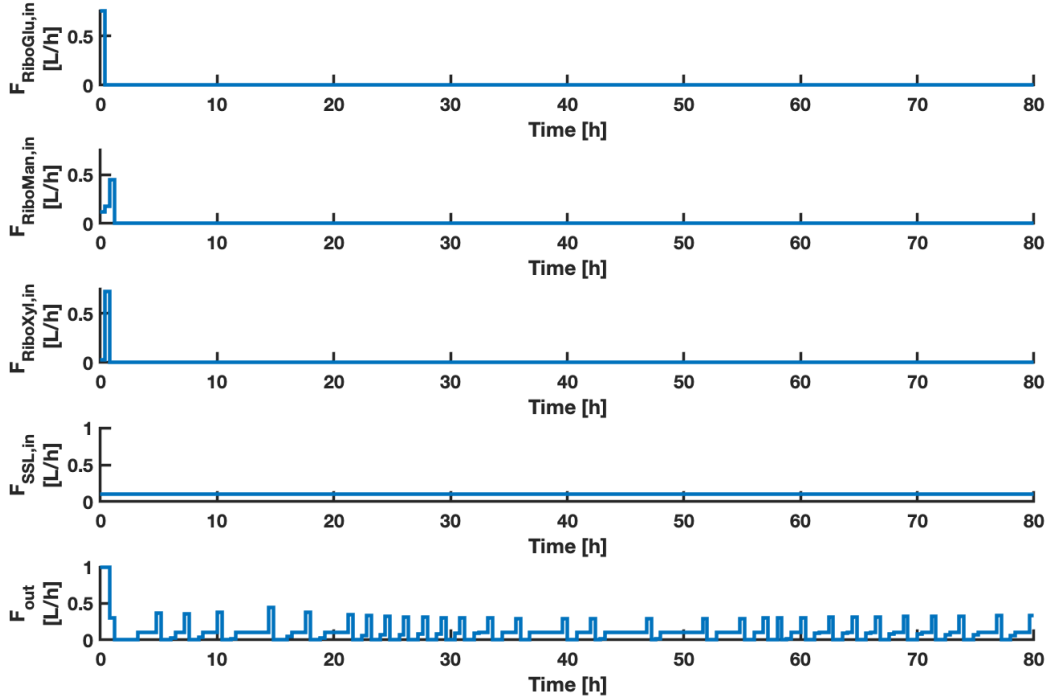


Figure 4.13: The plots shows the inputs $F_{RiboGlu,in}$, $F_{RiboMan,in}$, $F_{RiboXyl,in}$, $F_{SSL,in}$ and F_{out} as a function of time. The MPC inputs were calculated using the objective function of Case A (described in Equation (3.7)). The $F_{SSL,in}$ was set to 0.1 L/h.

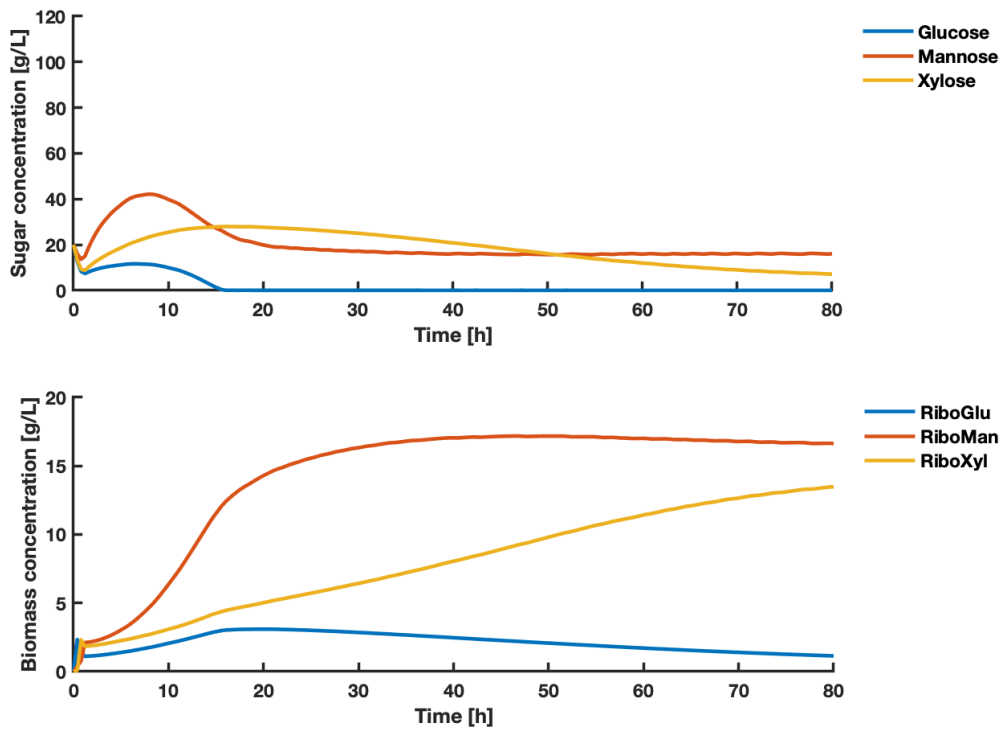


Figure 4.14: The upper plot shows the concentrations of the states glucose, mannose, xylose as a function of time. The lower plot shows the concentrations of states RiboGlu, RiboMan and RiboXyl as a function of time. The states are a result of the inputs shown in Figure 4.13. MPC states were calculated using the objective function of Case A (described in Equation (3.7)). The $F_{SSL,in}$ was set to 0.1 L/h.

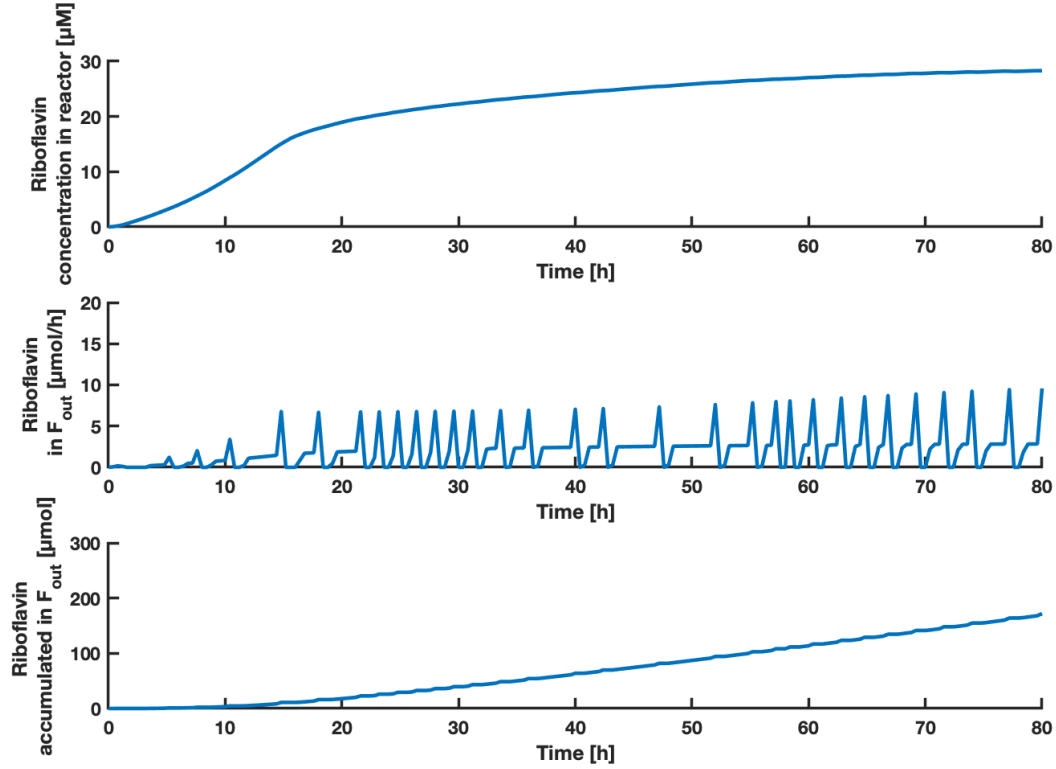


Figure 4.15: The upper plot shows the concentration of riboflavin as a function of time. The middle plot shows the amount of riboflavin in the F_{out} stream as a function of time. The lower plot shows the accumulated amount of riboflavin in the F_{out} stream as a function of time. The predicted states of riboflavin concentration in the reactor are a result of the inputs shown in Figure 4.13. MPC states were calculated using the objective function of Case A (described in Equation (3.7)). The $F_{SSL,in}$ was set to 0.1 L/h.

For Case A with a SSL stream of 0.1 L/h, the MPC predicted accumulated amounts of biomass, riboflavin and associated yields as shown in Table 4.3.

Table 4.3: The table shows the accumulated amounts of RiboGlu, RiboMan and RiboXyl strains, with associated biomass yield, X . The accumulated amount of the product riboflavin P , and the associated yield is shown. The values were calculated based on simulation results for Case A using 0.1 L/h SSL.

RiboGlu [g]	RiboMan [g]	RiboXyl [g]	X yield [g/g SSL]	P [μmol]	P yield [$\mu\text{g/g SSL}$]
18.23	116.08	66.017	0.1311	171.9	42.34

4.2.1.3 Comparison of Case A simulations

A constant SSL feed of 0.1 L/h, predicted higher biomass and riboflavin yields after 80 hours, compared to using the same SSL composition, but with a varying stream of 0-1 L/h. However by using the SSL stream of 0.1 L/h, after 200 iterations the MPC problem converged to a point of local infeasibility, probably due to the strict volume constraints combined with the rapid F_{out} steps. Since the problem was not solved, the results obtained by using a fixed stream are not representative for optimality.

As the objective function aims to maximize the biomass, once the SSL stream is more flexible, high flows of SSL are added in the start to increase the substrate available and hence the formation. The strict volume constraints of the main reactor is an obstacle. With the aim of increasing the biomass concentration of the main reactor, the MPC suggests to feed all of the biomass to the reactor simultaneously, and after approximately 2 hours all of the feed reactors have reached their minimum volume. To satisfy the maximum constraint of the main reactor, it starts pumping out liquid immediately as well. This high out-stream can be assumed to prevent the biomass growth, and hence the riboflavin production. The case using 0-1 L/h of SSL, uses approximately 20% more SSL than when using a constant stream of 0.1 L/h, which consequently reduces the yields.

Both versions used the maximum amount of all strains available, and due to the bad description of mannose consumption by the RiboMan strain, it can be assumed that the actual biomass- and riboflavin yield will be lower than predicted.

4.2.2 Case B: Maximize product in F_{out}

From the simulations using the objective function of maximizing product concentration in F_{out} (Equation (3.8)), the system was simulated under two different conditions when using real SSL: one with a variable feed stream and one with a fixed feed stream. This provided different results regarding biomass and product yields. The MPC simulation results of Case B can be graphically described by Figure 4.16 to 4.21. Results obtained using a variable feed stream of synthetic SSL, are attached in Appendix Section F.2. A comparison of the versions is presented in Subsection 4.2.2.3.

4.2.2.1 SSL with flow rate of 0-1 L/h

Figure 4.16, 4.17 and 4.18 shows the inputs, states and riboflavin results respectively obtained from MPC simulations using the objective function of Case B (Equation (3.8)) with a varying SSL flow rate in the range 0-1 L/h.

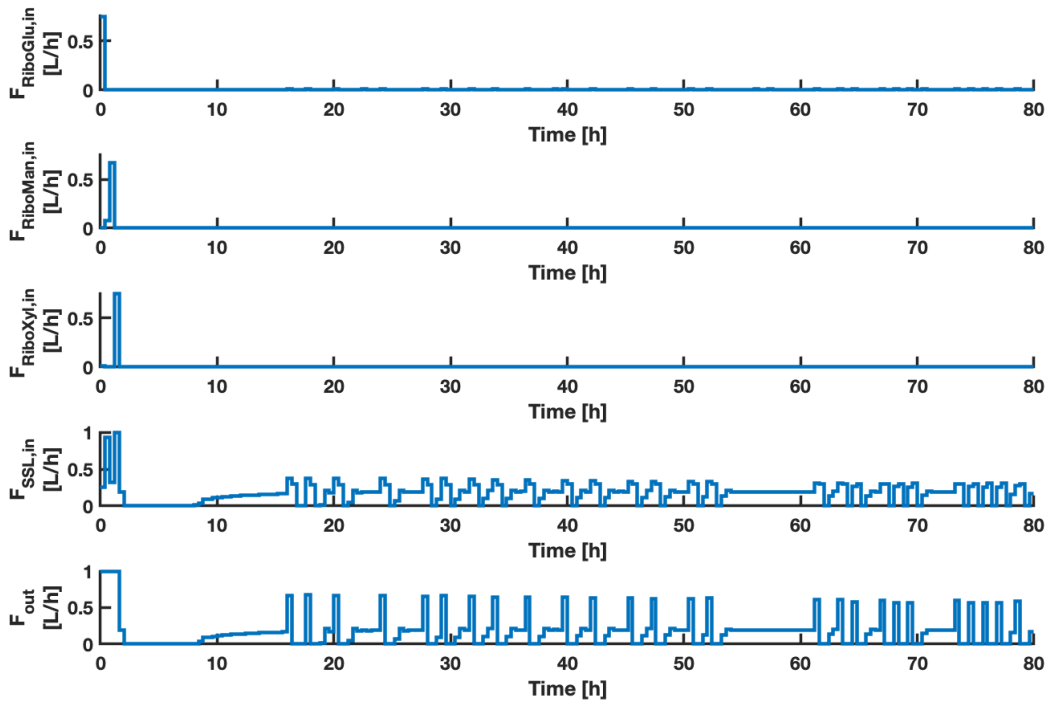


Figure 4.16: The plots shows the inputs $F_{RiboGlu,in}$, $F_{RiboMan,in}$, $F_{RiboXyl,in}$, $F_{SSL,in}$ and F_{out} as a function of time. The MPC inputs were calculated using the objective function of Case B (described in Equation (3.8)). The $F_{SSL,in}$ had a lower constraint of 0 and an upper constraint of 1 L/h.

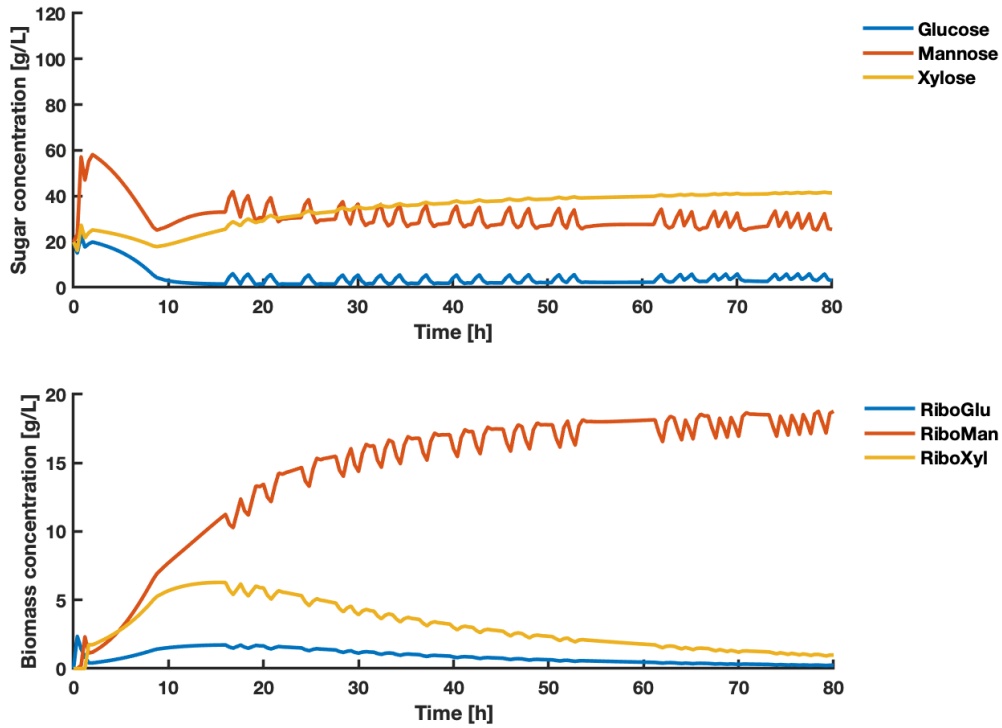


Figure 4.17: The upper plot shows the concentrations of the states glucose, mannose, xylose as a function of time. The lower plot shows the concentrations of states RiboGlu, RiboMan and RiboXyl as a function of time. The states are a result of the inputs shown in Figure 4.16. MPC states were calculated using the objective function of Case B (described in Equation (3.8)). The $F_{SSL,in}$ had a lower constraint of 0 and an upper constraint of 1 L/h.

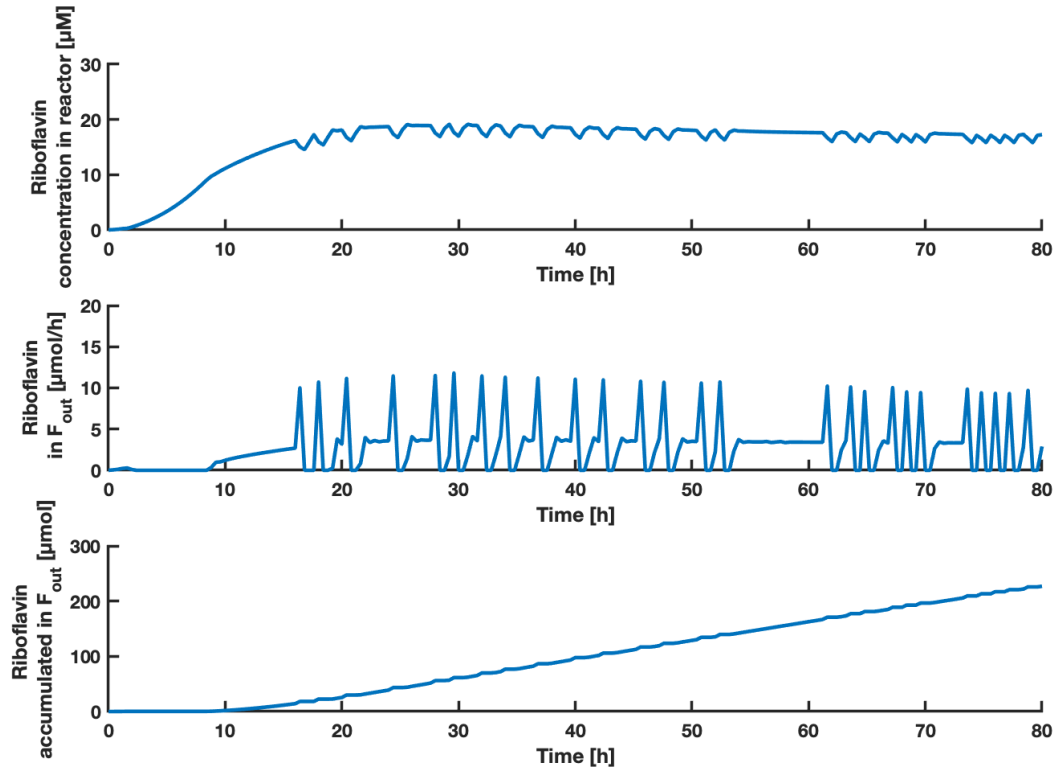


Figure 4.18: The upper plot shows the concentration of riboflavin as a function of time. The middle plot shows the amount of riboflavin in the F_{out} stream as a function of time. The lower plot shows the accumulated amount of riboflavin in the F_{out} stream as a function of time. The predicted states of riboflavin concentration in the reactor are a result of the inputs shown in Figure 4.16. MPC states were calculated using the objective function of Case B (described in Equation (3.8)). The $F_{SSL,in}$ had a lower constraint of 0 and an upper constraint of 1 L/h.

For Case B with a SSL stream of 0-1 L/h, the MPC predicted accumulated amounts of biomass, riboflavin and associated yields as shown in Table 4.4.

Table 4.4: The table shows the accumulated amounts of RiboGlu, RiboMan and RiboXyl strains, with associated biomass yield, X . The accumulated amount of the product riboflavin P , and the associated yield is shown. The values were calculated based on simulation results for Case B using 0-1 L/h SSL.

RiboGlu [g]	RiboMan [g]	RiboXyl [g]	X yield [g/g SSL]	P [μmol]	P yield [$\mu\text{g/g SSL}$]
13.21	212.3	41.36	0.0980	226.9	31.35

4.2.2.2 SSL with flow rate of 0.1 L/h

Figure 4.19, 4.20 and 4.21 shows the inputs, states and riboflavin results respectively obtained from MPC simulations using the objective function of Case B (Equation (3.8)) with a SSL flow rate of 0.1 L/h.

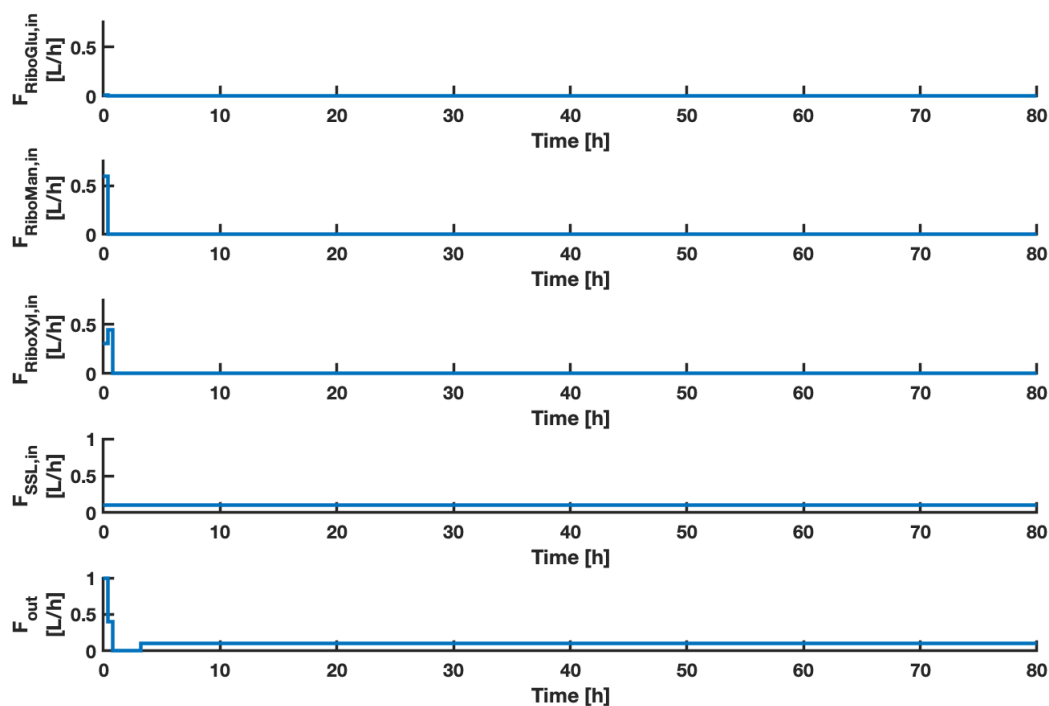


Figure 4.19: The plots shows the inputs $F_{RiboGlu,in}$, $F_{RiboMan,in}$, $F_{RiboXyl,in}$, $F_{SSL,in}$ and F_{out} as a function of time. The MPC inputs were calculated using the objective function of Case B (described in Equation (3.8)). The $F_{SSL,in}$ was set to 0.1 L/h.

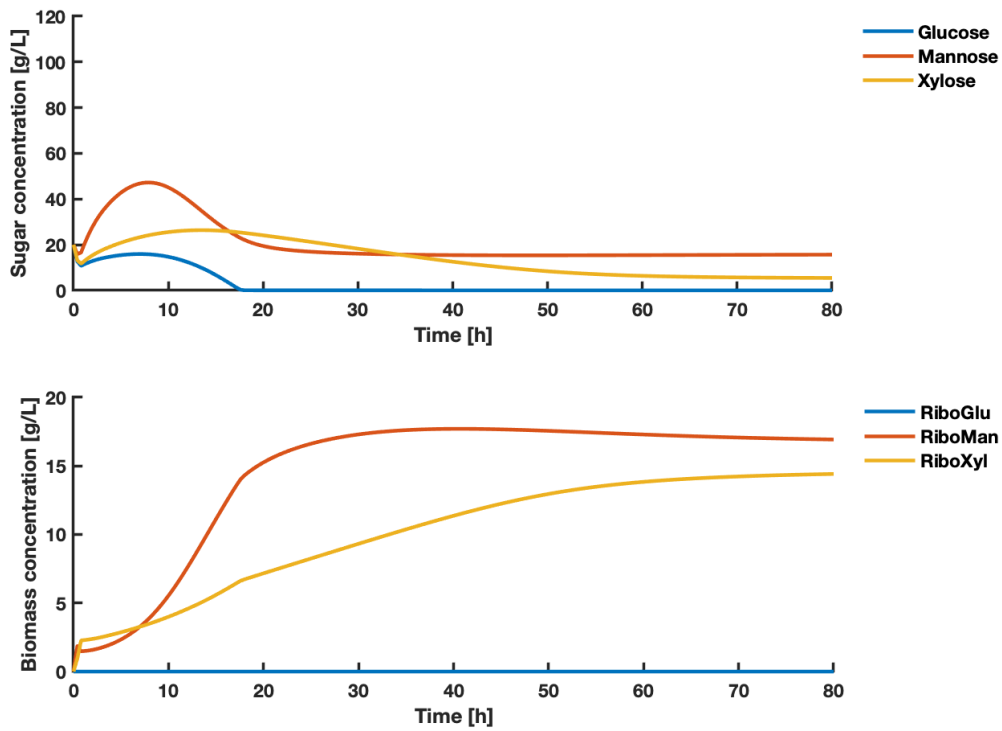


Figure 4.20: The upper plot shows the concentrations of the states glucose, mannose, xylose as a function of time. The lower plot shows the concentrations of states RiboGlu, RiboMan and RiboXyl as a function of time. The states are a result of the inputs shown in Figure 4.19. MPC states were calculated using the objective function of Case B (described in Equation (3.8)). The $F_{SSL,in}$ was set to 0.1 L/h.

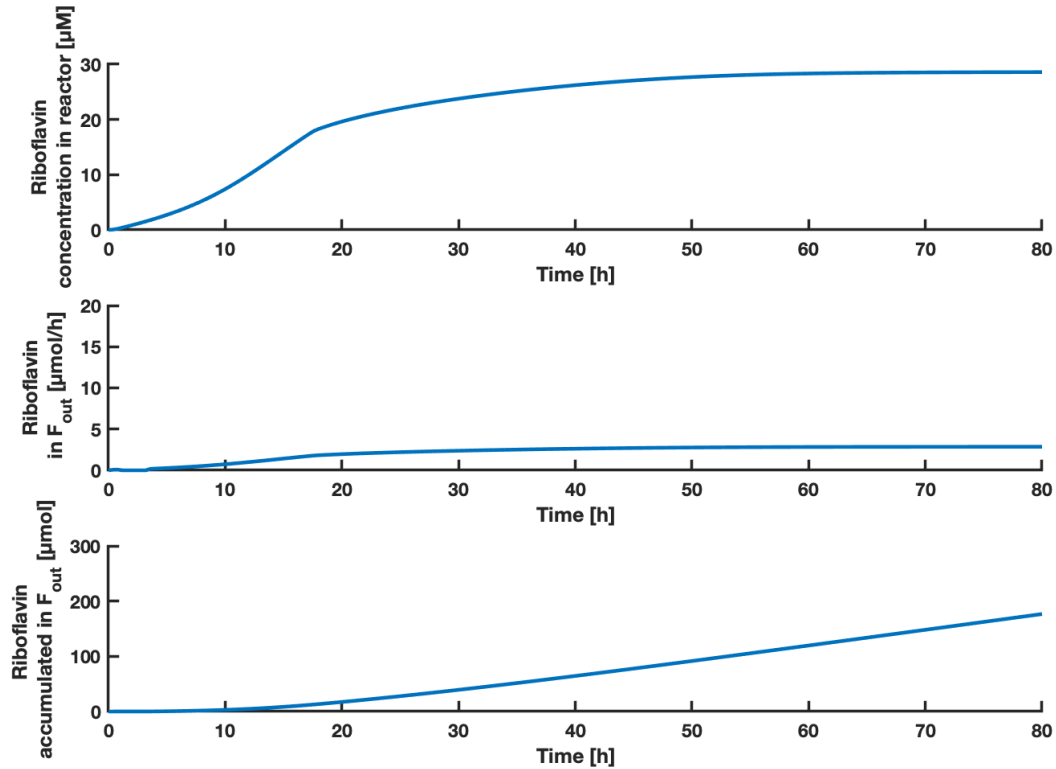


Figure 4.21: The upper plot shows the concentration of riboflavin as a function of time. The middle plot shows the amount of riboflavin in the F_{out} stream as a function of time. The lower plot shows the accumulated amount of riboflavin in the F_{out} stream as a function of time. The predicted states of riboflavin concentration in the reactor are a result of the inputs shown in Figure 4.19. MPC states were calculated using the objective function of Case B (described in Equation (3.8)). The $F_{SSL,in}$ was set to 0.1 L/h.

For Case B with a SSL stream of 0.1 L/h, the MPC predicted accumulated amounts of biomass, riboflavin and associated yields as shown in Table 4.5.

Table 4.5: The table shows the accumulated amounts of RiboGlu, RiboMan and RiboXyl strains, with associated biomass yield, X . The accumulated amount of the product riboflavin P , and the associated yield is shown. The values were calculated based on simulation results for Case B using 0.1 L/h SSL.

RiboGlu [g]	RiboMan [g]	RiboXyl [g]	X yield [g/g SSL]	P [µmol]	P yield [µg/g SSL]
0.00003	117.8	81.46	0.1304	176.6	43.49

4.2.2.3 Comparison of Case B simulations

In this case as well, using a constant SSL feed stream of 0.1 L/h, obtained the highest predicted accumulated riboflavin yield in the out stream after 80 hours, as well as the biomass yield when using real SSL. For this case, the MPC suggests almost no usage of the RiboGlu strain, and the feed of RiboMan strain is not reaching its maximum volume of 0.3 L. With the high concentration of mannose in the SSL, it makes sense that the *C. glutamicum* strains consuming mannose is fed at a high rate. Since the estimated RiboMan model shows an even better consumption of mannose than the experimental data showed, and regarding it providing a higher riboflavin titer than the RiboGlu strain, it makes sense that the RiboMan strain dominates over the RiboGlu strain. As the objective function aims to maximize the product multiplied with the out stream, the case with a varying stream of 0-1 L/h seems to increase the amount of sugars pumped into the reactor. When increasing the feed to the reactor, in order to satisfy the volume constraints of the main reactor, the solution is to increase the feed out as well. This case produces higher total amounts of biomass, at the cost of leaving more sugars unconsumed.

4.2.3 Case C: Maximize biomass yield

From the simulations using the objective function of maximizing the biomass yield (Equation (3.9)), the system was simulated under two different conditions when using real SSL: one with a variable feed stream and one with a fixed feed stream. This provided different results regarding biomass and product yields. The MPC simulation results of Case C can be graphically described by Figure 4.22 to 4.27. Results obtained using a variable feed stream of synthetic SSL, are attached in Appendix Section F.3. A comparison of the versions is presented in Subsection 4.2.3.3.

4.2.3.1 SSL with flow rate of 0-1 L/h

Figure 4.22, 4.23 and 4.24 shows the inputs, states and riboflavin results respectively obtained from MPC simulations using the objective function of Case C (Equation (3.9)) with a varying SSL flow rate in the range 0-1 L/h.

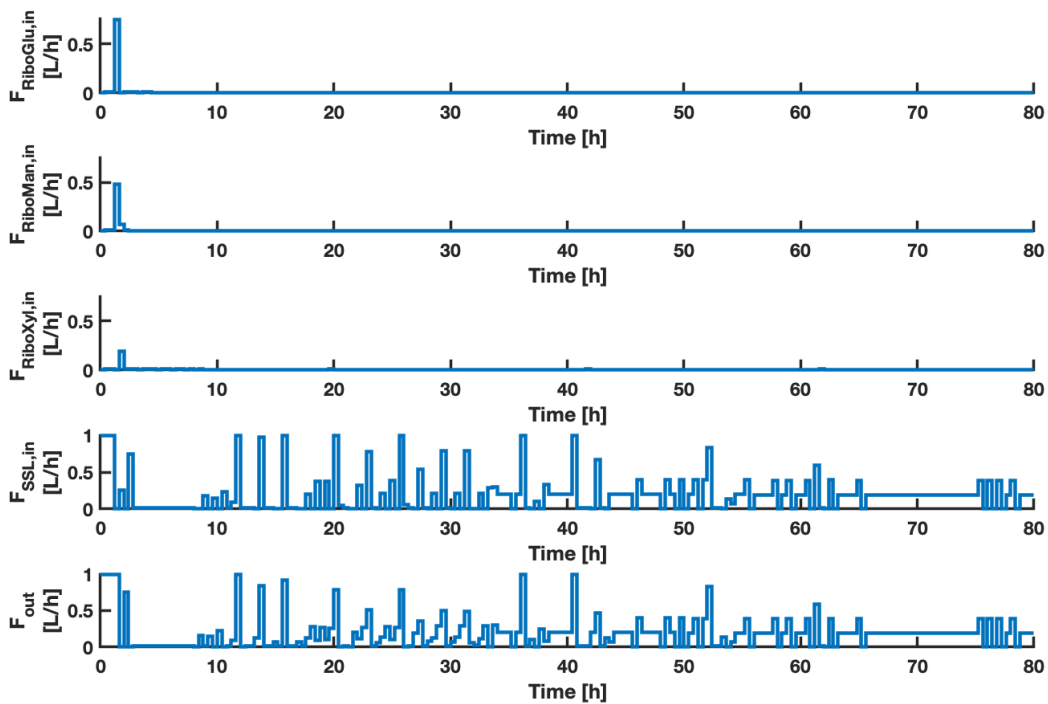


Figure 4.22: The plots shows the inputs $F_{RiboGlu,in}$, $F_{RiboMan,in}$, $F_{RiboXyl,in}$, $F_{SSL,in}$ and F_{out} as a function of time. The MPC inputs were calculated using the objective function of Case C (described in Equation (3.9)). The $F_{SSL,in}$ had a lower constraint of 0 and an upper constraint of 1 L/h.

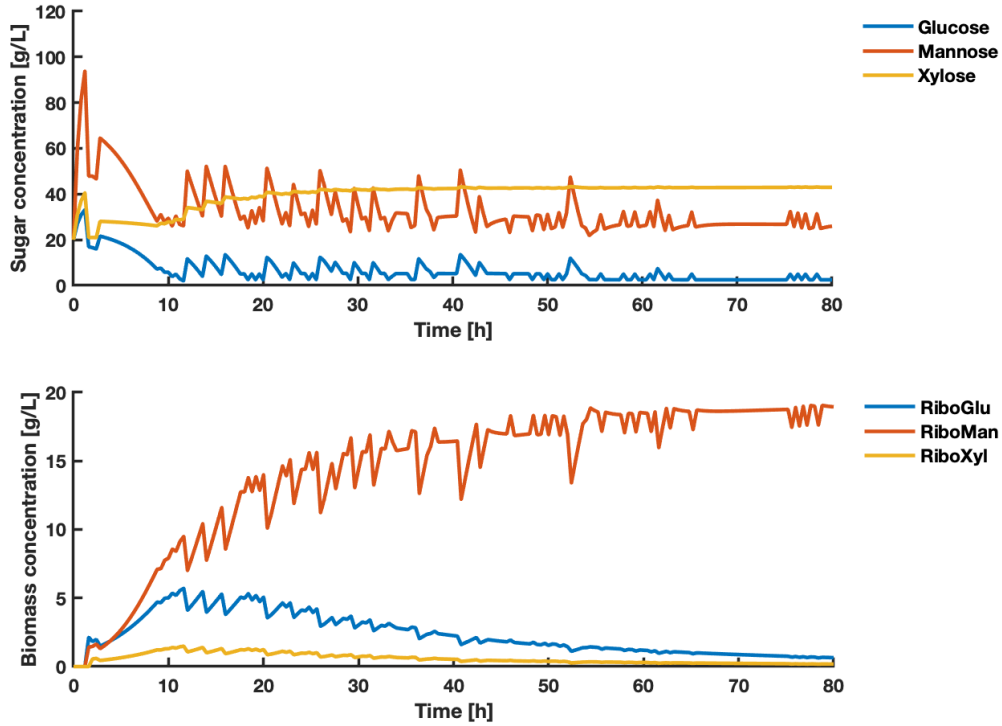


Figure 4.23: The upper plot shows the concentrations of the states glucose, mannose, xylose as a function of time. The lower plot shows the concentrations of states RiboGlu, RiboMan and RiboXyl as a function of time. The states are a result of the inputs shown in Figure 4.22. MPC states were calculated using the objective function of Case C (described in Equation (3.9)). The $F_{SSL,in}$ had a lower constraint of 0 and an upper constraint of 1 L/h.

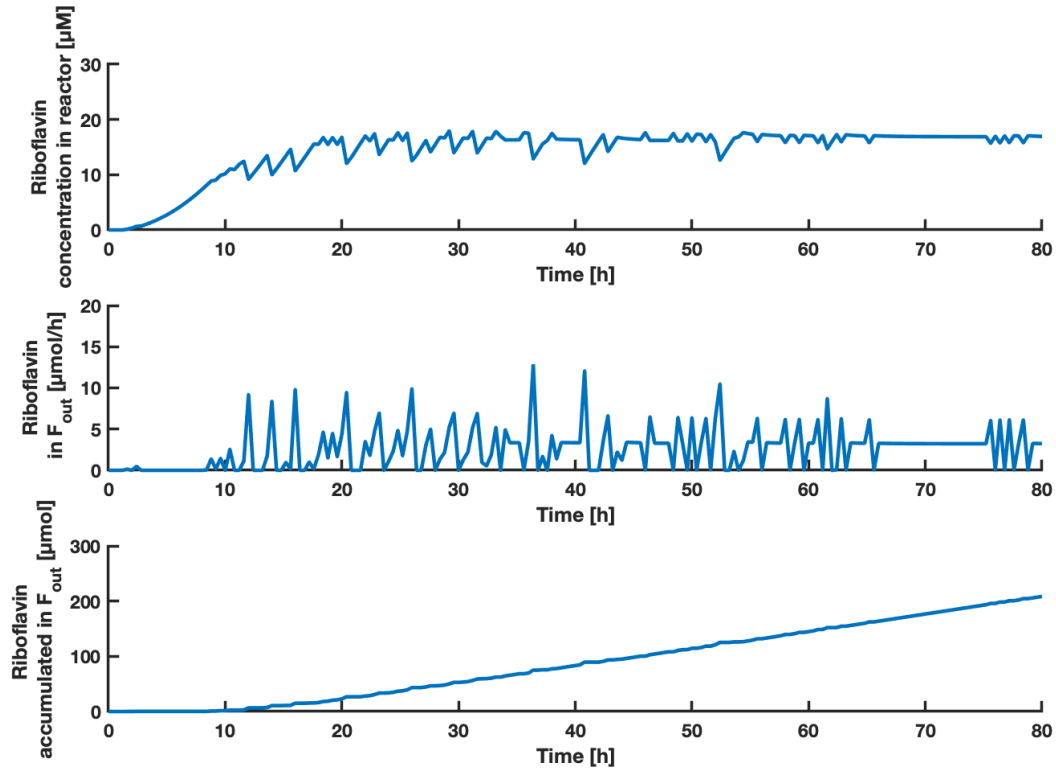


Figure 4.24: The upper plot shows the concentration of riboflavin as a function of time. The middle plot shows the amount of riboflavin in the F_{out} stream as a function of time. The lower plot shows the accumulated amount of riboflavin in the F_{out} stream as a function of time. The predicted states of riboflavin concentration in the reactor are a result of the inputs shown in Figure 4.22. MPC states were calculated using the objective function of Case C (described in Equation (3.9)). The $F_{SSL,in}$ had a lower constraint of 0 and an upper constraint of 1 L/h.

For Case C with a SSL stream of 0-1 L/h, the MPC predicted accumulated amounts of biomass, riboflavin and associated yields as shown in Table 4.6.

Table 4.6: The table shows the accumulated amounts of RiboGlu, RiboMan and RiboXyl strains, with associated biomass yield, X . The accumulated amount of the product riboflavin P , and the associated yield is shown. The values were calculated based on simulation results for Case C using 0-1 L/h SSL.

RiboGlu [g]	RiboMan [g]	RiboXyl [g]	X yield [g/g SSL]	P [μmol]	P yield [$\mu\text{g/g SSL}$]
31.67	210.3	7.565	0.08530	208.4	26.81

4.2.3.2 SSL with flow rate of 0.1 L/h

Figure 4.25, 4.26 and 4.27 shows the inputs, states and riboflavin results respectively obtained from MPC simulations using the objective function of Case C (Equation (3.9)) with a SSL flow rate of 0.1 L/h.

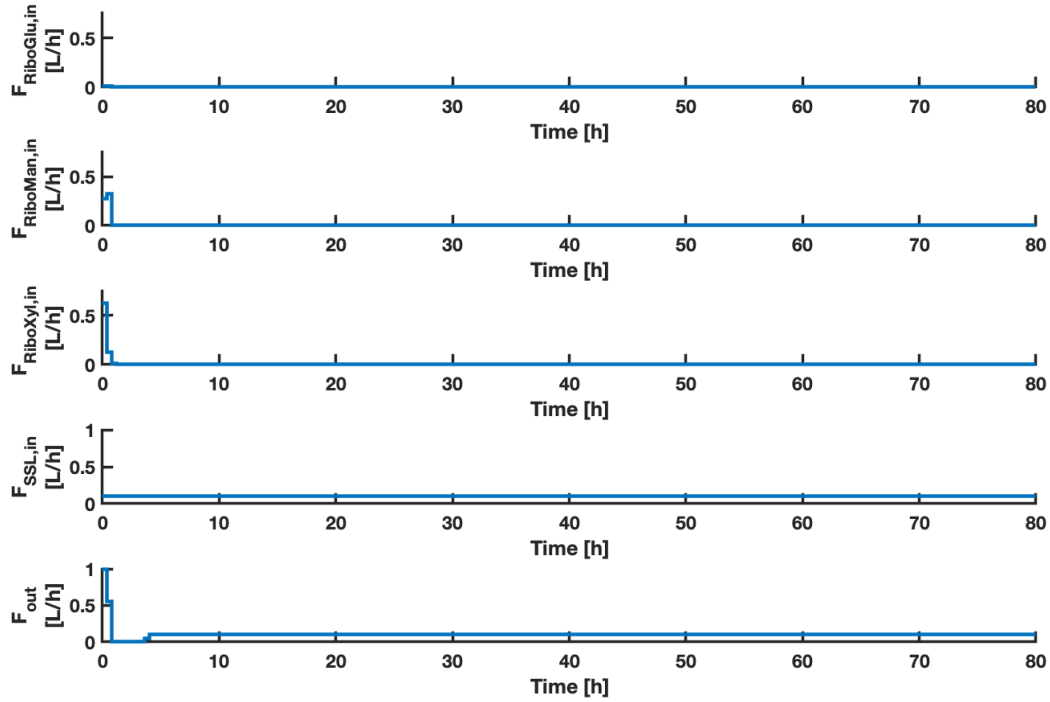


Figure 4.25: The plots shows the inputs $F_{RiboGlu,in}$, $F_{RiboMan,in}$, $F_{RiboXyl,in}$, $F_{SSL,in}$ and F_{out} as a function of time. The MPC inputs were calculated using the objective function of Case C (described in Equation (3.9)). The $F_{SSL,in}$ was set to 0.1 L/h.

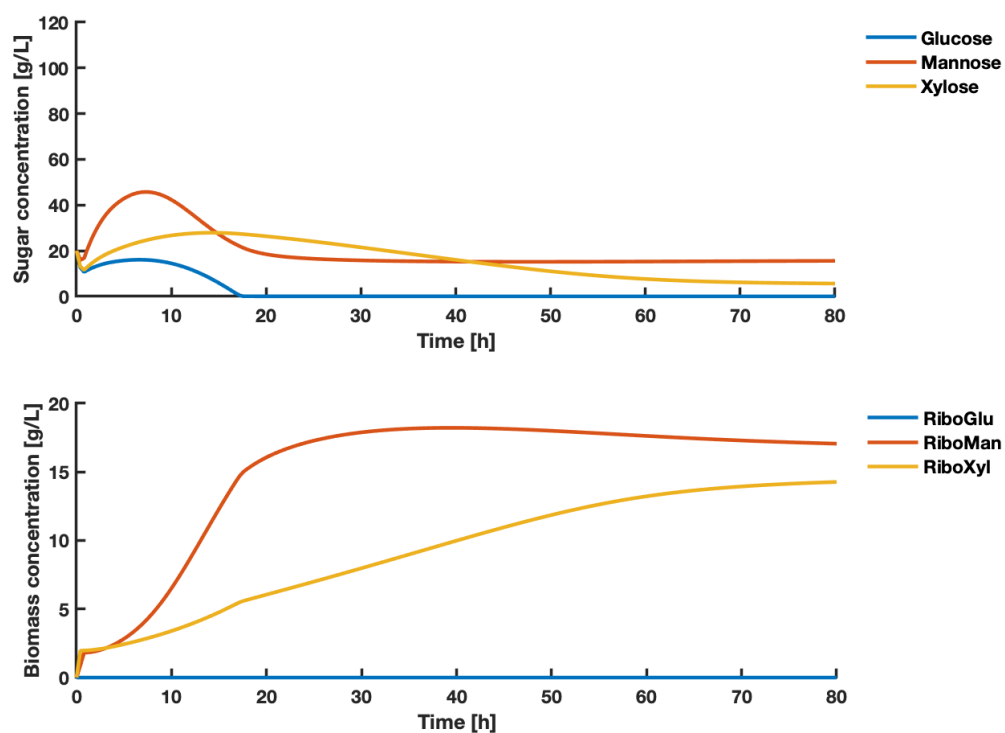


Figure 4.26: The upper plot shows the concentrations of the states glucose, mannose, xylose as a function of time. The lower plot shows the concentrations of states RiboGlu, RiboMan and RiboXyl as a function of time. The states are a result of the inputs shown in Figure 4.25. MPC states were calculated using the objective function of Case C (described in Equation (3.9)). The $F_{SSL,in}$ was set to 0.1 L/h.

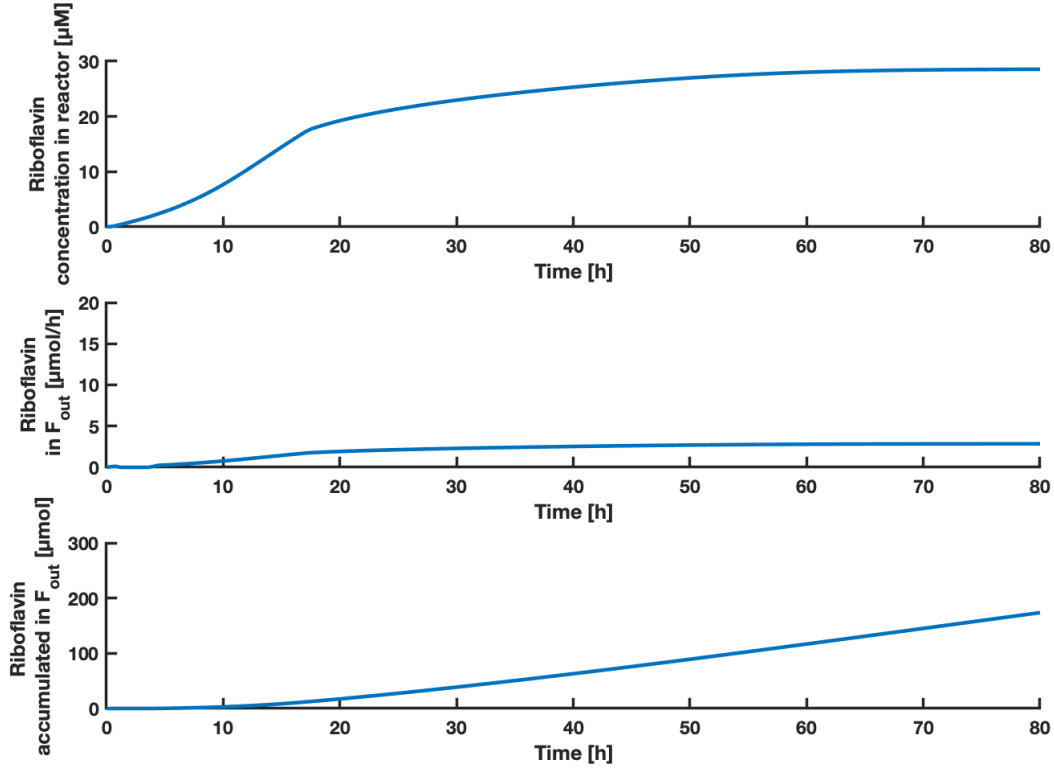


Figure 4.27: The upper plot shows the concentration of riboflavin as a function of time. The middle plot shows the amount of riboflavin in the F_{out} stream as a function of time. The lower plot shows the accumulated amount of riboflavin in the F_{out} stream as a function of time. The predicted states of riboflavin concentration in the reactor are a result of the inputs shown in Figure 4.25. MPC states were calculated using the objective function of Case C (described in Equation (3.9)). The $F_{SSL,in}$ was set to 0.1 L/h.

For Case C with a SSL stream of 0.1 L/h, the MPC predicted accumulated amounts of biomass, riboflavin and associated yields as shown in Table 4.7.

Table 4.7: The table shows the accumulated amounts of RiboGlu, RiboMan and RiboXyl strains, with associated biomass yield, X . The accumulated amount of the product riboflavin P , and the associated yield is shown. The values were calculated based on simulation results for Case C using 0.1 L/h SSL.

RiboGlu [g]	RiboMan [g]	RiboXyl [g]	X yield [g/g SSL]	P [μmol]	P yield [$\mu\text{g/g SSL}$]
0.03300	121.4	75.24	0.1287	173.6	42.77

4.2.3.3 Comparison of Case C simulations

Regarding biomass and riboflavin yields obtained, this version shows the same trend as Case A and Case B has showed. When using real SSL, a constant SSL stream of 0.1 L/h provides the highest yields. As the aim of this objective function was to maximize the biomass yield, it was assumed that this case would lead to higher yields than the other cases. When using a varying stream of 0-1 L/h real SSL however, it predicted the lowest biomass yield compared to the other cases (See Figure 4.35). This can be reflected through the high amount of SSL fed to the reactor (See Figure 4.37). Compared to Case A with the objective function of maximizing the biomass concentrations in the reactor, it was assumed that by replacing it with the biomass yield, the MPC using 0-1 L/h SSL would predict better yields. The MPC suggests to pump out high and rapid streams, in order to maximize the numerator term ($Biomass \cdot F_{out}$) of the yield expressions in the stage cost. To satisfy the volume constraints of the main reactor, high and rapid streams of SSL are pumped into the reactor as well, decreasing the yield results. For Case C, compared to Case A, not all of the biomass available from the feed reactors were used. A possible strategy to still satisfy the volume constraint of the main reactor could be to prioritize the biomass available from the feed reactors, before the high amounts of SSL were added. It can be concluded that the objective function of Case C was incorrectly formulated with the aim of maximizing the biomass yield.

4.2.4 Case D: Maximize product yield - linearized approximation

From the simulations using the objective function of maximizing product in F_{out} , while minimizing sugars from $F_{SSL,in}$ (Equation (3.10)), the system was simulated under two different conditions when using real SSL: one with a variable feed stream and one with a fixed feed stream. This provided different results regarding biomass and product yields. The MPC simulation results of Case D can be graphically described by Figure 4.28 to 4.33. Results obtained using a variable feed stream of synthetic SSL, are attached in Appendix Section F.4. A comparison of the versions is presented in Subsection 4.2.4.3.

4.2.4.1 SSL with flow rate of 0-1 L/h

Figure 4.28, 4.29 and 4.30 shows the inputs, states and riboflavin results respectively obtained from MPC simulations using the objective function of Case D (Equation (3.10)) with a varying SSL flow rate in the range 0-1 L/h.

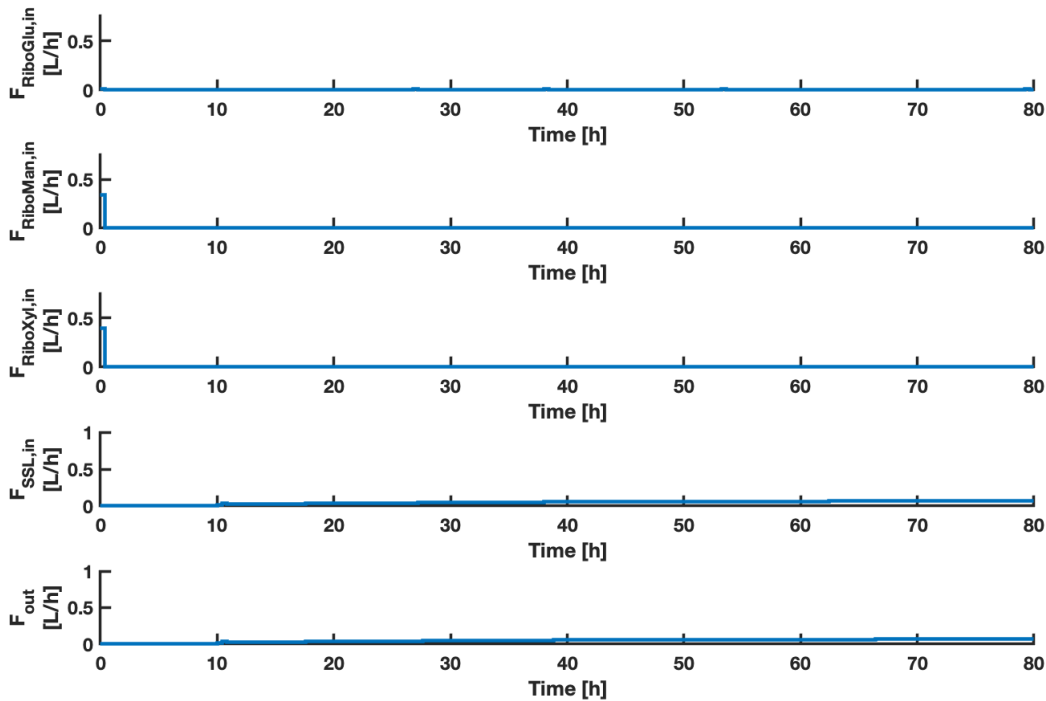


Figure 4.28: The plots shows the inputs $F_{RiboGlu,in}$, $F_{RiboMan,in}$, $F_{RiboXyl,in}$, $F_{SSL,in}$ and F_{out} as a function of time. The MPC inputs were calculated using the objective function of Case D (described in Equation (3.10)). The $F_{SSL,in}$ had a lower constraint of 0 and an upper constraint of 1 L/h.

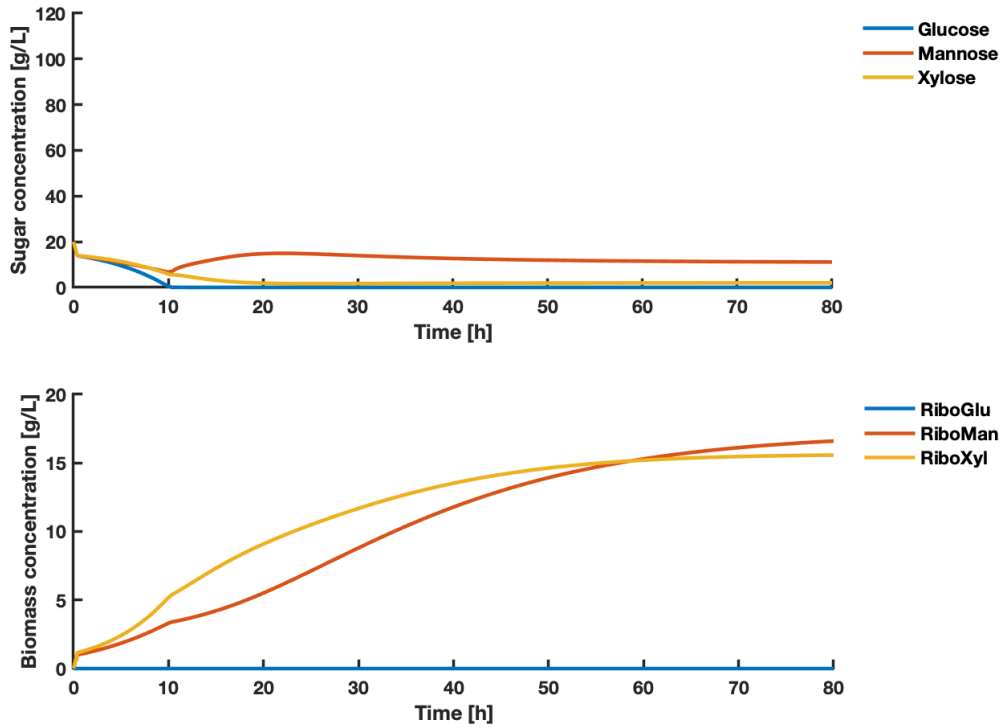


Figure 4.29: The upper plot shows the concentrations of the states glucose, mannose, xylose as a function of time. The lower plot shows the concentrations of states RiboGlu, RiboMan and RiboXyl as a function of time. The states are a result of the inputs shown in Figure 4.28. MPC states were calculated using the objective function of Case D (described in Equation (3.10)). The $F_{SSL,in}$ had a lower constraint of 0 and an upper constraint of 1 L/h.

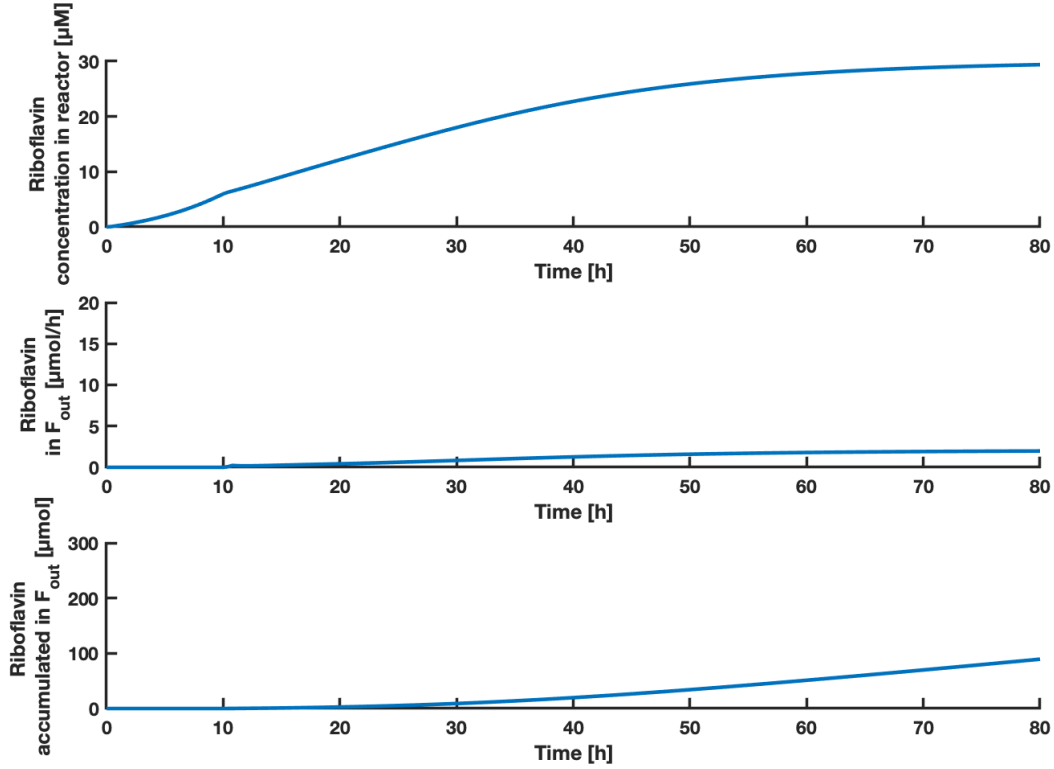


Figure 4.30: The upper plot shows the concentration of riboflavin as a function of time. The middle plot shows the amount of riboflavin in the F_{out} stream as a function of time. The lower plot shows the accumulated amount of riboflavin in the F_{out} stream as a function of time. The predicted states of riboflavin concentration in the reactor are a result of the inputs shown in Figure 4.28. MPC states were calculated using the objective function of Case D (described in Equation (3.10)). The $F_{SSL,in}$ had a lower constraint of 0 and an upper constraint of 1 L/h.

For Case D with a SSL stream of 0-1 L/h, the MPC predicted accumulated amounts of biomass, riboflavin and associated yields as shown in Table 4.8.

Table 4.8: The table shows the accumulated amounts of RiboGlu, RiboMan and RiboXyl strains, with associated biomass yield, X . The accumulated amount of the product riboflavin P , and the associated yield is shown. The values were calculated based on simulation results for Case D using 0-1 L/h SSL.

RiboGlu [g]	RiboMan [g]	RiboXyl [g]	X yield [g/g SSL]	P [μmol]	P yield [μg/g SSL]
0.0001	47.92	51.35	0.1380	89.35	46.75

4.2.4.2 SSL with flow rate of 0.1 L/h

Figure 4.31, 4.32 and 4.33 shows the inputs, states and riboflavin results respectively obtained from MPC simulations using the objective function of Case D (Equation (3.10)) with a SSL flow rate of 0.1 L/h.

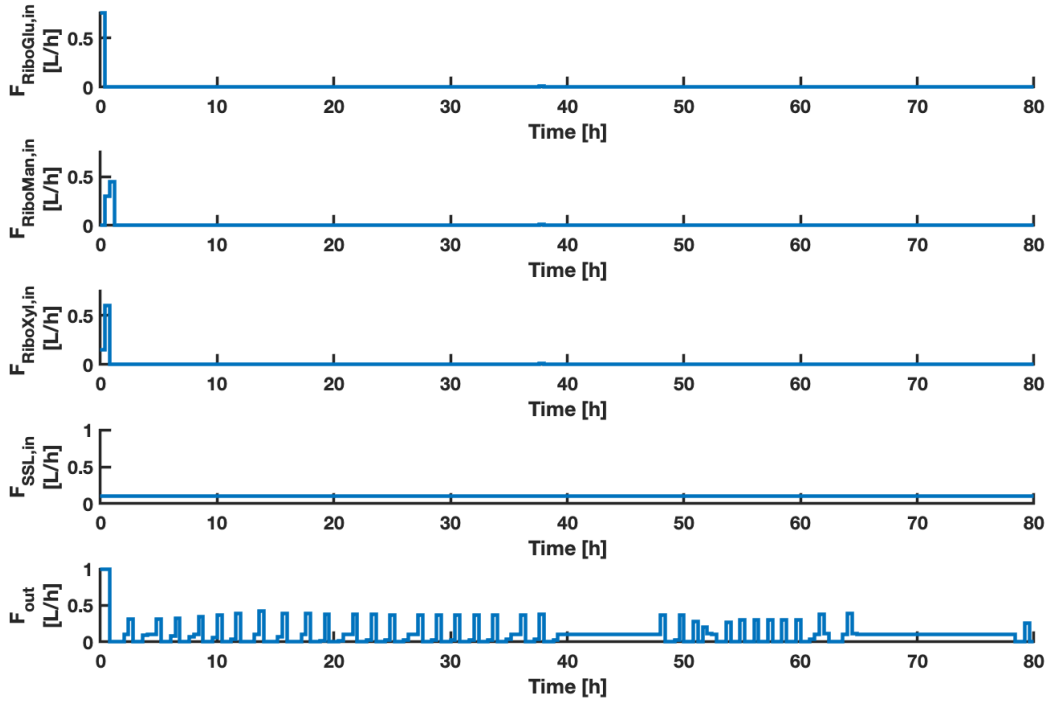


Figure 4.31: The plots shows the inputs $F_{RiboGlu,in}$, $F_{RiboMan,in}$, $F_{RiboXyl,in}$, $F_{SSL,in}$ and F_{out} as a function of time. The MPC inputs were calculated using the objective function of Case D (described in Equation (3.10)). The $F_{SSL,in}$ was set to 0.1 L/h.

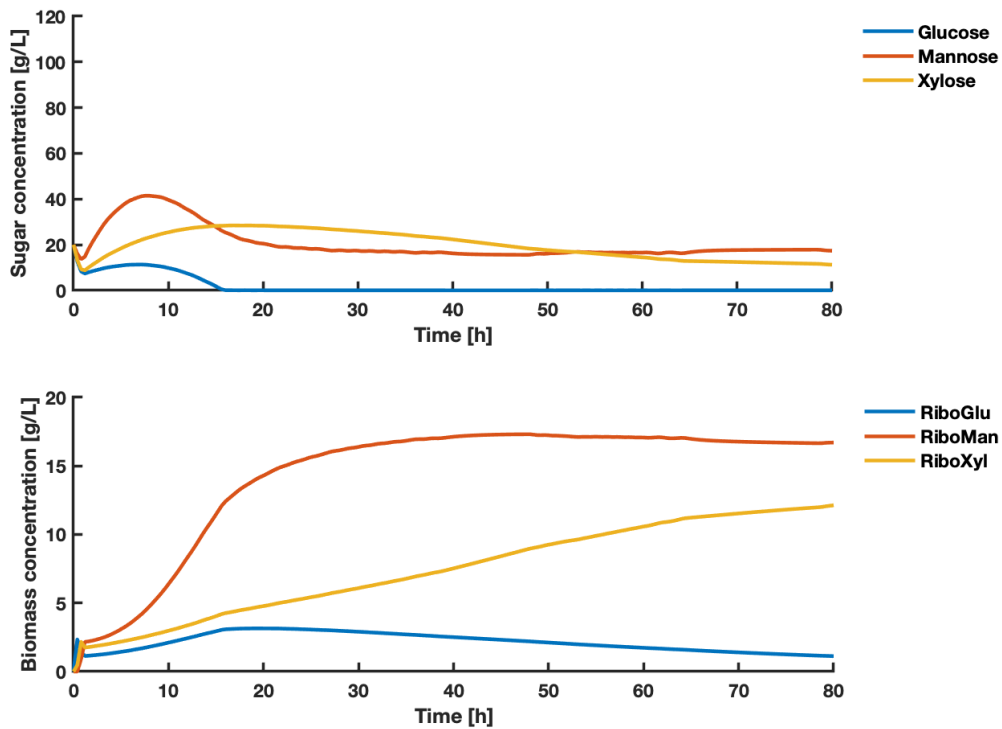


Figure 4.32: The upper plot shows the concentrations of the states glucose, mannose, xylose as a function of time. The lower plot shows the concentrations of states RiboGlu, RiboMan and RiboXyl as a function of time. The states are a result of the inputs shown in Figure 4.31. MPC states were calculated using the objective function of Case D (described in Equation (3.10)). The $F_{SSL,in}$ was set to 0.1 L/h.

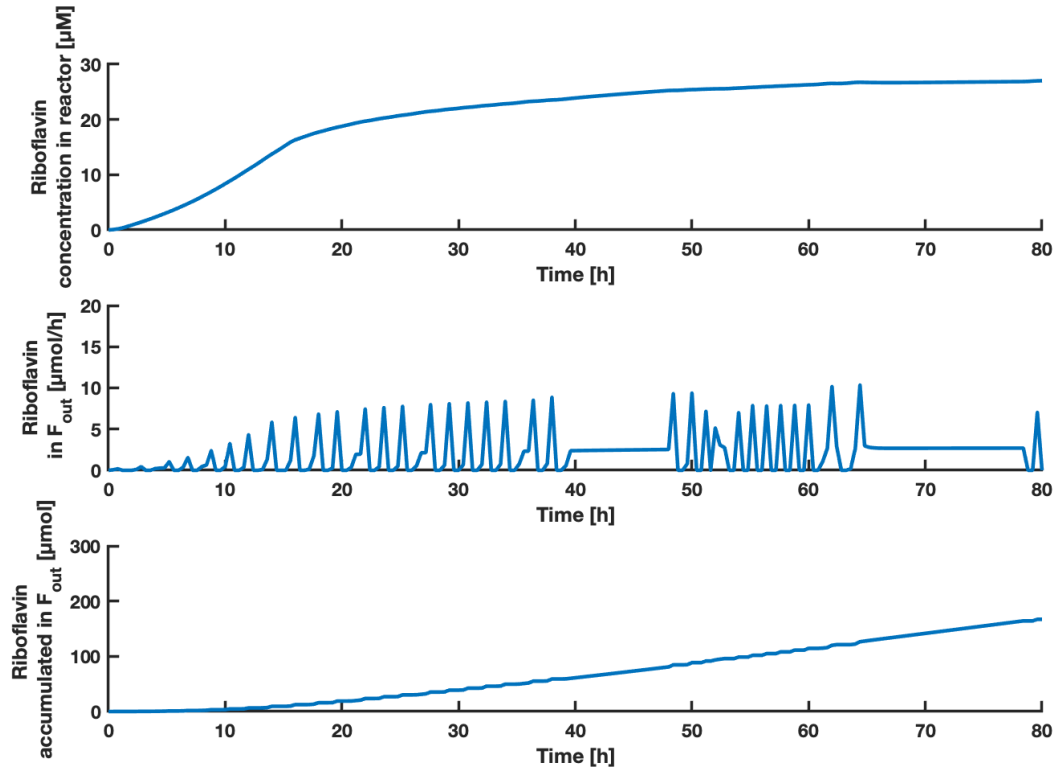


Figure 4.33: The upper plot shows the concentration of riboflavin as a function of time. The middle plot shows the amount of riboflavin in the F_{out} stream as a function of time. The lower plot shows the accumulated amount of riboflavin in the F_{out} stream as a function of time. The predicted states of riboflavin concentration in the reactor are a result of the inputs shown in Figure 4.31. MPC states were calculated using the objective function of Case D (described in Equation (3.10)). The $F_{SSL,in}$ was set to 0.1 L/h.

For Case D with a SSL stream of 0.1 L/h, the MPC predicted accumulated amounts of biomass, riboflavin and associated yields as shown in Table 4.9.

Table 4.9: The table shows the accumulated amounts of RiboGlu, RiboMan and RiboXyl strains, with associated biomass yield, X . The accumulated amount of the product riboflavin P , and the associated yield is shown. The values were calculated based on simulation results for Case D using 0.1 L/h SSL.

RiboGlu [g]	RiboMan [g]	RiboXyl [g]	X yield [g/g SSL]	P [μmol]	P yield [μg/g SSL]
18.52	115.7	61.00	0.1278	167.0	41.12

4.2.4.3 Comparison of Case D simulations

The MPC simulation results of Case D using a linear approximation of product yield predicted results with a different trend than previously observed. The version using 0-1 L/h SSL obtained higher yields than with a constant stream of 0.1 L/h SSL. The version using 0-1 L/h of real SSL in fact predicts a biomass yield of 0.138 g/g SSL - higher than all other cases when using real SSL. From Figure 4.37 it can be seen that this version uses the lowest amount of real SSL, resulting in higher yields. It does not start pumping in SSL until after approximately 10 hours, and with a continuous feed between 0.018 and 0.067 L/h. The feed out is consequently within the same interval. In this case, a negligible amount of the RiboGlu strain is fed into the reactor, but as the other strains consume glucose as well, the biomass formation of the other strains is still higher. The formation of the RiboXyl strain in this case is better than for all other cases. This may also cause the higher riboflavin yield obtained. From the experimental data and the estimated RiboXyl model in Figure 4.9, it was showed that the RiboXyl strain produces a higher titer of riboflavin when growing on synthetic SSL. RiboGlu however produces the lowest titer (Figure 4.3). With the aim of maximizing the product, it makes sense to rather utilize the RiboMan and RiboXyl strain, than the RiboGlu strain. For the case using 0.1 L/h SSL, the outcome of the states depicted in Figure 4.32 had a similar behaviour as for Case A with the same conditions (Figure 4.14). The inputs after approximately 40 hours differs, where Case D avoids the rapid inputs, and suggests periods of continuous feed out. This may be a reason for the problem being solved, compared to for Case A where the problem may have been infeasible.

4.2.5 Summary of simulation results

A summary of results obtained from the different simulations are presented in this section, to compare the results from the different cases. The results includes final accumulated amount of riboflavin and biomass produced, corresponding yields, amount of biomass and sugar used to feed the main reactor. In this section the key results obtained when using synthetic SSL are included as well (the simulation results are attached in Section F).

4.2.5.1 Riboflavin production

Figure 4.34 shows the final accumulated amount of riboflavin in the F_{out} stream predicted after 80 hours for the different cases, and the riboflavin yield obtained.

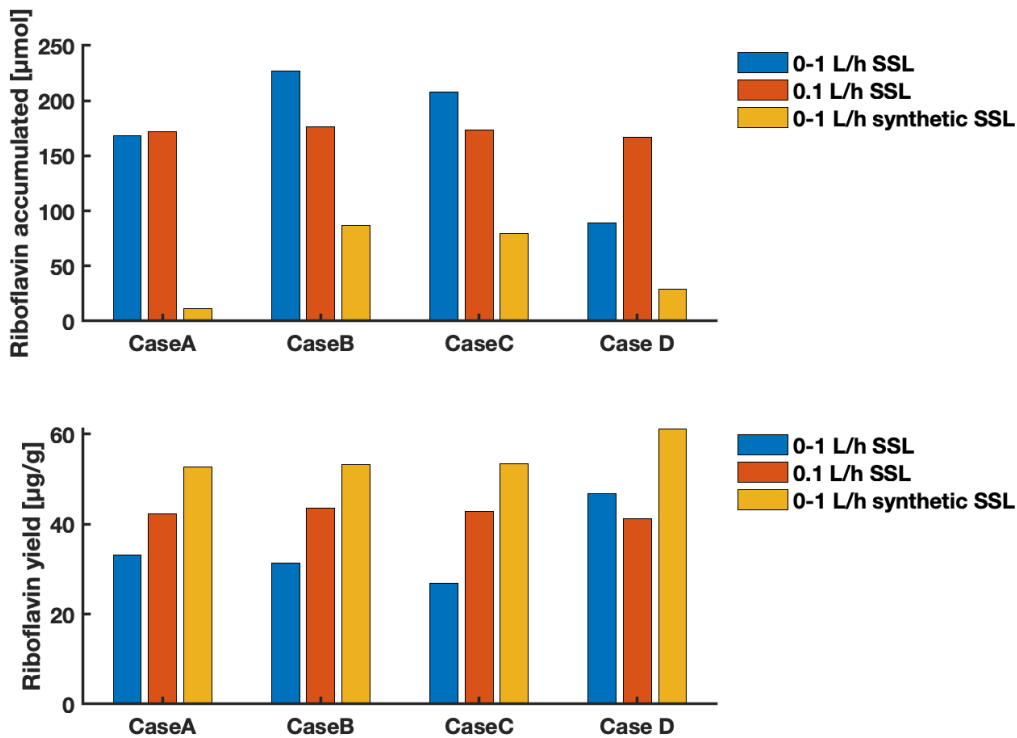


Figure 4.34: The upper plot shows the final accumulated amount of riboflavin in the F_{out} stream predicted after 80 hours for the different cases presented in Equation (3.7) to (3.10). The lower plot shows the yield of riboflavin in $\mu\text{g/g}$ sugars obtained after 80 hours. Both plots shows the results obtained using 0-1 L/h SSL (blue bars), 0.1 L/h SSL (orange bars) and 0-1 L/h synthetic SSL (yellow bars).

For all cases the predicted riboflavin yields after 80 hours are highest when using 0-1 L/h of synthetic SSL. This shows the importance of the sugar composition, not only

the sugar concentration. With the exception of Case D, there is also a trend of varying flow of real SSL leading to the lowest riboflavin yield. The highest predicted riboflavin yield overall is obtained by using the objective function of Case D (linear approximation of maximizing riboflavin yield) with synthetic SSL. The riboflavin results obtained are suspected to have the highest uncertainty, due to the difficulties of an accurate model for describing the product formation. The models of all the strains describing the product formation usually predicts lower concentrations of riboflavin, than the experimental data showed - except for when growing on synthetic SSL. It is therefore a possibility that the actual riboflavin concentrations in reality could become higher.

4.2.5.2 Biomass formation

Figure 4.35 shows the final accumulated amount of biomass in the F_{out} stream predicted after 80 hours for the different cases, and the biomass yield obtained.

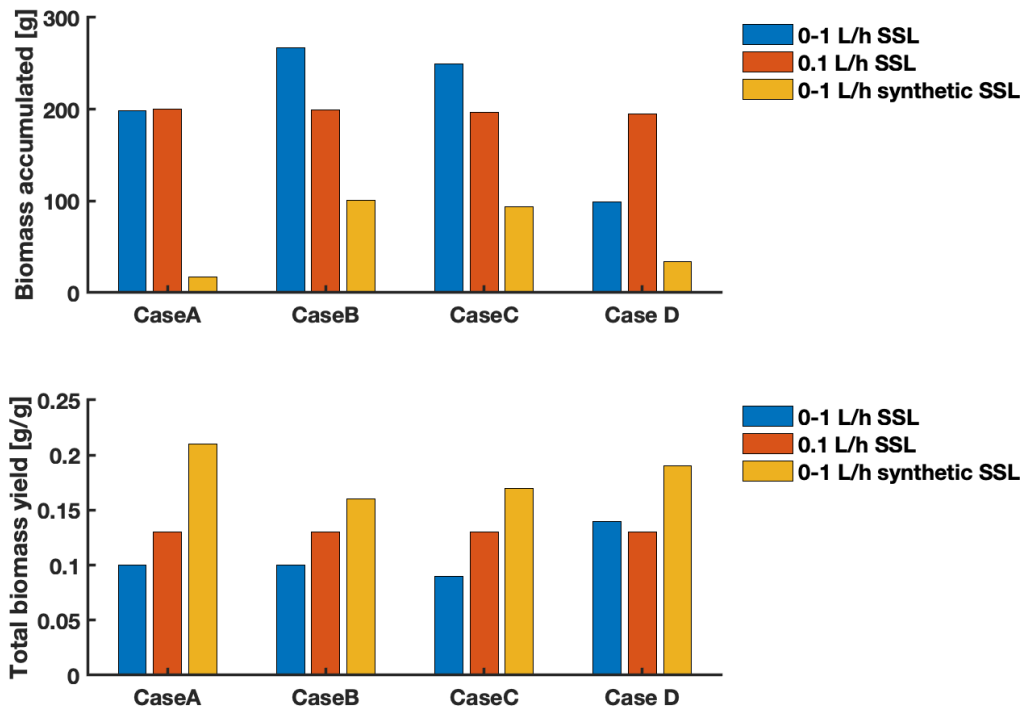


Figure 4.35: The upper plot shows the final accumulated amount of biomass in the F_{out} stream predicted after 80 hours for the different cases presented in Equation (3.7) to (3.10). The lower plot shows the biomass yield in g/g sugars predicted after 80 hours. The plot shows the results obtained using 0-1 L/h SSL (blue bars), 0.1 L/h SSL (orange bars) and 0-1 L/h synthetic SSL (yellow bars).

Figure 4.36 shows the predicted volumes of biomass used from the three feeding reactors of the RiboGlu, RiboMan and RiboXyl strains for the different cases.

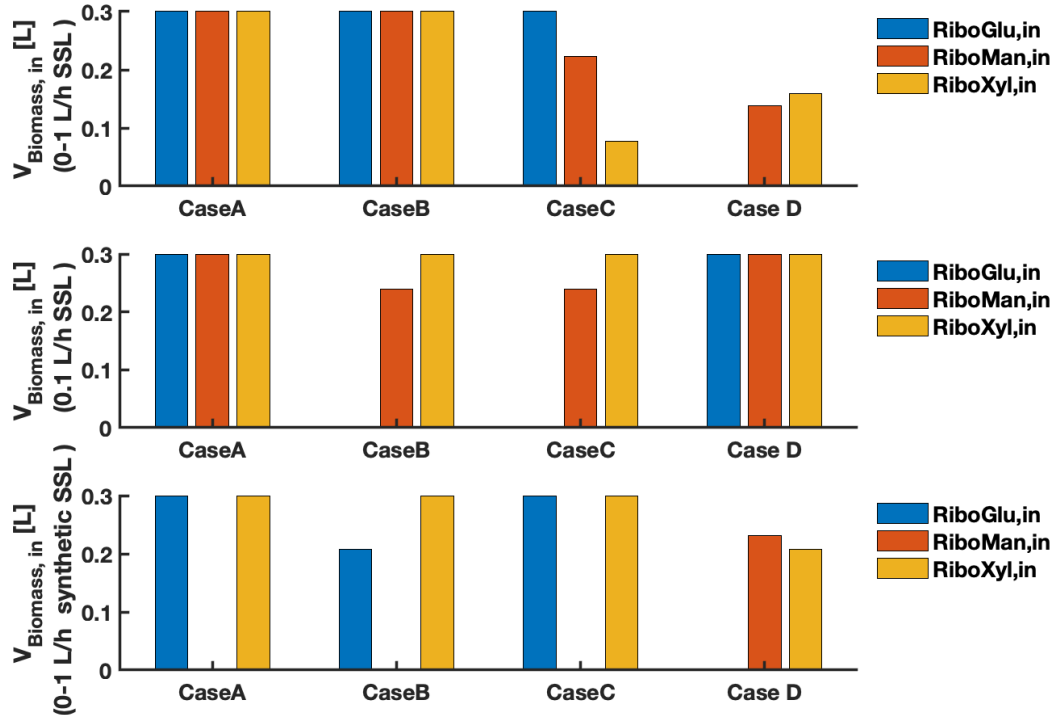


Figure 4.36: The plots shows the volume of biomass used to feed the main reactor for the different cases presented in Equation (3.7) to (3.10). The blue, orange and yellow bars represents the volume of the RiboGlu, RiboMan, and RiboXyl strain respectively fed into the main reactor. The upper plot shows the results obtained using 0-1 L/h SSL, the middle plot shows the results obtained using 0.1 L/h SSL, and the lower plot shows the results obtained using 0-1 L/h synthetic SSL.

The aim of this thesis was to optimize the biomass formation of *C. glutamicum* strains when growing on SSL-sugars. Therefore the biomass yields depicted in Figure 4.35 were considered important when analyzing the MPC simulation results. The models estimated for the different strains showed a good fit with the experimental data regarding biomass formation, which contributed to the assumption of more reliable results (compared to riboflavin yields). However since the biomass and riboflavin concentrations are modeled to be proportional, the biomass yields generally shows the same trends as the riboflavin yields presented in Figure 4.34. The exception is that the highest predicted biomass yield was obtained by using the objective function of Case A (maximize biomass concentration)

with synthetic SSL. This case utilizes more biomass, compared to Case D with the higher riboflavin yield. As mentioned in Section 4.2.3.3, it was assumed that Case C (maximize biomass yield) would obtain the highest biomass yield, but in this case almost 7 times as much synthetic SSL was used (See Figure 4.37). A linear approximation of Case C was performed, as the objective function was formulated incorrectly (See Appendix Section H). The simulation results were approximately equal to the results obtained from Case D, as the biomass and product formation are modeled to be proportional.

From Figure 4.36 the lower plot shows the biomass used when 0-1 L/h synthetic SSL was used. The usage of synthetic SSL predicted the highest biomass yields, and a common feature observed is that practically only two of the strains were being fed to the reactor when using synthetic SSL. The usage of only two strains was also a feature of Case D when using 0-1 real SSL - which was the case obtaining the highest biomass yield when using real SSL. Case C using 0-1 L/h SSL obtained the lowest biomass yield. It is also the case using the least of the RiboXyl strain, which was the strain experimentally achieving the highest biomass concentrations when growing on synthetic SSL. The middle plot of Figure 4.36 shows the biomass utilized when 0.1 L/h SSL was used. For Case A and Case D, all three strains are used. The biomass yields obtained when using 0.1 L/h SSL are similar, but as mentioned in the discussion of Case A (Section 4.2.1.3), the MPC algorithm did not find an optimal solution to the problem. A hypothesis could be that the combination of strict feed constraints, and the use of all three strains made the problem more difficult to solve, and a reduction to two strains could improve the converging.

4.2.5.3 Sugar usage

Figure 4.37 shows the amount of sugars fed into the reactor for the different cases after 80 hours.

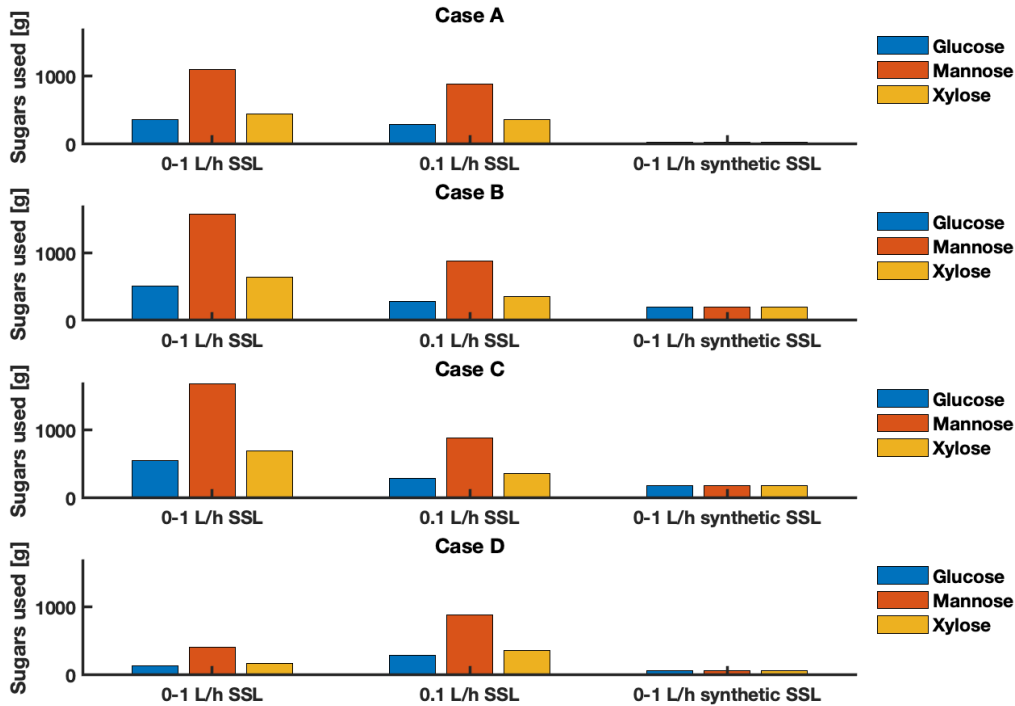


Figure 4.37: The plot shows the final amount of sugars used, predicted after 80 hours for the different cases presented in Equation (3.7) to (3.10). The blue, orange and yellow bars represents the amount of glucose, mannose and xylose respectively fed into the main reactor. From the top, Case A to D are presented.

As Figure 4.37 shows, when the SSL stream is flexible, there is a variation of the amount of sugars used. This affected the predicted yields. The use of synthetic SSL in general predicted high yields, a consequence of a the significant low utilization of sugars, leading to a low production rate. It can be observed that Case B uses approximately 30 % more SSL than Case A with a variable feed stream. Still the biomass yields depicted in Figure 4.35 shows similar yields achieved. Hence not only the amount of substrate used in total is of importance, the size and quantity of streams in and out of the reactor matters as well.

4.3 MPC simulation results of simplified system

This section presents the MPC simulation results from the simplified system described in Figure 3.2. This was the MPC that was implemented to the laboratory, to compare the performance of the MPC on the real system with that of the simulations. The OCP had the time horizon, number of control intervals and number of collocation points outlined in Table 3.7. The constraints are presented in Table 3.8 and 3.9. Synthetic SSL was used as carbon source (composition is described in Table 3.6). The system was simulated for 24 hours. Figure 4.38 to 4.40 shows the results obtained after 24 hours.

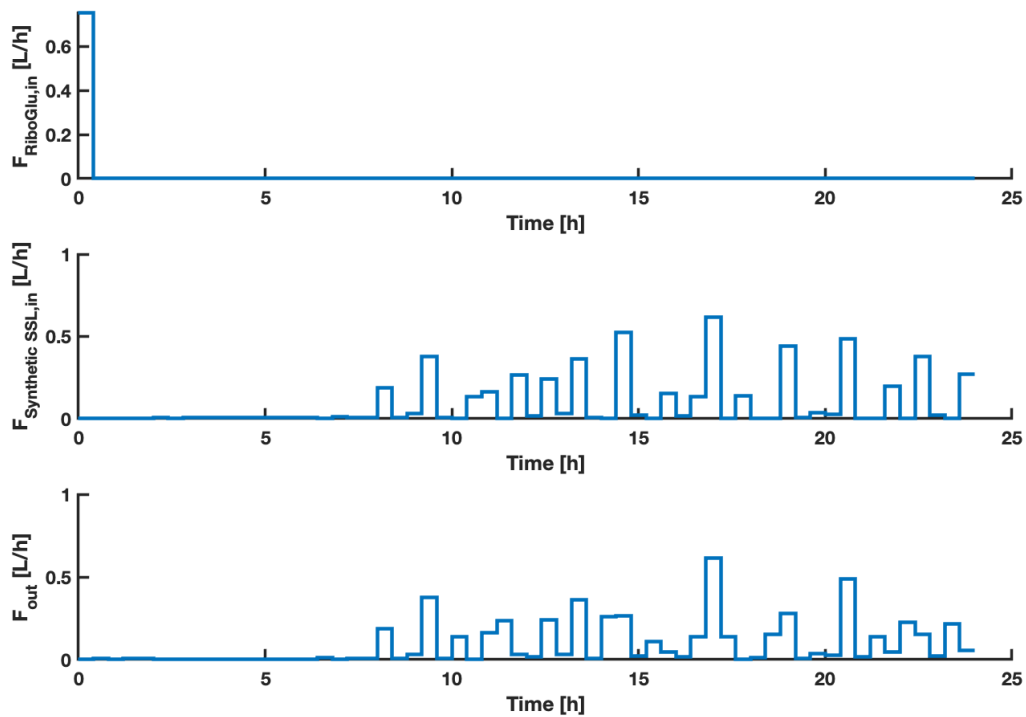


Figure 4.38: The plots shows the inputs $F_{\text{RiboGlu},in}$, $F_{\text{Synthetic SSL},in}$ and F_{out} as a function of time. The MPC inputs were calculated using the objective function described in Equation (3.11). The $F_{\text{Synthetic SSL},in}$ had a lower constraint of 0 and an upper constraint of 1 L/h.

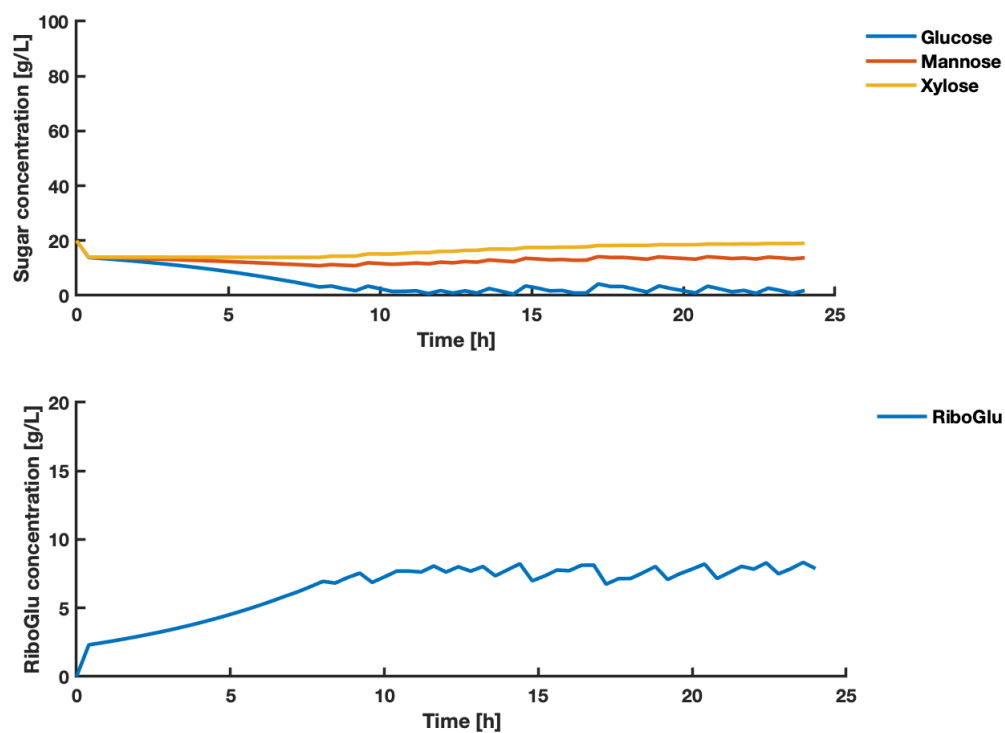


Figure 4.39: The upper plot shows the concentrations of the states glucose, mannose, xylose as a function of time. The lower plot shows the concentration of the state RiboGlu as a function of time. The states are a result of the inputs shown in Figure 4.38, using the objective function described in Equation (3.11). The $F_{\text{Synthetic SSL},in}$ had a lower constraint of 0 and an upper constraint of 1 L/h.

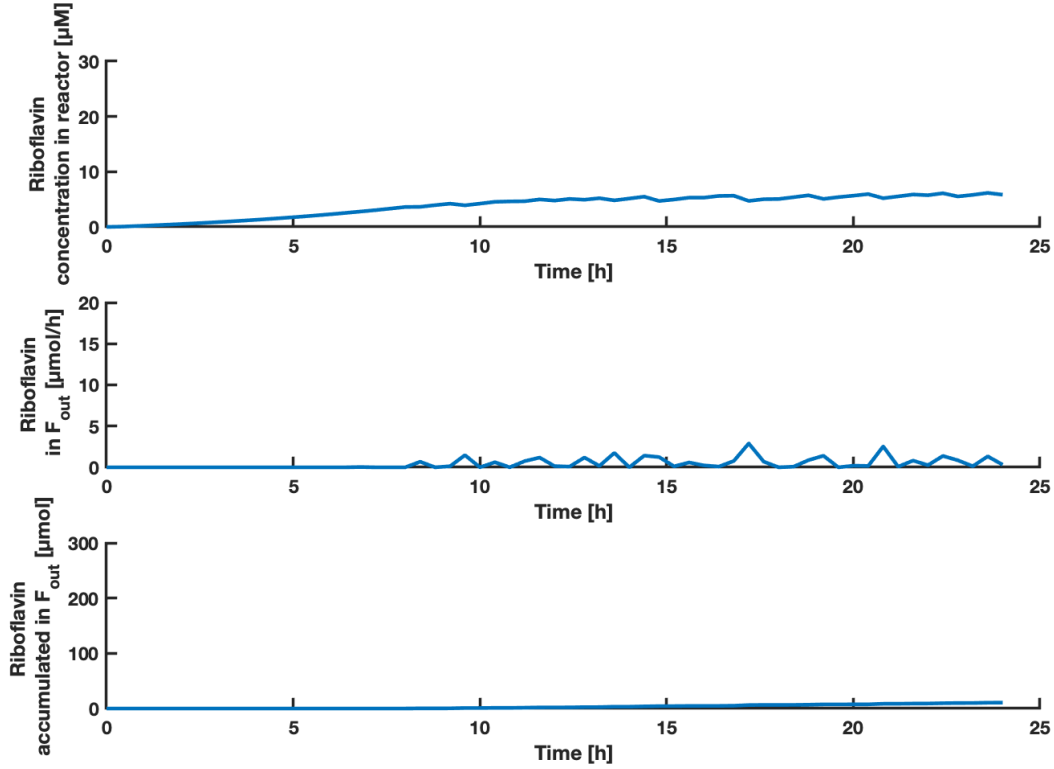


Figure 4.40: The upper plot shows the concentration of riboflavin as a function of time. The middle plot shows the amount of riboflavin in the F_{out} stream as a function of time. The lower plot shows the accumulated amount of riboflavin in the F_{out} stream as a function of time. The predicted states of riboflavin concentration in the reactor are a result of the inputs shown in Figure 4.38, using the objective function described in Equation (3.11). The $F_{Synthetic\ SSL,in}$ had a lower constraint of 0 and an upper constraint of 1 L/h.

For the simplified system with a synthetic SSL stream of 0-1 L/h, the MPC predicted accumulated amounts of biomass, riboflavin and associated yields as shown in Table 4.10.

Table 4.10: The table shows the accumulated amounts of RiboGlu, RiboMan and RiboXyl strains, with associated biomass yield, X . The accumulated amount of the product riboflavin P , and the associated yield is shown. The values were calculated based on simulation results for simplified system with a synthetic SSL stream of 0-1 L/h

RiboGlu [g]	X yield [g/g syn SSL]	P [μmol]	P yield [μg/g syn SSL]
15.81	0.1243	10.67	31.56

The inoculation of the RiboGlu strain starts immediately as seen in the upper plot of Figure 4.38. With the objective function of maximizing the biomass yield, the synthetic SSL fed into the reactor starts after approximately 7 hours. At this time most of the glucose has been consumed, and the biomass needs more substrate for growth. The consumption of xylose in this case was poor, as expected as the RiboGlu strain can not consume xylose (See Figure 4.3).

4.3.1 Summary of simulation results of simplified system

Simulations were also performed with a prediction of 80 hours, to better compare with the results obtained using multiple strains. The graphical simulation results are attached in Appendix Section G. The key results compared to the results from Case C with 0-1 L/h synthetic SSL are shown in Figure 4.41 to 4.44.

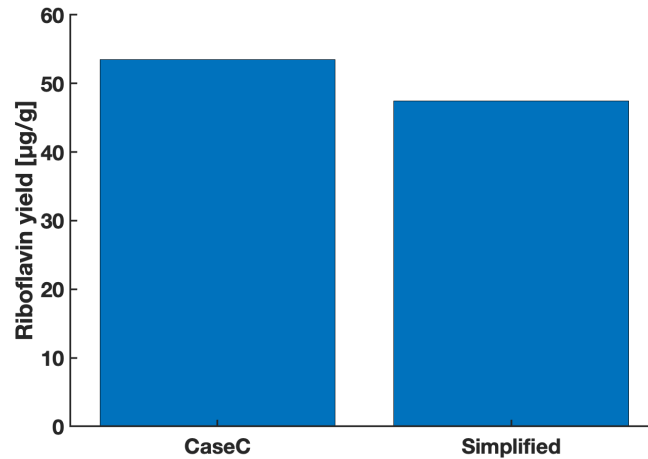


Figure 4.41: The plot shows the yield of riboflavin in $\mu\text{g/g}$ synthetic SSL obtained after 80 hours for Case C (Equation (3.9)) and the simplified version using only the RiboGlu strain (Equation (3.11)). The plot shows the results obtained using 0-1 L/h synthetic SSL.

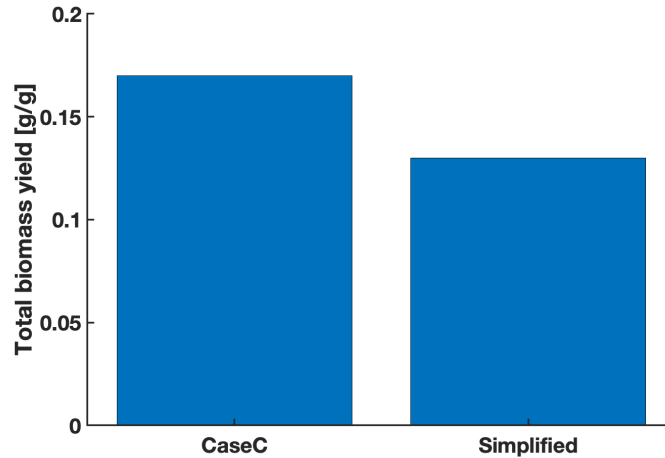


Figure 4.42: The plot shows the final biomass yield in g/g synthetic SSL predicted after 80 hours for Case C (Equation (3.9)) and the simplified version using only the RiboGlu strain (Equation (3.11)). The plot shows the results obtained using 0-1 L/h synthetic SSL.

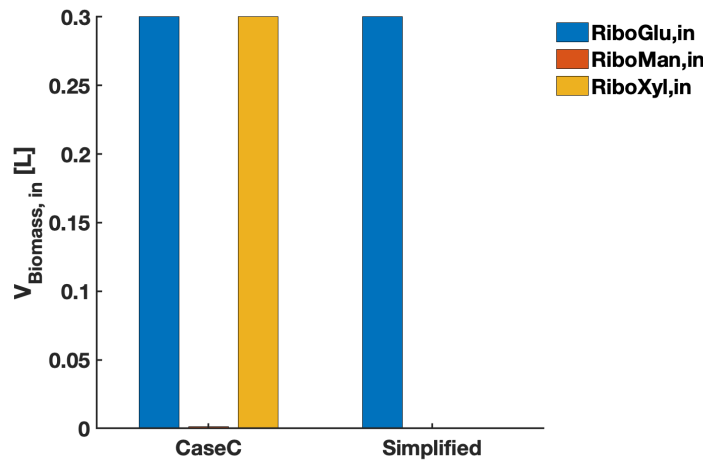


Figure 4.43: The plots shows the volume of biomass used to feed the main reactor predicted after 80 hours for Case C (Equation (3.9)) and the simplified version using only the RiboGlu strain (Equation (3.11)). The blue, orange and yellow bars represents the volume of the RiboGlu, RiboMan, and RiboXyl strain respectively fed into the main reactor. The plot shows the results obtained using 0-1 L/h synthetic SSL.

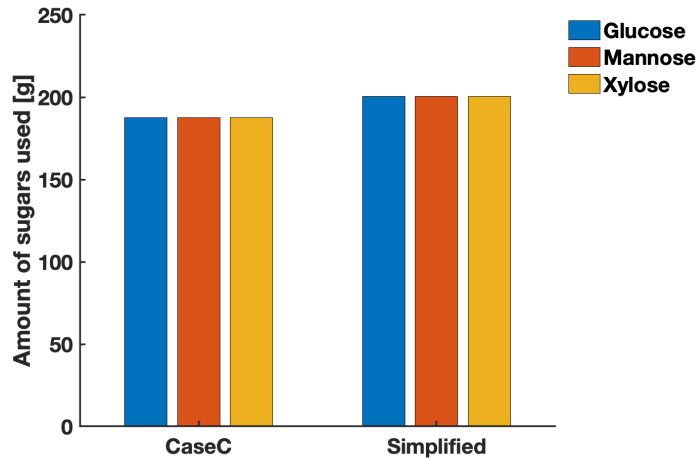


Figure 4.44: The plot shows the final amount of sugars used, predicted after 80 hours for Case C (Equation (3.9)) and the simplified version using only the RiboGlu strain (Equation (3.11)).

By comparing the original system containing three feeds of *C. glutamicum* strains, with the simplified idea using only the RiboGlu strain it was showed that a combination of strains predicts higher biomass and riboflavin yields. The simplified system uses more synthetic SSL. However the main difference is presumably the effect of using the RiboXyl strain, as this strain provided higher biomass concentrations as well as riboflavin titers.

4.4 Comparison of single strains and combination of strains

To further see if the combination of strains could improve the biomass and riboflavin production, and the effect of the RiboXyl strain, new simulations were performed. The cases presented in Equation (3.7) to (3.10) were used as objective functions, with some modifications. A variable feed stream of 0-1 L/h real SSL was used. Because of the error of the RiboMan model, this strain was excluded. Simulations using only RiboGlu, only RiboXyl, and a combination of the two were performed. Figure 4.45 shows the final accumulated amount of riboflavin in the F_{out} stream predicted after 80 hours for the different cases, and the riboflavin yield obtained.

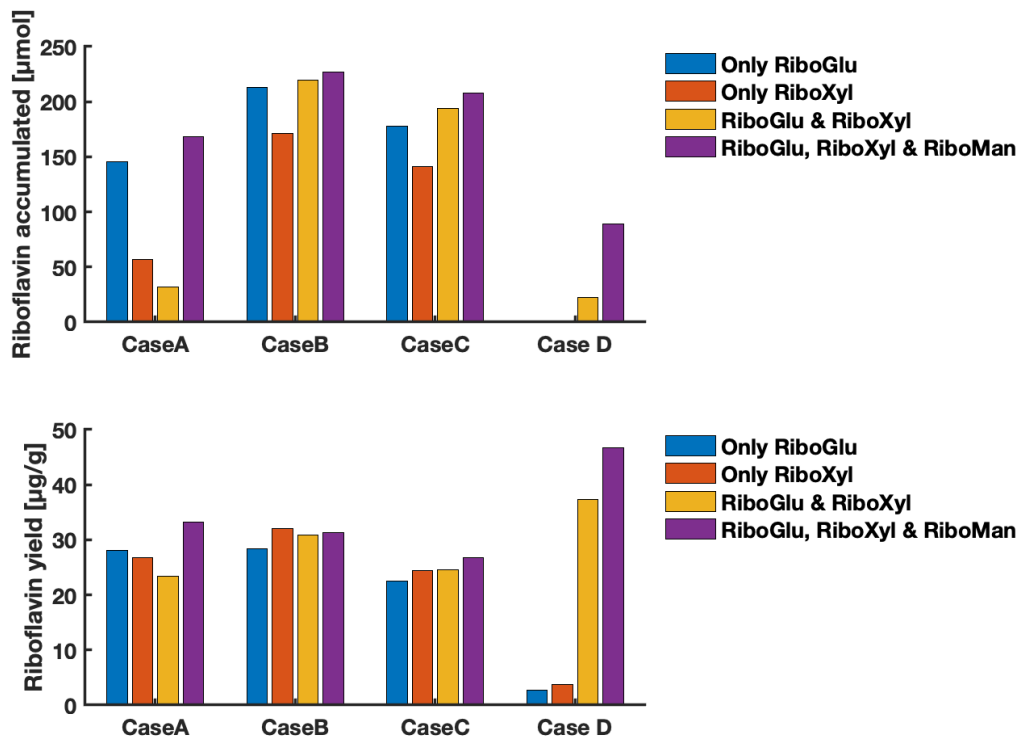


Figure 4.45: The upper plot shows the final accumulated amount of riboflavin in the F_{out} stream predicted after 80 hours for the different cases presented in Equation (3.7) to (3.10). The lower plot shows the yield of riboflavin in $\mu\text{g/g}$ SSL. The plots shows the results obtained using only RiboGlu strain (blue bars), only RiboXyl strain (orange bars), RiboGlu and RiboXyl strains (yellow bars), and RiboGlu, RiboMan and RiboXyl strains (purple bars).

Figure 4.46 shows the final accumulated amount of biomass in the F_{out} stream predicted after 80 hours for the different cases, and the biomass yield obtained.

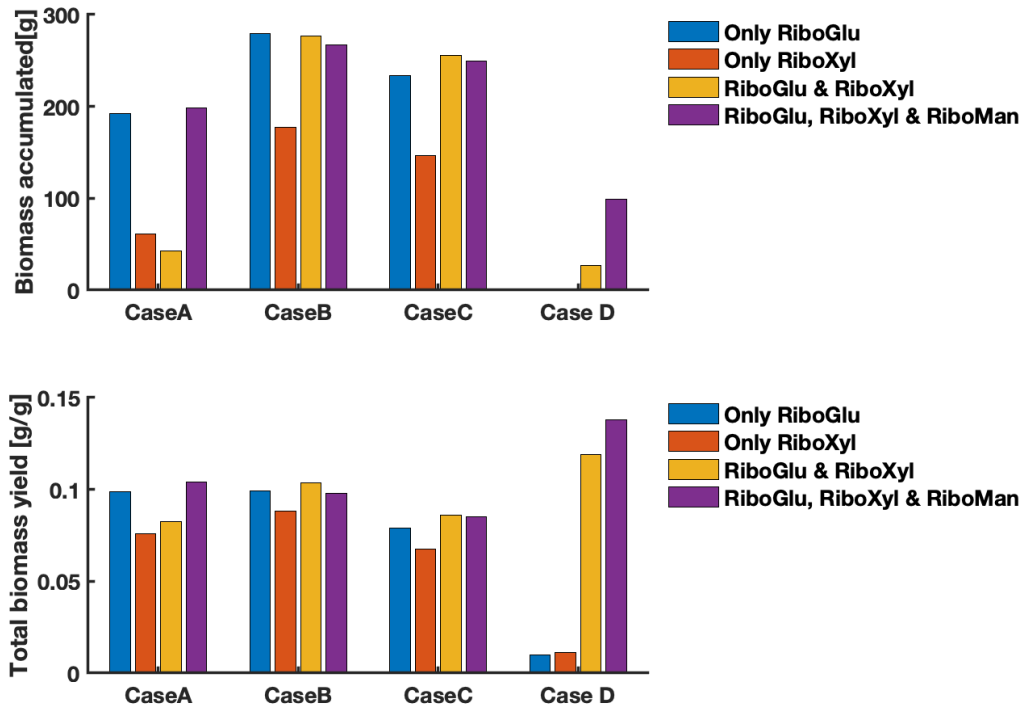


Figure 4.46: The upper plot shows the final accumulated amount of biomass in the F_{out} stream predicted after 80 hours for the different cases presented in Equation (3.7) to (3.10). The lower plot shows the yield of biomass in g/g SSL. The plots shows the results obtained using only RiboGlu strain (blue bars), only RiboXyl strain (orange bars), RiboGlu and RiboXyl strains (yellow bars), and RiboGlu, RiboMan and RiboXyl strains (purple bars).

It can be seen that the highest biomass and riboflavin yield predicted when using 0-1 L/h SSL, is still by using the original version of Case D, and combining all the strains. For all cases it seems that the biomass yield gets higher by either combining the RiboGlu and RiboXyl strain, or by using all three strains. It should be noted that the objective functions of Case A and B does not optimize for the yields. It can be seen that the production rates of biomass and riboflavin are higher for Case B. In this case it can be beneficial to only use the RiboGlu strain as the production and yields obtained are similar to when a combination of strains are used.

5 Discussion

5.1 Modeling and parameter estimation

As Szallasi et al. [56] stated, biological systems are inherently complex, and should be modeled to see if it can reflect the experimental data. This way the effect of manipulating experimental conditions can be analyzed, without performing costly and complex experiments.

For the models describing each strain, the biomass growth is described better than the sugar consumption and product formation. This is the natural consequence of the biomass part being weighted more to achieve a better fit, as explained in Section 3.4. Further improvements could have been implemented to the model, by including a substrate inhibition model or the product inhibition model developed by Khan et al. [76]. They established proof of growth inhibition of *C. glutamicum* by the product L-glutamate, and showed that the specific growth rate of *C. glutamicum* decreased with increasing L-glutamate concentrations [76]. For describing the biomass, in this case it seemed that the simple Monod kinetics was sufficiently accurate, and was therefore used for the further construction of the MPC algorithm as well.

For the models presented in Section 4.1.4, the specific rate of product formation due to maintenance was neglected. As described in Figure 2.2, the riboflavin pathway of *C. glutamicum* is connected to the PPP, while the main pathways for generating energy or ATP in *C. glutamicum* are through the glycolysis and the TCA cycle (See Figure 2.3). Two other models were tested, with the aim of improving the product to fit experimental data. A model including maintenance coefficients, and a model including three separate Y_{px} 's - one for each sugar were tested. The parameter results are attached in Appendix Section D. However the results obtained did not change the behavior of the model describing product formation, as the shape of the curve does not change by adding the extra term.

As mentioned in Section 4.1.1, there was carried out an improvement of the RiboGlu parameters estimated. The change of parameters was subsequently implemented to the

MPC algorithm. It was observed that a change of a few parameters, could have a great impact on the performance. A summary of the simulation results obtained using the old version of parameters estimated can be seen in Appendix Section E.1. It was assumed that the better fit of the RiboGlu model, with a worse consumption of xylose would affect the input of the strains. However a drawback of the MPC for this system was the strict volume constraints of the feed reactors. If the amount of RiboXyl strain added to the main reactor using the old parameters had already reached the maximum volume of 0.3 L, it was not feasible to add more RiboXyl. Where the previous version did not maximize the RiboXyl usage, an improvement of the parameters generally lead to an increase of the RiboXyl feed. It can be assumed that if the constraints were more relaxed, the change of the parameters would increase the feed of RiboXyl strain further to better consume the xylose. It can be observed that for some cases the amount of RiboGlu added to the main reactor was reduced, now that the RiboGlu model showed a worse consumption of xylose. Although the RiboGlu model was improved, there were difficulties modeling the mannose consumption of the RiboMan strain when growing on multiple substrates. There have been developed several other kinetic expressions for cell growth, providing better correlations for experimental data in certain situations [84, 85], and especially for the RiboMan strain consuming SSL it could be useful to test other models.

Further analysis such as the root mean square of the models, could have been performed to see the actual errors between models and experimental data. A sensitivity analysis could have been performed to better understand how the parameter values affects the system behavior. A sensitivity analysis helps determining the accuracy needed in the estimation of the parameters to make the models valid [86].

5.2 MPC simulations

From Section 4.2.5, it can be seen that for all cases, the highest biomass yields were obtained by using synthetic SSL. As the synthetic SSL has a mannose concentration 5.5 times lower than the real SSL, it does not need as much of the RiboMan strain for mannose consumption. From the experimental data it seems that both RiboGlu and RiboXyl actually consumes mannose from synthetic SSL faster than the RiboMan strain. The RiboXyl strain produces the highest titer of riboflavin when growing on synthetic SSL. As shown in Figure 2.3, an overexpression of *xylAB* increases the conversion of D-xylose

to ribose 5-phosphate, an intermediate in the PPP, making it an intermediate in the riboflavin biosynthesis pathway as well (Figure 2.2). The PPP may be more active when *xylAB* is overexpressed and, therefore, the consumption of glucose through the PPP increases to the detriment of the consumption through the glycolysis. As a consequence, RiboXyl is the strain with the highest feed to the main reactor for most cases.

Although MPC simulations were performed using synthetic SSL as well, the results obtained of using real SSL are of a higher importance. The idea of the industrial application is having the system described in Figure 3.1 as a downstream process, with the SSL as a direct waste stream from the bio-refineries. The constraints of the industrial scale system are likely to vary, depending on availability of biomass. By up-scaling the system, and hence the constraints of reactor volumes and flow sizes, some of the weaknesses of the MPC the way it is implemented here may be reduced. All the simulations performed for this thesis were done with feasible constraints of the equipment available in the laboratory. With the aim of optimizing biomass growth, the MPC algorithm suggests to inoculate the strains of *C. glutamicum* immediately. To satisfy the volume constraints, if high amounts of inoculum are added, the stream out of the reactor is subsequently high in the beginning. The use of small scale reactors was a major limitation, and the capacity of bacteria strains could be increased drastically by up-scaling.

The linearized approximation of maximizing the riboflavin yield (Case D) using 0-1 L/h real SSL obtained the highest riboflavin and biomass yields when real SSL was used. In this case, smaller amounts of biomass were used for feed and two strains were combined - RiboMan and RiboXyl. The RiboMan strain is overexpressing the *manA* gene. The gene *manA* connects the glycolysis pathway with the cell wall biosynthesis pathway [87]. Its overexpression may change the carbon flux ratios between the pathways, providing a more robust cell wall and increasing the biomass yield. A similar linear approximation was subsequently done with the maximization of the biomass yield (Case C) as well. The results obtained were approximately equal (See Appendix Section H). As the kinetic expressions used shows a proportionality between the biomass and product formation, this was anticipated. For optimization of biomass yields it seems that an objective function with a linearized approximation of either the riboflavin or biomass yield is preferable.

As seen in Figure 4.45 and 4.46, a combination of all the strains predicts the highest biomass and riboflavin yield for Case D. However costs of operating an extra reactor should also be considered. By down-scaling the process to using two feed reactors with the RiboGlu and RiboXyl strain, the biomass yield predicted was 16 % lower than when using all three strains. Nevertheless it predicted at least a 14.3 % higher biomass yield than for the other cases when using 0-1 L/h SSL. There is a trade-off between obtaining high biomass yields, and high production rates. If the sugars are cheap, it may be preferable to increase the production rate, at the cost of leaving more sugars unconsumed. As shown in Figure 4.45 and 4.46, when using Case B as objective function it can be beneficial to only use the RiboGlu strain as feed. The yields obtained will not be as high, but the production rate will increase, and the costs of operating two extra reactors will be eliminated.

As mentioned in Section 3.6, due to limitations of access to the NTNU campus the spring of 2020, the number of physical experiments planned were reduced to one. The aim of this first experiment was to compare the performance of the MPC on the real system with that of the simulations, not to experimentally optimize the biomass growth. Consequently objective function did not include the linearized yield approximation (which provided better results regarding biomass yields), but rather an objective function providing rapid changes in the inputs.

5.3 Riboflavin biosynthesis genes

The strains of *C. glutamicum* described in Table 3.1 are overexpressing the gene *sigH*, leading to an increased expression of riboflavin biosynthesis genes, described in Figure 2.2 [25]. According to the riboflavin pathway of *C. glutamicum*, riboflavin could be further degraded to FMN and FAD due to the gene *ribF*. However *ribF* is not located in the same operon as the riboflavin synthesis genes *ribA*, *ribH*, and *ribC* which are suspected to belong to the operon OP_cg1804 [88]. Taniguchi and Wendisch showed in their research from 2015 that *ribF* mRNA levels of *C. glutamicum* were not affected notably by *sigH* overexpression [11]. They also overexpressed the *ribF* gene, leading to lower riboflavin concentrations [11]. It could possibly be of interest to do a further study involving *ribF* deficient strains. In that case FMN and FAD would have to be provided in another

way, as they are important cofactors, and as *sigH* overexpression upregulates enzymes depending on them [11].

5.4 Future work

SSL is widely used as a substrate for industrial ethanol production, a product with a cheaper selling price than riboflavin. In addition to the economical aspect, ethanol production can emit large amounts of CO₂ [89]. An environmental evaluation can therefore be done to measure the CO₂ emitted by riboflavin production from SSL.

The rate of riboflavin production by *C. glutamicum* strains can be improved. For instance by overexpressing the operon containing *ribAHC* genes, instead of overexpressing *sigH*.

The experimental work using the MPC developed in this thesis will be performed by the Bio-systems research group at NTNU once the technical challenges of the laboratory are solved. The automatic transfer of samples from NUMERA to the HPLC will also be implemented in the future, which will reduce the measurement delay. Firstly the experiment described in Section 3.6 will be performed again. Once the MPC algorithm is implemented in the laboratory and works properly, the objective function can be changed with the aim of optimizing the biomass formation and hence the riboflavin production. It is further suggested to expand the experiment to two feeding reactors, using the RiboGlu and the RiboXyl strain. The final step will be to expand the experiment and combine the strains as the main idea described in Figure 3.1 shows. Before this final step is implemented, it is recommended to try to improve the RiboMan model.

6 Conclusion

This report showed that genetically modified strains of *C. glutamicum* producing riboflavin by consuming SSL sugars could be modeled, and further used to construct an MPC algorithm combining the strains. The models, describing biomass formation, substrate consumption and product formation were based on experimental work performed in the specialization project the fall of 2019. The models followed Monod kinetics, and captured the behavior of biomass formation well. The consumption of mannose by the RiboMan strain was difficult to model, and was a source of error for the further work.

An MPC algorithm was constructed to see if a combination of the genetically modified strains of *C. glutamicum* could improve the biomass formation and hence the riboflavin production by consuming SSL sugars. The MPC algorithm predicted future output values to optimize the chosen objective function. Four different objective functions were presented in this report, providing different results regarding biomass and riboflavin yields. The MPC algorithm included constraints that were feasible for laboratory-scale experiments.

The results of this study indicates that a combination of *C. glutamicum* strains can provide an improvement of the biomass yield. The results showed that the usage of RiboXyl strain was crucial for predicting the highest biomass yields. This is the only strain consuming xylose. When using real SSL (composition is described in Table 3.6), the highest biomass yield is predicted by using smaller amounts of biomass for feed and by combining two strains - RiboMan and RiboXyl (Case D). It is assumed that by improving the RiboMan model, the addition of RiboMan will be reduced, and replaced by the RiboGlu strain to better consume the SSL sugars.

If the efficient consumption of SSL sugars is not prioritized, high production rates of biomass and riboflavin can be obtained only by using the RiboGlu strain (Case B). This will reduce the costs of operating extra reactors, and the complexity of the system.

References

- [1] G. F. Combs and J. P. McClung, *The vitamins : fundamental aspects in nutrition and health*, pp. 327–330, ISBN: 0128029838.
- [2] J. Becker, C. M. Rohles, and C. Wittmann, *Metabolically engineered Corynebacterium glutamicum for bio-based production of chemicals, fuels, materials, and health-care products*, Nov. 2018. DOI: 10.1016/j.ymben.2018.07.008.
- [3] C. Rueda, P. A. Calvo, G. Moncalián, G. Ruiz, and A. Coz, “Biorefinery options to valorize the spent liquor from sulfite pulping,” *Journal of Chemical Technology & Biotechnology*, vol. 90, no. 12, pp. 2218–2226, Dec. 2015, ISSN: 02682575. DOI: 10.1002/jctb.4536. [Online]. Available: <http://doi.wiley.com/10.1002/jctb.4536>.
- [4] P. M. Doran, “Chapter 14.4 Monitoring and Control of Bioreactors,” in *Bioprocess Engineering Principles*, 2nd ed., Elsevier, Jan. 2013, pp. 778–789. DOI: 10.1016/b978-0-12-220851-5.00014-9.
- [5] D. E. Seborg, T. F. Edgar, D. A. Mellichamp, and F. J. Doyle, “Chapter 20 Model Predictive Control,” in *Process Dynamics and Control*, 3rd ed., 2011, pp. 414–438.
- [6] G. F. Combs, “Chapter 11 – Riboflavin,” in *The Vitamins*, 4th ed., Academic Press, 2012, ch. 11, pp. 277–289, ISBN: 9780123819802. DOI: 10.1016/B978-0-12-381980-2.00011-6.
- [7] K. P. Stahmann, J. L. Revuelta, and H. Seulberger, *Three biotechnical processes using Ashbya gossypii, Candida famata, or Bacillus subtilis compete with chemical riboflavin production*, 2000. DOI: 10.1007/s002530051649.
- [8] S. K. Schwechheimer, E. Y. Park, J. L. Revuelta, J. Becker, and C. Wittmann, “Biotechnology of riboflavin,” DOI: 10.1007/s00253-015-7256-z.
- [9] Z. Yuan, J. Bi, and Y. Moriguchi, *The circular economy: A new development strategy in China*, Dec. 2006. DOI: 10.1162/108819806775545321.
- [10] D. Peters, “Carbohydrates for fermentation,” *Biotechnology Journal*, vol. 1, no. 7-8, pp. 806–814, Aug. 2006, ISSN: 1860-6768. DOI: 10.1002/biot.200600041. [Online]. Available: <http://doi.wiley.com/10.1002/biot.200600041>.
- [11] H. Taniguchi and V. F. Wendisch, “Exploring the role of sigma factor gene expression on production by *Corynebacterium glutamicum*: Sigma factor H and FMN as

- example,” *Frontiers in Microbiology*, vol. 6, no. JUL, 2015, ISSN: 1664302X. DOI: 10.3389/fmicb.2015.00740.
- [12] E. F. Camacho and C. Bordons, “Introduction to model predictive control,” in *Model Predictive Control, Advanced Textbooks in Control and Signal Processing*, 9781852336943, Springer International Publishing, 2007, pp. 1–11. DOI: 10.1007/978-0-85729-398-5{_}1.
- [13] M. Hovd and R. R. Bitmead, “Interaction Between Control and State Estimation in Nonlinear MPC,” *Dynamics and Control of Process Systems*, vol. 1, pp. 119–125, 2004.
- [14] A. Zheng, “Computationally efficient nonlinear MPC algorithm,” in *Proceedings of the American Control Conference*, vol. 3, IEEE, 1997, pp. 1623–1627. DOI: 10.1109/acc.1997.610858.
- [15] F. Allgöwer, T. A. Badgwell, J. S. Qin, J. B. Rawlings, and S. J. Wright, “Nonlinear Predictive Control and Moving Horizon Estimation — An Introductory Overview,” in *Advances in Control*, Springer London, 1999, pp. 391–449. DOI: 10.1007/978-1-4471-0853-5{_}19.
- [16] M. Diehl, H. J. Ferreau, and N. Haverbeke, “Efficient numerical methods for nonlinear MPC and moving horizon estimation,” in *Lecture Notes in Control and Information Sciences*, vol. 384, Springer, Berlin, Heidelberg, 2009, pp. 391–417, ISBN: 9783642010934. DOI: 10.1007/978-3-642-01094-1{_}32.
- [17] D. R. Kallman, “Riboflavin production from genetically modified strains of *Corynebacterium glutamicum* using sugars present in spent sulfite liquor,” 2019.
- [18] F. Aramouni and K. Deschenes, *Methods for Developing New Food Products: An Instructional Guide*. 2015, p. 115.
- [19] S. A. Mapari, K. F. Nielsen, T. O. Larsen, J. C. Frisvad, A. S. Meyer, and U. Thrane, *Exploring fungal biodiversity for the production of water-soluble pigments as potential natural food colorants*, 2005. DOI: 10.1016/j.copbio.2005.03.004.
- [20] P. Karrer, K. Schöpp, and F. Benz, “Synthesis of Flavins. 4.,” *Helvetica Chimica Acta*, vol. 18, no. 1, pp. 426–429, 1935, ISSN: 15222675. DOI: 10.1002/hlca.19350180152.
- [21] P. Hoyos, M. Hernáiz, and A. Alcántara, “Biocatalyzed Production of Fine Chemicals,” in *Reference Module in Life Sciences*, Elsevier, 2017.

- [22] L. J. WICKERHAM, M. H. FLICKINGER, and R. M. JOHNSTON, “The production of riboflavin by *Ashbya gossypii*,” *Arch. Biochem.*, vol. 9, pp. 95–98, 1946.
- [23] D. L. Heefner, C. A. Weaver, M. J. Yarus, and L. A. Burdzinski, “Riboflavin Producing Strains of Microorganisms,” Tech. Rep., 1992.
- [24] U. Sauer, V. Hatzimanikatis, H. P. Hohmann, M. Manneberg, A. P. Van Loon, and J. E. Bailey, “Physiology and metabolic fluxes of wild-type and riboflavin-producing *Bacillus subtilis*,” *Applied and Environmental Microbiology*, vol. 62, no. 10, pp. 3687–3696, Oct. 1996, ISSN: 00992240.
- [25] *KEGG PATHWAY: Riboflavin metabolism - Corynebacterium glutamicum ATCC 13032 (Bielefeld)*.
- [26] Z. Lin, Z. Xu, Y. Li, Z. Wang, T. Chen, and X. Zhao, “Metabolic engineering of *Escherichia coli* for the production of riboflavin,” Tech. Rep., 2014, pp. 1–12.
- [27] L Eggeling and M Bott, “Handbook of *Corynebacterium glutamicum*,” 2005.
- [28] B. Blombach and G. M. Seibold, “Carbohydrate metabolism in *Corynebacterium glutamicum* and applications for the metabolic engineering of L-lysine production strains,” DOI: 10.1007/s00253-010-2537-z.
- [29] J. Becker, O. Zelder, S. Häfner, H. Schröder, and C. Wittmann, “From zero to hero-Design-based systems metabolic engineering of *Corynebacterium glutamicum* for l-lysine production,” *Metabolic Engineering*, vol. 13, no. 2, pp. 159–168, Mar. 2011, ISSN: 10967176. DOI: 10.1016/j.ymben.2011.01.003.
- [30] V. F. Wendisch, L. F. Brito, M. Gil Lopez, G. Hennig, J. Pfeifenschneider, E. Sgobba, and K. H. Veldmann, *The flexible feedstock concept in Industrial Biotechnology: Metabolic engineering of Escherichia coli, Corynebacterium glutamicum, Pseudomonas, Bacillus and yeast strains for access to alternative carbon sources*, Sep. 2016. DOI: 10.1016/j.jbiotec.2016.07.022.
- [31] S. N. Lindner, G. M. Seibold, A. Henrich, R. Krämer, and V. F. Wendisch, “Phosphotransferase system-independent glucose utilization in *Corynebacterium glutamicum* by inositol permeases and glucokinases,” *Applied and Environmental Microbiology*, vol. 77, no. 11, pp. 3571–3581, Jun. 2011, ISSN: 00992240. DOI: 10.1128/AEM.02713-10.
- [32] M. W. Moon, H. J. Kim, T. K. Oh, C. S. Shin, J. S. Lee, S. J. Kim, and J. K. Lee, “Analyses of enzyme II gene mutants for sugar transport and heterologous expres-

- sion of fructokinase gene in *Corynebacterium glutamicum* ATCC 13032,” *FEMS Microbiology Letters*, vol. 244, no. 2, pp. 259–266, Mar. 2005, ISSN: 03781097. DOI: 10.1016/j.femsle.2005.01.053.
- [33] H Dominguez, M Cocaign-Bousquet, and N. D. Lindley, “Simultaneous consumption of glucose and fructose from sugar mixtures during batch growth of *Corynebacterium glutamicum*,” Tech. Rep.
- [34] M. Sasaki, T. Jojima, M. Inui, and H. Yukawa, “Simultaneous utilization of D-cellobiose, D-glucose, and D-xylose by recombinant *Corynebacterium glutamicum* under oxygen-deprived conditions,” *Applied Genetics and Molecular Biotechnology*, DOI: 10.1007/s00253-008-1703-z.
- [35] M. Sasaki, H. Teramoto, M. Inui, and H. Yukawa, “Identification of mannose uptake and catabolism genes in *Corynebacterium glutamicum* and genetic engineering for simultaneous utilization of mannose and glucose,” *Applied Genetics and Molecular Biotechnology*, DOI: 10.1007/s00253-010-3002-8.
- [36] A. Arndt and B. J. Eikmanns, “Chapter 7 Regulation of carbon metabolism in *Corynebacterium glutamicum*,” *Corynebacteria: Genomics and Molecular Biology*, 2008.
- [37] C. Brüsseler, A. Radek, N. Tenhaef, K. Krumbach, S. Noack, and J. Marienhagen, “The myo-inositol/proton symporter IolT1 contributes to D-xylose uptake in *Corynebacterium glutamicum*,” *Bioresource Technology*, vol. 249, pp. 953–961, Feb. 2018, ISSN: 18732976. DOI: 10.1016/j.biortech.2017.10.098.
- [38] T. Llano, N. Quijorna, A. Andrés, and A. Coz, “Sugar, acid and furfural quantification in a sulphite pulp mill: Feedstock, product and hydrolysate analysis by HPLC/RID,” *Biotechnology Reports*, vol. 15, pp. 75–83, 2017.
- [39] M. Weissgram, J. Gstöttner, B. Lorantfy, R. Tenhaken, C. Herwig, and H. Weber, “Generation of PHB from Spent Sulfite Liquor Using Halophilic Microorganisms,” *Microorganisms*, vol. 3, no. 2, pp. 268–289, Jun. 2015, ISSN: 2076-2607. DOI: 10.3390/microorganisms3020268.
- [40] M. Alexandri, H. Papapostolou, L. Stragier, W. Verstraete, S. Papanikolaou, and A. A. Koutinas, “Succinic acid production by immobilized cultures using spent sulphite liquor as fermentation medium,” *Bioresource Technology*, vol. 238, pp. 214–222, 2017, ISSN: 18732976. DOI: 10.1016/j.biortech.2017.03.132.

- [41] A. M. Petersen, K. Haigh, and J. F. Görgens, “Techno-economics of integrating bioethanol production from spent sulfite liquor for reduction of greenhouse gas emissions from sulfite pulping mills,” *Biotechnology for Biofuels*, vol. 7, no. 1, 2014, ISSN: 17546834. DOI: 10.1186/s13068-014-0169-8.
- [42] S. S. Helle, A. Murray, J. Lam, D. R. Cameron, and S. J. Duff, “Xylose fermentation by genetically modified *Saccharomyces cerevisiae* 259ST in spent sulfite liquor,” *Bioresource Technology*, vol. 92, no. 2, pp. 163–171, 2004, ISSN: 09608524. DOI: 10.1016/j.biortech.2003.08.011.
- [43] Z. Szallasi, J. Stelling, and V. Periwal, “The Role of Modelling in Systems Biology,” in *System Modeling in Cellular Biology : From Concepts to Nuts and Bolts*, Cambridge, Mass: The MIT Press, 2006, ch. 1, pp. 3–18, ISBN: 9780262195485.
- [44] A. L. Lehninger, D. L. Nelson, and M. M. Cox, *Principles of Biochemistry Lehninger Sixth edition*. 2013, pp. 200–213, ISBN: 9781429234146.
- [45] P. M. Doran, “Chapter 12.3 General Reaction Kinetics for Biological Systems,” in *Bioprocess Engineering Principles*, 2nd ed., Elsevier, 2013, pp. 612–621, ISBN: 9780122208515.
- [46] —, “Chapter 12.8 Cell Growth Kinetics,” in *Bioprocess Engineering Principles*, 2013.
- [47] —, “Chapter 12.11 Kintetics of Substrate Uptake in Cell Culture,” in *Bioprocess Engineering Principles*, 2nd ed., Elsevier, 2013, pp. 645–648, ISBN: 9780122208515.
- [48] —, “Chapter 12.10 Production Kinetics in Cell Culture,” in *Bioprocess Engineering Principles*, 2nd ed., Elsevier, 2013, pp. 643–645.
- [49] H. S. Fogler, “1.4.1 Continous-Stirred Tank Reactor,” in *Elements of chemical reaction engineering*, Fourth edition., Upper Saddle River NJ: Prentice Hall PTR, 2006, pp. 12–14, ISBN: 9780130473943.
- [50] D.-E. Gratie, B. Iancu, and I. Petre, “ODE Analysis of Biological Systems,” *Formal Methods for Dynamical Systems*, pp. 29–63, 2013.
- [51] I. Mihai, M Turnea, and M Rotariu, “Ordinary differential equations with applications in molecular biology,” Universitatea de Medicină și Farmacie “Gr.T.Popa” Iași, Facultatea de Medicină, Tech. Rep., 2012.
- [52] J. Cronin, “Some Mathematics of Biological Oscillations*,” Tech. Rep. 1, 1977.

- [53] C. C. Chicone, *Ordinary differential equations with applications*. Springer, 2006, p. 623, ISBN: 0387357947.
- [54] *Ordinary Differential Equations - MATLAB & Simulink - MathWorks Nordic*.
- [55] G Lillacci and M Khammash, “Parameter Estimation and Model Selection in Computational Biology,” *PLoS Comput Biol*, vol. 6, no. 3, p. 1 000 696, 2010.
- [56] Z. Szallasi, J. Stelling, and V. Periwal, “Computational Constraints on Modeling in Systems Biology,” in *System modeling in cell biology : from concepts to nuts and bolts - NTNU Universitetsbiblioteket*, The MIT Press, 2006, ch. 15, pp. 315–329.
- [57] J. E. Dennis and R. B. Schnabel, “10. Nonlinear Least Squares,” in *Numerical Methods for Unconstrained Optimization and Nonlinear Equations*, Society for Industrial and Applied Mathematics, Jan. 1996, pp. 218–238. DOI: 10 . 1137 / 1 . 9781611971200 . ch10.
- [58] *Solve nonlinear least-squares (nonlinear data-fitting) problems - MATLAB lsqnonlin - MathWorks Nordic*.
- [59] A. Tzes, G. Nikolakopoulos, and K. Alexis, “Model predictive quadrotor control: attitude, altitude and position experimental studies,” *IET Control Theory & Applications*, vol. 6, no. 12, pp. 1812–1827, Aug. 2012.
- [60] M. Ellis, H. Durand, and P. D. Christofides, “A tutorial review of economic model predictive control methods,” *Journal of Process Control*, vol. 24, no. 8, pp. 1156–1178, 2014, ISSN: 09591524. DOI: 10.1016/j.jprocont.2014.03.010.
- [61] A. Beck, “Chapter 8: Convex Optimization,” in *Introduction to Nonlinear Optimization*, Society for Industrial and Applied Mathematics, Oct. 2014, pp. 147–168. DOI: 10.1137/1.9781611973655.ch8.
- [62] *Optimization Problem Types - Linear and Quadratic Programming / solver*.
- [63] F. Magnusson and J. Åkesson, “Dynamic optimization in JModelica.org,” *Processes*, vol. 3, no. 2, pp. 471–496, Jun. 2015, ISSN: 22279717. DOI: 10.3390/pr3020471.
- [64] F Topputo and C Zhang, “Survey of Direct Transcription for Low-Thrust Space Trajectory Optimization with Applications,” 2014.
- [65] *Collocation Point - an overview | ScienceDirect Topics*. [Online]. Available: <https://www.sciencedirect.com/topics/engineering/collocation-point>.

- [66] L. T. Biegler, “10. Simultaneous Methods for Dynamic Optimization,” in *Nonlinear Programming*, Society for Industrial and Applied Mathematics, Jan. 2010, pp. 287–324. DOI: 10.1137/1.9780898719383.ch10.
- [67] E. L. Haseltine and J. B. Rawlings, “Critical evaluation of extended Kalman filtering and moving-horizon estimation,” *Industrial and Engineering Chemistry Research*, vol. 44, no. 8, pp. 2451–2460, Apr. 2005, ISSN: 08885885. DOI: 10.1021/ie0343081.
- [68] C. V. Rao, J. B. Rawlings, and J. H. Lee, “Constrained linear state estimation - A moving horizon approach,” *Automatica*, vol. 37, no. 10, pp. 1619–1628, Oct. 2001, ISSN: 00051098. DOI: 10.1016/S0005-1098(01)00115-7.
- [69] Y. Ramamurthi, P. B. Sistu, and B. W. Bequette, “Control-relevant dynamic data reconciliation and parameter estimation,” *Computers and Chemical Engineering*, vol. 17, no. 1, pp. 41–59, Jan. 1993, ISSN: 00981354. DOI: 10.1016/0098-1354(93)80004-7.
- [70] J. M. Maciejowski, “Moving-Horizon estimation,” in *Predictive Control: With Constraints*, Pearson Education, 2002, ch. 10.4, pp. 289–290.
- [71] I. I. Sirmatel and N. Geroliminis, “Optimization-based state estimation for perimeter controlled large-scale urban road networks,” Tech. Rep.
- [72] *CasADi*. [Online]. Available: <https://web.casadi.org/>.
- [73] C. Stansen, D. Uy, S. Delaunay, L. Eggeling, J. L. Goergen, and V. F. Wendisch, “Characterization of a *Corynebacterium glutamicum* lactate utilization operon induced during temperature-triggered glutamate production,” *Applied and Environmental Microbiology*, vol. 71, no. 10, pp. 5920–5928, Oct. 2005, ISSN: 00992240. DOI: 10.1128/AEM.71.10.5920-5928.2005.
- [74] N. A. Henke, S. A. Heider, P. Peters-Wendisch, and V. F. Wendisch, “Production of the marine carotenoid astaxanthin by metabolically engineered *Corynebacterium glutamicum*,” *Marine Drugs*, vol. 14, no. 7, Jul. 2016, ISSN: 16603397. DOI: 10.3390/md14070124.
- [75] P. C. De Blanc, D. C. McKinney, and G. E. Speitel, “Chapter 1 Modeling subsurface biodegradation of non-aqueous phase liquids,” *Advances in Porous Media*, vol. 3, no. C, pp. 1–86, Jan. 1996, ISSN: 1873975X. DOI: 10.1016/S1873-975X(96)80003-5.

- [76] N. S. Khan, I. M. Mishra, R. P. Singh, and B. Prasad, “Modeling the growth of *Corynebacterium glutamicum* under product inhibition in L-glutamic acid fermentation,” *Biochemical Engineering Journal*, vol. 25, no. 2, pp. 173–178, Sep. 2005, ISSN: 1369703X. DOI: 10.1016/j.bej.2005.01.025.
- [77] K. Sun, A. Kasperski, Y. Tian, and L. Chen, “Modelling of the *Corynebacterium glutamicum* biosynthesis under aerobic fermentation conditions,” *Chemical Engineering Science*, vol. 66, no. 18, pp. 4101–4110, Sep. 2011, ISSN: 00092509. DOI: 10.1016/j.ces.2011.05.041.
- [78] *Choose Sample Time and Horizons - MATLAB & Simulink - MathWorks Nordic*. [Online]. Available: <https://se.mathworks.com/help/mpc/ug/choosing-sample-time-and-horizons.html>.
- [79] E. Lazutkin, A. Geletu, and P. Li, “An Approach to Determining the Number of Time Intervals for Solving Dynamic Optimization Problems,” 2018.
- [80] “The unique automated sampling and sample processing system for on-line analytics in up-and down-stream bioprocesses,” Tech. Rep.
- [81] *High-Pressure Liquid Chromatography - an overview (pdf) | ScienceDirect Topics*.
- [82] F. Pérez-García, P. Peters-Wendisch, and V. F. Wendisch, “Engineering *Corynebacterium glutamicum* for fast production of L-lysine and l-pipecolic acid,” *Applied Microbiology and Biotechnology*, vol. 100, no. 18, pp. 8075–8090, Sep. 2016, ISSN: 14320614. DOI: 10.1007/s00253-016-7682-6.
- [83] S. Kind, S. Neubauer, J. Becker, M. Yamamoto, M. Völkert, G. v. Abendroth, O. Zelder, and C. Wittmann, “From zero to hero - Production of bio-based nylon from renewable resources using engineered *Corynebacterium glutamicum*,” *Metabolic Engineering*, vol. 25, pp. 113–123, 2014, ISSN: 10967184. DOI: 10.1016/j.ymben.2014.05.007.
- [84] A. Moser, “The Principles of Bioprocess Technology,” in *Bioprocess Technology*, Springer New York, 1988, pp. 13–65. DOI: 10.1007/978-1-4613-8748-0_{_}2.
- [85] R. Dutta, “Chapter 6: Cell Kinetics and Fermenter Design,” in *Fundamentals of Biochemical Engineering*, Springer Berlin Heidelberg, 2008, pp. 162–167. DOI: 10.1007/978-3-540-77901-8.
- [86] S. Rosa and D. F. M. Torres, “Parameter Estimation, Sensitivity Analysis and Optimal Control of a Periodic Epidemic Model with Application to HRSV in Florida,”

- Statistics, Optimization & Information Computing*, vol. 6, no. 1, pp. 139–149, Feb. 2018.
- [87] A. K. Mishra, K. Krumbach, D. Rittmann, S. M. Batt, O. Y-C Lee, S. De, J. Frunzke, G. S. Besra, L. Eggeling, and C. K. Arun Mishra, “Deletion of *manC* in *Corynebacterium glutamicum* results in a phospho-myo-inositol mannoside-and lipoglycan-deficient mutant,” DOI: 10.1099/mic.0.057653-0. [Online]. Available: <http://mic.sgmjournals.org>.
- [88] CoryneRegNet, *Predicted operon: OP_cg1804*.
- [89] E. Palmqvist, M. Galbe, and B. Hahn-Hägerdal, “Evaluation of cell recycling in continuous fermentation of enzymatic hydrolysates of spruce with *Saccharomyces cerevisiae* and on-line monitoring of glucose and ethanol,” *Applied Microbiology and Biotechnology*, vol. 50, no. 5, pp. 545–551, 1998, ISSN: 01757598. DOI: 10.1007/s002530051332.
- [90] C. M. Rohles, G. Gießelmann, M. Kohlstedt, C. Wittmann, and J. Becker, “Systems metabolic engineering of *Corynebacterium glutamicum* for the production of the carbon-5 platform chemicals 5-aminovalerate and glutarate,” *Microb Cell Fact*, vol. 15, p. 154, 2016. DOI: 10.1186/s12934-016-0553-0.
- [91] F. Pérez-García, C. Ziert, J. M. Risse, and V. F. Wendisch, “Improved fermentative production of the compatible solute ectoine by *Corynebacterium glutamicum* from glucose and alternative carbon sources,” *Journal of Biotechnology*, vol. 258, pp. 59–68, Sep. 2017, ISSN: 18734863. DOI: 10.1016/j.jbiotec.2017.04.039.

Appendix A Raw data: OD_{600} and HPLC values

A.1 RiboGlu strain with glucose as sole carbon source

Raw data of the experiment using RiboGlu strain with glucose as sole carbon source is shown in Table A.1.

Table A.1: Raw data from RiboGlu strain with glucose as sole carbon source experiment. OD_{600} was measured manually. Area values (A) of sugar and riboflavin were collected from the HPLC software Chromeleon.

Time[h]	OD_{600} RiboGlu	A glucose [μ RIU*min]	A riboflavin [μ RIU*min]
0	1.61	14.5786	0
2	1.78	13.7018	
4	2.31		15
6	3.85		
8	3.55		32.67
10	4.2	11.422	
12	4.8		56.5165
14	5.95		
16	7.1	7.96	60.3218
18	12.8	6.4047	
20	22	2.1273	67.2746
22	22.9	0	
29	15.6	0	68.3359

A.2 RiboGlu strain with mannose as sole carbon source

Raw data of the experiment using RiboGlu strain with mannose as sole carbon source is shown in Table A.2.

Table A.2: Raw data from RiboGlu strain with mannose as sole carbon source experiment.

OD₆₀₀ was measured manually. Area values (A) of sugar and riboflavin were collected from the HPLC software Chromeleon.

Time[h]	OD ₆₀₀ RiboGlu	A mannose [μ RIU*min]	A riboflavin [μ RIU*min]
0	0.97	17.51	0
2	1.23	17.24	
4	1.24	17.65	4.5
6	1.35	15.81	
8	1.28	16.76	7.43
10	1.39	17.27	
12	1.5	16.98	11.23
14	1.55	16.8	
16	1.59	17.04	26.23
18	1.72	16.7	
20	1.77	16.62	31.23
22	1.84	16.77	
24	2.2	16.29	46.51
26	2.21	16.15	
28	2.24	16.21	76.51
30	2.35	15.98	
32	2.8	15.86	100.03
34	2.5	16.38	
36	2.5	16.15	89.49
38	2.7	16.21	
40	2.8	15.91	102.37
42	2.9	14.02	
44	3	12.69	140.87
46	2.9	13.63	
48	2.9	14.38	189.01
50	3.2	13.9	
52	3.3	14.04	212.51
56	3.4	14.45	
58	3.6	14.1	259.88
60	3.4	14.08	

Time[h]	OD ₆₀₀	RiboGlu	A mannose [μ RIU*min]	A riboflavin [μ RIU*min]
62	3.8		13.85	238.7
64	3.8		13.53	
66	4		12.46	300.53
68	4.3		12.96	
70	4.3		12.1	305.97
72	4.5		13.92	
74	3.7		12.86	
76	2.2		12.15	
78				305.85
82	4.7		11.96	
84				383.94
88	5		11.48	
90				377.83
94	5.8		10.70	
96				425.86
100	5.9		10.03	
102				451.85
106	6.3		8.96	
108				483.48
112	6.5		8.29	
114				507.68
118	7.2		8.10	
120				558.88
124	7.2		8.46	
126				589.96
130	7.1		5.87	663.25
134				665.34
136	7.9		3.28	
140				667.89
142	7.2		2.82	

A.3 RiboGlu strain with synthetic SSL as carbon source

Raw data of the experiment using RiboGlu strain with synthetic SSL as sole carbon source is shown in Table A.3.

Table A.3: Raw data from RiboGlu strain with synthetic SSL as carbon source experiment. OD₆₀₀ was measured manually. Area values (A) of sugars and riboflavin were collected from the HPLC software Chromeleon.

Time[h]	OD ₆₀₀ RiboGlu	A glucose [μ RIU*min]	A mannose [μ RIU*min]	A xylose [μ RIU*min]	A riboflavin [μ RIU*min]
0	0.93	12.11	10.93	9.91	21.88
2					
4	1.84	12.68	11.77	10.68	19.63
6					
8	3.10	12.06	12.27	11.13	20.62
10	4.00				
12		9.20	10.36	9.65	22.24
14	6.90				
16		8.95	14.16	12.68	26.54
18	15.05				
20		0.85	9.17	8.48	33.03
22	28.60				
24	26.60		7.44	8.71	40.72
26					
28	26.60	0.12	6.05	9.78	38.67
30					
32	25.80		4.58	7.85	34.48
34					
36		0.07	5.01	9.92	38.25
38	26.00				
40	26.20		3.73	8.57	34.79
42	25.80				
44			3.14	9.33	32.53
46	26.40				
48	27.20		2.77	9.54	30.18
50					
52	23.20		1.98	8.79	31.54
54					
56					31.70
58					
60	24.40		1.30	9.31	34.21
62					
64			1.14	8.67	34.93
66					
68	24.40		1.07	8.84	36.71

A.4 RiboMan strain with glucose as sole carbon source

Raw data of the experiment using RiboMan strain with glucose as sole carbon source is shown in Table A.4.

Table A.4: Raw data from RiboMan strain with glucose as sole carbon source experiment. OD₆₀₀ was measured manually. Area values (A) of sugar and riboflavin were collected from the HPLC software Chromeleon.

Time[h]	OD ₆₀₀ RiboMan	A glucose [μ RIU*min]	A riboflavin [μ RIU*min]
0	1.28	13.894	3
2	1.48	13.7453	
4	1.8	13.4247	23.7483
6	2.24	12.8798	
8	2.6	12.2388	39.5568
10	2.75	11.9986	
12	2.9		51.974
14	3.2	10.4679	
16	3.2	10.1234	60.3971
18	4	9.3425	
20	5.7		64.6756
22	8.9	8.754	
29	15.75	6.1674	88.1614
31	17.85	4.1265	
33	28.95		91.8552
35	27.45	2.0065	

A.5 RiboMan strain with mannose as sole carbon source

Raw data of the experiment using RiboMan strain with mannose as sole carbon source is shown in Table A.5.

Table A.5: Raw data from RiboMan strain with mannose as sole carbon source experiment. OD₆₀₀ was measured manually. Area values (A) of sugar and riboflavin were collected from the HPLC software Chromeleon.

Time[h]	OD ₆₀₀ RiboMan	A mannose [μ RIU*min]	A riboflavin [μ RIU*min]
0	1.14	17.54	6.34
2	1.43	15.93	
4	1.89	13.27	9.35
6	2.45	16.26	
8	3.2	15.94	18.82
10	3.4	15.53	
12	3.7	12.44	23.66
14	4.8	13.27	
16	4.8	11.93	55.22
18	7.2	11.68	
20	8.8	9.1	78.5
22	10.9	7.74	
24	12.1	6.66	132.14
26	12.8	5.8	
28	11.6	5.58	185.47
30	11.8	17.65	
32	12	4.87	242.26
34	11.4	4.62	
36	10.5	4.44	322
38	11.4	4.03	
40	11	3.76	385.63
42	11.7	3.35	
44	12.4	3.12	391.49
46	11.1	2.76	
48	10	2.2	369.08
50	9.2	1.79	
52	10.4	1.42	379.47
54	9.9	0	
56		0	364.06
58	9.2	0.65	
60	10.6	0.34	354.44
62	9.4	0.06	
64	10.4	0.019	378.32
66	10.4	0.0178	
68	10.7	0.0149	374.74

A.6 RiboMan strain with synthetic SSL as carbon source

Raw data of the experiment using RiboMan strain with synthetic SSL as sole carbon source is shown in Table A.6.

Table A.6: Raw data from RiboMan strain with synthetic SSL as carbon source experiment. OD₆₀₀ was measured manually. Area values (A) of sugars and riboflavin were collected from the HPLC software Chromeleon.

Time[h]	OD ₆₀₀ RiboMan	A glucose [μ RIU*min]	A mannose [μ RIU*min]	A xylose [μ RIU*min]	A riboflavin [μ RIU*min]
0	0,84	13,21	11,90	10,90	41,70
2					
4	2,46	11,04	10,51	9,64	44,91
6					
8	3,68	11,11	11,72	10,67	43,86
10	4,70				
12		8,30	9,79	9,74	44,47
14	7,10				
16		8,64	13,45	12,64	45,82
18	9,75				
20		4,72	11,13	10,33	48,86
22	13,20				
24	12,40	2,39	15,12	13,89	52,23
26					
28	13,40	0,08	9,58	7,91	55,66
30					
32	10,60		11,58	10,93	52,41
34					
36			12,70	12,60	53,30
38	11,80				
40	16,00		8,11	10,07	51,07
42	21,00				
44			8,16	10,87	53,26
46	21,60				
48	22,40	0,02	6,13	9,31	54,36
50					
52	21,20	0,03	4,78	8,56	53,15
54					
56					45,78
58					
60	21,20		3,76	8,80	52,56

Appendix A - RiboMan strain with synthetic SSL as carbon source

Time[h]	OD ₆₀₀	RiboMan	A glucose [μ RIU*min]	A mannose [μ RIU*min]	A xylose [μ RIU*min]	A riboflavin [μ RIU*min]
62						
64				3,07	8,24	53,12
66						
68		21,40		2,97	10,31	55,81
70						
72				2,09	9,33	55,14
74						
76		22,00		1,81	9,15	57,12
78						
80				1,28	8,24	56,60
82						
84		23,20		1,04	8,08	57,42
86						
88				1,22	11,29	63,28
90						
92		23,00		0,68	8,71	62,35

A.7 RiboXyl strain with glucose as sole carbon source

Raw data of the experiment using RiboXyl strain with glucose as sole carbon source is shown in Table A.7.

Table A.7: Raw data from RiboXyl strain with glucose as sole carbon source experiment. OD₆₀₀ was measured manually. Height values (H) of sugar and riboflavin were collected from the HPLC software Chromeleon.

Time[h]	OD ₆₀₀	RiboXyl	H glucose [μ RIU]	H riboflavin [μ RIU]
0	0.4		28.52	17.5
2	1.29		27.94	35.61
4	1.54		27.69	
6	1.64		27.71	55.78
8	1.79		27.11	
10	1.84		27.08	72.03
12	1.91		26.86	
14	2.02		26.44	78.6
16	2.12		26.11	101.77
18	2.23		25.96	
20	2.2		25.22	148.2
22	2.5		25.57	
24	2.5		24.87	
26			24.66	165.4
28	2.7			
30	2.9		24.38	179
32	3.1		24.29	
34	3.5		23.84	183.88
36	3.7		23.05	186
38	4.5		21.69	
40	5.4		17.25	
42			15.16	195.96
44	7.1		12.75	
46	8.3			215.99
48	10.1		9.95	
50	11.4		7.6	217.58
52	13.2		4.42	
54	14.3		1.49	220.84
56	16.1		0	236.06
58	15.2		0.28	
60	14.5		0.37	235.57

A.8 RiboXyl strain with xylose as sole carbon source

Raw data of the experiment using RiboXyl strain with xylose as sole carbon source is shown in Table A.8.

Table A.8: Raw data from RiboXyl strain with xylose as sole carbon source experiment.

OD₆₀₀ was measured manually. Height values (H) of sugar and riboflavin were collected from the HPLC software Chromeleon.

Time[h]	OD ₆₀₀ RiboXyl	H xylose [μ RIU]	H riboflavin [μ RIU]
0	1.34	24.24	20.87
2	1.47	23.92	
4	1.75	22.71	38.83
6	1.94	22.42	
8	2.6	21.41	42.94
10	3.5	20.65	
12	4.4	19.13	53.92
14	5.6	17.82	
16	6.9	16.13	79.24
18	8.1	14.33	83.39
20	9.5	12.08	
22	11.5	9.98	138.25
24	13	7.59	
26	16.4	4.75	152.27
28	16.7	1.95	
30	19.2	0.24	338.09
32	18.2	0.13	
34	18	0	330.75
36	18.4	0	379.5
38	19.6	0	
40	19.2	0	359.07

A.9 RiboXyl strain with synthetic SSL as carbon source

Raw data of the experiment using RiboXyl strain with synthetic SSL as sole carbon source is shown in Table A.9.

Table A.9: Raw data from RiboXyl strain with synthetic SSL as carbon source experiment. OD₆₀₀ was measured manually. Area values (A) of sugars and riboflavin were collected from the HPLC software Chromeleon.

Time[h]	OD ₆₀₀ RiboXyl	A glucose [μ RIU*min]	A mannose [μ RIU*min]	A xylose [μ RIU*min]	A riboflavin [μ RIU*min]
0	0.94	15.62	12.99	12.89	56.05
2					
4	2.57	13.37	14.87	14.33	56.46
6					
8	3.55	12.24	10.96	10.59	55.64
10	4.75				
12		9.16	10.87	10.49	58.60
14	7.95				
16		3.17	10.89	9.36	64.67
18	14.85				
20		2.10	9.24	7.43	73.47
22	30.40				
24	31.60		7.41	4.38	97.37
26					
28	32.60	0.10	6.84	2.45	90.14
30		0.10			
32	31.40		6.21	1.79	83.50
34					
36			5.04	1.32	79.32
38	29.00				
40	29.50		4.43	1.10	78.43
42	31.00				
44			3.11	0.84	82.85
46	33.00				
48	24.00		2.39	0.80	77.49
50					
52	34.00		0.40	0.57	78.55
54					
56			0.05	0.52	83.01
58					
60	32.60		0.05	0.37	82.63
62					
64			0.04	0.30	94.12

A.10 Sugar and riboflavin standards

To calculate the concentrations of sugars and riboflavin, data obtained from HPLC chromatograms of sugar and riboflavin standards of known concentrations were used. The data used for RiboGlu and RiboMan strains is presented in Table A.10.

Table A.10: Standards of sugars, riboflavin, and area peaks (A) from HPLC chromatograms.

The data was used for calculating sugar and riboflavin concentrations from experiments using RiboGlu and RiboMan strains.

Glucose				
C_{Glucose} [mM]	25.000	12.500	6.250	3.125
A_{Glucose} [$\mu\text{RIU} \cdot \text{min}$]	28.674	12.447	6.147	3.061
$C_{\text{Riboflavin}}$ [mM]	0.1000	0.0100	0.0050	0.0025
$A_{\text{Riboflavin}}$ [$\mu\text{RIU} \cdot \text{min}$]	5471.52	651.82	359.43	198.36
Mannose				
C_{Mannose} [mM]	25.000	12.500	6.250	3.125
A_{Mannose} [$\mu\text{RIU} \cdot \text{min}$]	42.940	19.24	11.570	4.350
$C_{\text{Riboflavin}}$ [mM]	0.00500	0.00250	0.00125	
$A_{\text{Riboflavin}}$ [$\mu\text{RIU} \cdot \text{min}$]	2541.71	1174.330	553.34	
Synthetic SSL				
C_{Sugars} [mM]	25.000	12.500	6.250	3.125
A_{Glucose} [$\mu\text{RIU} \cdot \text{min}$]	28.11	15.21	6.05	2.96
A_{Mannose} [$\mu\text{RIU} \cdot \text{min}$]	33.66		7.38	3.55
A_{Xylose} [$\mu\text{RIU} \cdot \text{min}$]	26.76	2.32	5.35	2.56
$C_{\text{Riboflavin}}$ [mM]	0.0100	0.0050	0.0025	
$A_{\text{Riboflavin}}$ [$\mu\text{RIU} \cdot \text{min}$]	344.86	168.20	94.84	

The data used for RiboXyl strain is presented in Table A.11.

Table A.11: Standards of sugars, riboflavin, area (A) and height (H) peaks from HPLC chromatograms. The data was used for calculating sugar and riboflavin concentrations from experiments using RiboXyl strains.

Glucose				
C_{Glucose} [mM]	25,000	12,500	6,250	3,125
H_{Glucose} [mM]	56,61	23,84	12,39	5,53
$C_{\text{Riboflavin}}$ [mM]	0,0100	0,0050	0,0025	
$H_{\text{Riboflavin}}$ [$\mu\text{RIU} \cdot \text{min}$]	2301	1121,7	608,34	
Xylose				
C_{Xylose} [mM]	25,000	12,500	6,250	3,125
H_{Xylose} [mM]	39,24	15,75	7,87	3,83
$C_{\text{Riboflavin}}$ [mM]	0,01	0,005	0,0025	
$H_{\text{Riboflavin}}$ [$\mu\text{RIU} \cdot \text{min}$]	2301	1121,7	608,34	
Synthetic SSL				
C_{Sugars} [mM]	25.000	12.500	6.250	3.125
A_{Glucose} [$\mu\text{RIU} \cdot \text{min}$]	28.11	15.21	6.05	2.96
A_{Mannose} [$\mu\text{RIU} \cdot \text{min}$]	33.66		7.38	3.55
A_{Xylose} [$\mu\text{RIU} \cdot \text{min}$]	26.76	2.32	5.35	2.56
$C_{\text{Riboflavin}}$ [mM]	0.0100	0.0050	0.0025	
$A_{\text{Riboflavin}}$ [$\mu\text{RIU} \cdot \text{min}$]	344.86	168.20	94.84	

Appendix B Calculating cell concentration

Under the conditions used in the experiments performed in the specialization project, the concentration of cell dry weight (CDW) was calculated from the optical density using a correlation factor of $\text{CDW} [\text{g/L}] = 0.3634 \times \text{OD}_{600}$ [Unpublished data]. Similar values of the correlation factor has been found in similar conditions [90, 91].

Appendix C Stock solutions

C.1 Minimal medium - CGXII

CGXII is a minimal medium used for for microplate, flask, and bioreactor fermentations with *C. glutamicum* strains. The medium was prepared using the recipe showed in Table C.1.

Table C.1: Recipe for CGXII buffer for batch reactor, where the total volume of the fermentation broth was 5 L. CGXII, trace elements, biotin, antibiotics and ITPG (See Table C.4) represents 75% of the total broth. The pH was corrected with KOH to 7.00. Recipes of stock solutions of Ca and Mg are attached in Appendix Section C.4.

Component	Concentration	Unit	Measure	Unit
(NH ₄) ₂ SO ₄	10	g/L	50	g
Urea	5	g/L	25	g
KH ₂ PO ₄	0.5	g/L	2.5	g
K ₂ HPO ₄	0.5	g/L	2.5	g
Ca-stock 1000X	1	mL/L	5	mL
Mg-stock 1000X	1	mL/L	5	mL
Fill up with H ₂ O to reach total volume of			3740	mL

C.2 Complex Medium - BHI

The complex media BHI (Brain heart infusion) was used for the precultures of *C. glutamicum* strains. The recipe of the BHI stock is showed in Table C.2.

Table C.2: Recipe for 1 liter stock solution of BHI medium for batch reactor.

Component	Concentration	Unit	Measure	Unit
BHI	37	g/L	37	g
Fill up with H ₂ O to reach total volume of			1000	mL

C.2.1 Carbon source solution

Glucose, mannose, xylose and a combination of them as a synthetic SSL were used for the bioreactor fermentations. The carbon sources were prepared using the recipe shown in Table C.3, and filtered for sterilization.

Table C.3: Recipe of carbon source stock solution for batch reactor. Carbon sources used for the experiments were glucose, mannose, xylose or a combination of them.

Component	Concentration	Unit	Measure	Unit
Carbon source	40	%	200	g
Fill up with H ₂ O to reach total volume of			500	mL

C.3 Final solution in reactor after sterilization

The final solution used for the feed reactor after autoclave sterilization was prepared using the recipe shown in Table C.4.

Table C.4: Recipe of final solution added to batch reactor after sterilization. The recipe for CGXII and C-source are found in Table C.1 and C.3 respectively. Recipes of stock solutions of trace elements, biotin, Kanamycin, Spectinomycin and IPTG are attached in Appendix Section C.4.

Component	Concentration	Unit	Measure	Unit
Trace element solution	1	mL/L	1	mL
Biotin solution	1	mL/L	1	mL
Kanamycin stock	0.5	mL/L	0.5	mL
Spectinomycin stock	1	mL/L	1	mL
IPTG-stock	1	mL/L	10	μ L
CGXII			745.5	mL
C-source	2	%	200	mL
Inoculum			50	mL
Fill up with H ₂ O to reach total volume of			1000	mL

The final solution used for the main reactor after autoclave sterilization was prepared using the recipe shown in Table C.5.

Table C.5: Recipe of final solution added to main reactor after sterilization. The recipe for CGXII and C-source are found in Table C.1 and C.3 respectively. In this case the C-source was synthetic SSL (2% of glucose + 2% of mannose and 2% of xylose). Recipes of stock solutions of trace elements, biotin, Kanamycin, Spectinomycin and IPTG are attached in Appendix Section C.4.

Component	Concentration	Unit	Measure	Unit
Trace element solution	1	mL/L	700	μL
Biotin solution	1	mL/L	700	μL
Kanamycin stock	0.5	mL/L	350	μL
Spectinomycin stock	1	mL/L	700	μL
IPTG-stock	1	mL/L	7	μL
CGXII			521.85	mL
C-source	6	%	178.15	mL
Inoculum			50	mL
Fill up with H ₂ O to reach total volume of			700	mL

C.4 Stocks used in minimal media and solution of reactor

Recipes of the stocks used for minimal media, and solution of reactor (Table C.1, C.4 are presented in the following sections.

C.4.1 Biotin Solution

The recipe of the biotin solution used is presented in Table C.6.

Table C.6: Recipe of biotin solution used in solution of reactor (Table C.4)

Component	Concentration	Unit	Measure	Unit
Biotin	0.2	g/L	0.02	g
Fill up with NaOH to reach a total volume of	1	M	100	mL

C.4.2 Trace elements solution

The recipe of the trace elements solution used is presented in Table C.7.

Table C.7: Recipe of trace elements solution used in solution of reactor (Table C.4)

Component	Concentration	Unit	Measure	Unit
FeSO ₄ * 7 H ₂ O	16.4	g/L	1.64	g
MnSO ₄ * H ₂ O	10	g/L	1	g
ZnSO ₄ * 7 H ₂ O	1	g/L	0.1	g
CuSO ₄ * 5 H ₂ O	0.31	g/L	0.031	g
NiCl ₂ * 6 H ₂ O	0.02	g/L	0.002	g
Fill up with H ₂ O to reach a total volume of			100	mL

C.4.3 Ca-stock

The recipe of the Ca-stock solution used is presented in Table C.8.

Table C.8: Recipe of Ca-stock solution used in minimal media (Table C.1)

Component	Concentration	Unit	Measure	Unit
CaCl ₂ * 2 H ₂ O	13.25	g/L	1.325	g
Fill up with H ₂ O to reach a total volume of			100	mL

C.4.4 Mg-stock

The recipe of the Mg-stock solution used is presented in Table C.9.

Table C.9: Recipe of Mg-stock solution used in minimal media (Table C.1)

Component	Concentration	Unit	Measure	Unit
MgSO ₄ * 7 H ₂ O	250	g/L	25	g
Fill up with H ₂ O to reach a total volume of			100	mL

C.4.5 IPTG stock

The recipe of the IPTG stock solution used is presented in Table C.10.

Table C.10: Recipe of IPTG stock solution used in solution of reactor (Table C.4)

Component	Concentration	Unit	Measure	Unit
IPTG	23.8	g/L	2.38	g
Fill up with H ₂ O to reach a total volume of			100	mL

C.4.6 Kanamycin stock

The recipe of the Kanamycin stock solution used is presented in Table C.11.

Table C.11: Recipe of Kanamycin stock solution used in solution of reactor (Table C.4)

Component	Concentration	Unit	Measure	Unit
Kanamycin	50	g/L	5	g
Fill up with H ₂ O to reach a total volume of			100	mL

C.4.7 Spectinomycin stock

The recipe of the Spectinomycin stock solution used is presented in Table C.12.

Table C.12: Recipe of Spectinomycin stock solution used in solution of reactor (Table C.4)

Component	Concentration	Unit	Measure	Unit
Spectinomycin	100	g/L	10	g
Fill up with H ₂ O to reach a total volume of			100	mL

Appendix D Parameter estimations including extra terms

Two other versions of parameter estimations were tested, to see if the model describing riboflavin fit better. Parameter estimations were performed where the specific rate of product formation due to maintenance (m_p) was included. The results are showed in Table D.1.

Table D.1: Parameters estimated for the three strains presented in Table 3.1, including m_p . Estimations were based on experiments performed during the specialization project of the fall 2019. Raw data is attached in Appendix Section A.

Parameter	RiboGlu	RiboMan	RiboXyl	Lower constraint	Upper constraint
$\mu_{max,1}$	0.1290	0.0798	0.0678	0	5
$\mu_{max,2}$	0.7222	3.4218	0.0003	0	5
$\mu_{max,3}$	0.0008	0.0008	0.1191	0	5
$K_{s,1}$	0.0725	0.0700	0.0425	0	1000
$K_{s,2}$	520.3251	745.6475	619.6938	0	1000
$K_{s,3}$	867.6271	943.1094	3.7320	0	1000
$Y_{xs,1}$	-0.3783	-0.2408	-0.2391	-1	0
$Y_{xs,2}$	-0.1799	-0.1343	-0.0001	-1	0
$Y_{xs,3}$	-0.0030	-0.0022	-0.2894	-1	0
Y_{px}	0.7953	0.9999	0.9997	0	1
m_p	-0.0005	-0.0047	-0.0091	-1	0

Parameter estimations were performed with three separate theoretical yields of product from biomass ($Y_{px,1}$, $Y_{px,2}$ and $Y_{px,3}$), used in three separate rates of product formation (Equation (2.5)). The results are showed in Table D.2.

Table D.2: Parameters estimated for the three strains presented in Table 3.1, including three separate yields of product from biomass. Estimations were based on experiments performed during the specialization project of the fall 2019. Raw data is attached in Appendix Section A.

Parameter	RiboGlu	RiboMan	RiboXyl	Lower constraint	Upper constraint
$\mu_{max,1}$	0.1289	0.0820	0.0671	0	5
$\mu_{max,2}$	0.7298	4.4082	0.0003	0	5
$\mu_{max,3}$	0.0013	0.0210	0.1086	0	5
$K_{s,1}$	0.0512	0.5396	0.0208	0	1000
$K_{s,2}$	524.0348	957.7716	596.2498	0	1000
$K_{s,3}$	837.0179	931.4301	2.1175	0	1000
$Y_{xs,1}$	-0.3809	-0.2380	-0.2400	-1	0
$Y_{xs,2}$	-0.1716	-0.1341	-0.0001	-1	0
$Y_{xs,3}$	-0.0049	-0.0600	-0.2881	-1	0
$Y_{px,1}$	0.4014	0.5494	0.7027	0	1
$Y_{px,2}$	0.4088	0.6144	0.0889	0	1
$Y_{px,3}$	0.3249	0.1380	0.7424	0	1

Appendix E Previous versions of parameter estimations

E.1 Previous version of parameter estimation of RiboGlu strain

Figure E.1 shows model simulations with previous version of RiboGlu parameters (Table E.1), together with the experimental data when using synthetic SSL.

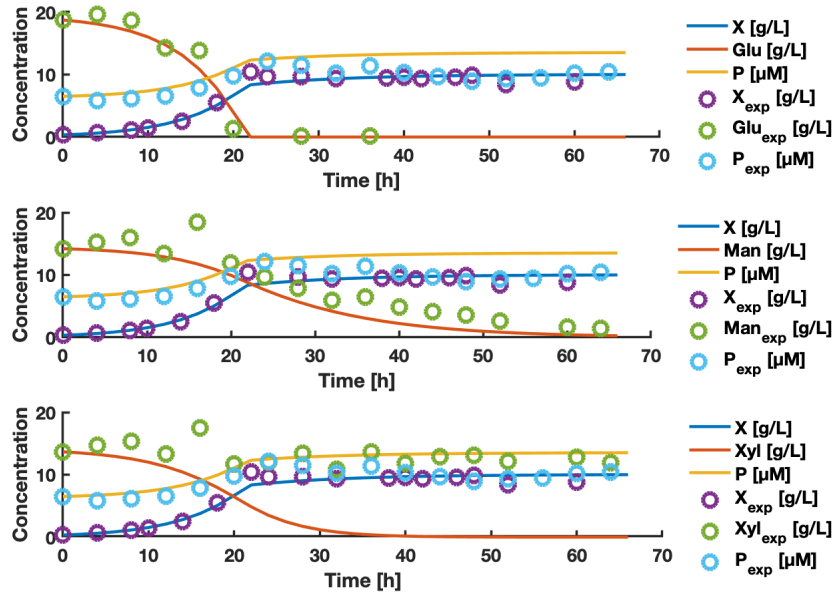


Figure E.1: Previous version of RiboGlu strain model simulations with synthetic SSL as its carbon source. Circles represents experimental data, while solid lines represents the data fitted using estimated parameters. X and Glu represents biomass and glucose concentrations respectively in g/L, P represents product concentration of riboflavin in μM .

The parameters estimated for modeling biomass formation of RiboGlu, sugar consumption and product formation are presented in Table E.1.

Table E.1: Previous version of parameters estimated for the RiboGlu strain. Estimations were based on experiments performed during the specialization project of the fall 2019. Raw data is attached in Appendix Section A. Description of the parameters is presented in Table 3.3.

Parameter	Value	Lower constraint	Upper constraint
$\mu_{max,1}$	0.1224	0	5
$\mu_{max,2}$	1.1261	0	5
$\mu_{max,3}$	0.0545	0	5
$K_{s,1}$	0.1251	0	1000
$K_{s,2}$	851.0659	0	1000
$K_{s,3}$	43.2716	0	1000
$Y_{xs,1}$	-0.3539	-1	0
$Y_{xs,2}$	-0.1589	-1	0
$Y_{xs,3}$	-0.0595	-1	0
Y_{px}	0.7244	0	1

E.1.1 Summary of MPC results based on previous version of RiboGlu parameter estimation

A summary of results obtained from the different simulations using the previous version of the RiboGlu parameters are presented in this section, to compare the results from the different cases.

E.1.1.1 Riboflavin results

Figure E.2 shows the final accumulated amount of riboflavin in the F_{out} stream predicted after 80 hours for the different cases, and the riboflavin yield obtained.

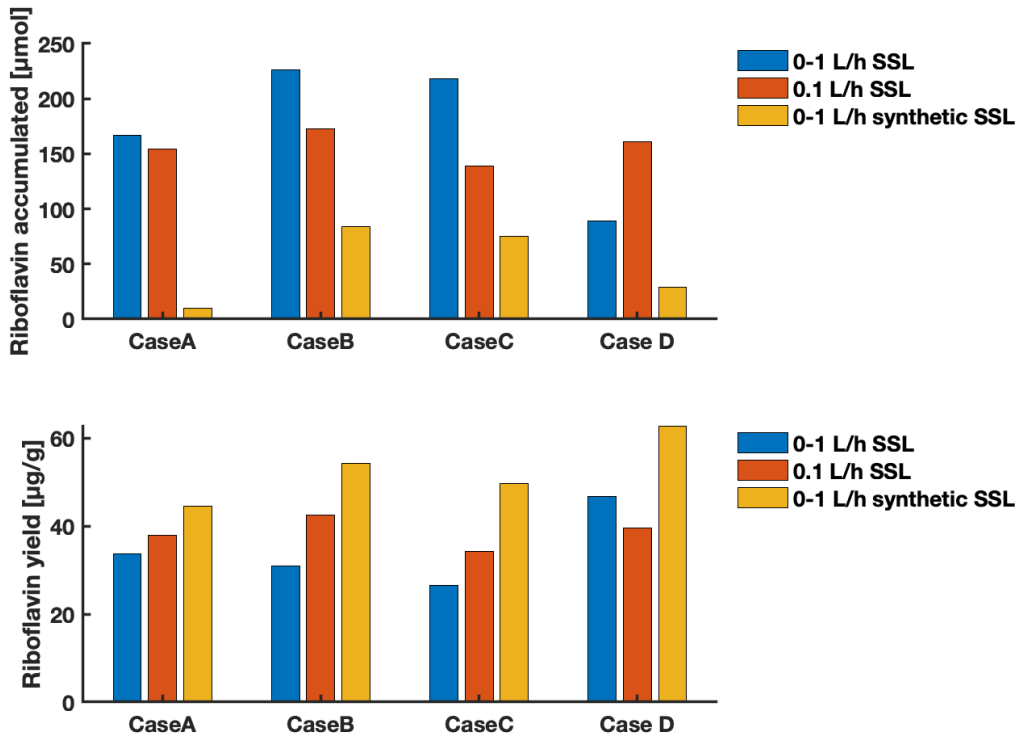


Figure E.2: The upper plot shows the final accumulated amount of riboflavin in the F_{out} stream predicted after 80 hours for the different cases presented in Equation (3.7) to (3.10). The lower plot shows the yield of riboflavin in $\mu\text{g/g}$ sugars obtained after 80 hours. Both plots shows the results obtained using 0-1 L/h SSL (blue bars), 0.1 L/h SSL (orange bars) and 0-1 L/h synthetic SSL (yellow bars). Results are obtained using the previous version of RiboGlu parameters.

E.1.1.2 Biomass results

Figure E.3 shows the predicted yields of biomass obtained from the different cases after 80 hours.

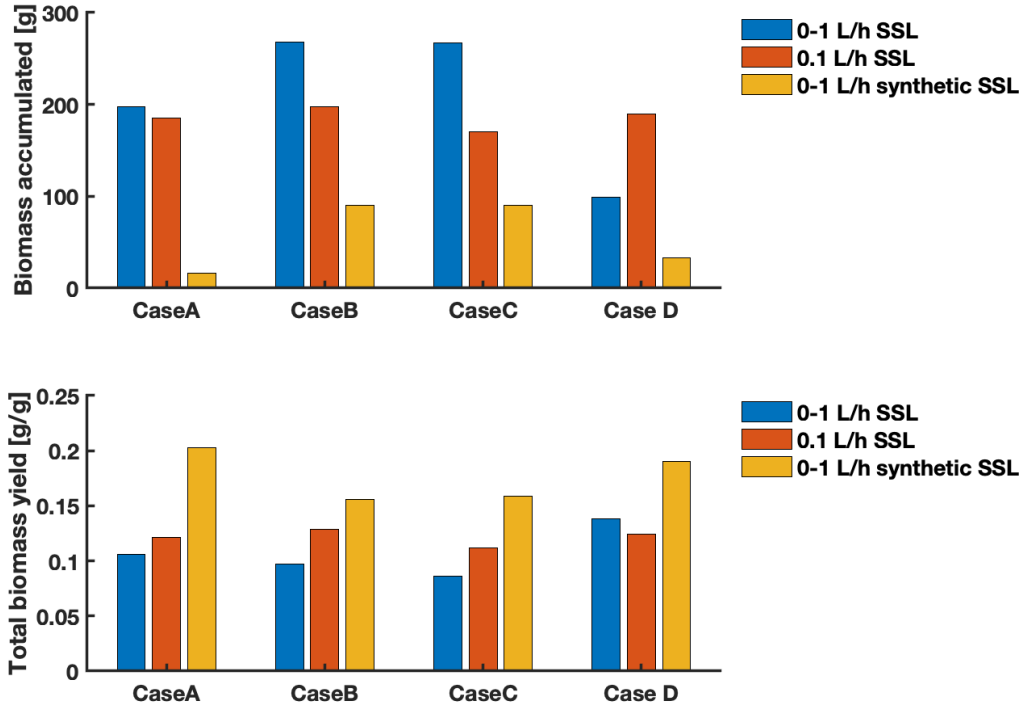


Figure E.3: The upper plot shows the final accumulated amount of biomass in the F_{out} stream predicted after 80 hours for the different cases presented in Equation (3.7) to (3.10). The lower plot shows the biomass yield in g/g sugars predicted after 80 hours. The plot shows the results obtained using 0-1 L/h SSL (blue bars), 0.1 L/h SSL (orange bars) and 0-1 L/h synthetic SSL (yellow bars). Results are obtained using the previous version of RiboGlu parameters.

Figure E.4 shows the predicted volumes of biomass used from the three feeding reactors of the RiboGlu, RiboMan and RiboXyl strains for the different cases.

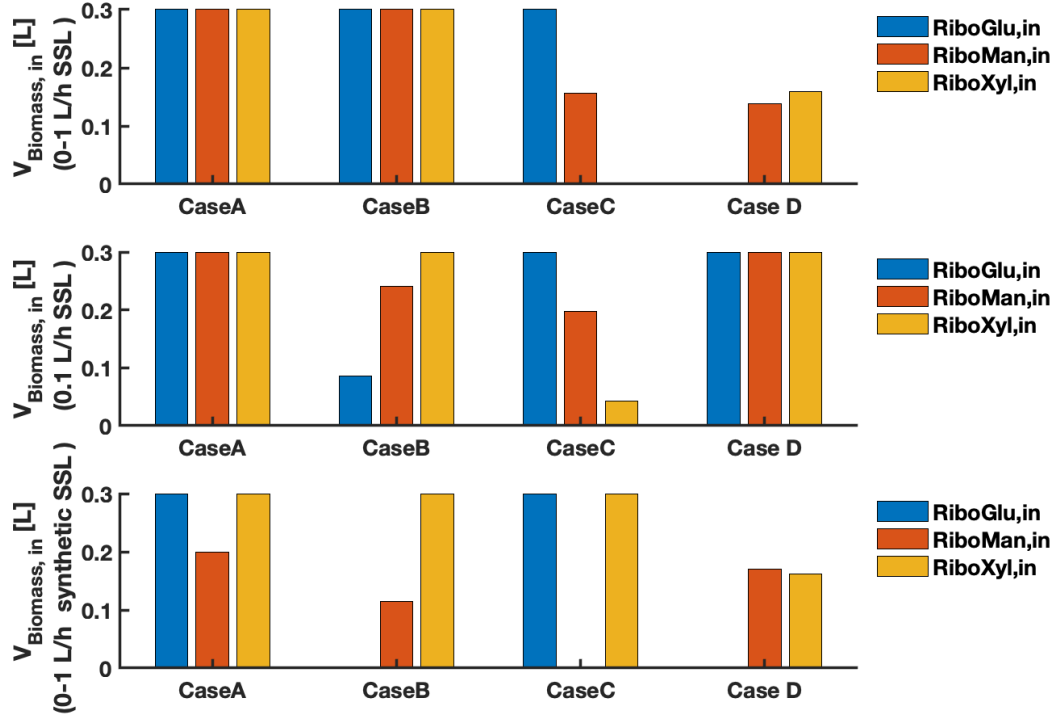


Figure E.4: The plots shows the volume of biomass used to feed the main reactor for the different cases presented in Equation (3.7) to (3.10). The blue, orange and yellow bars represents the volume of the RiboGlu, RiboMan, and RiboXyl strain respectively fed into the main reactor. The upper plot shows the results obtained using 0-1 L/h SSL, the middle plot shows the results obtained using 0.1 L/h SSL, and the lower plot shows the results obtained using 0-1 L/h synthetic SSL. Results are obtained using the previous version of RiboGlu parameters.

E.1.1.3 SSL results

Figure E.5 shows the amount of SSL fed into the reactor for the different cases after 80 hours.

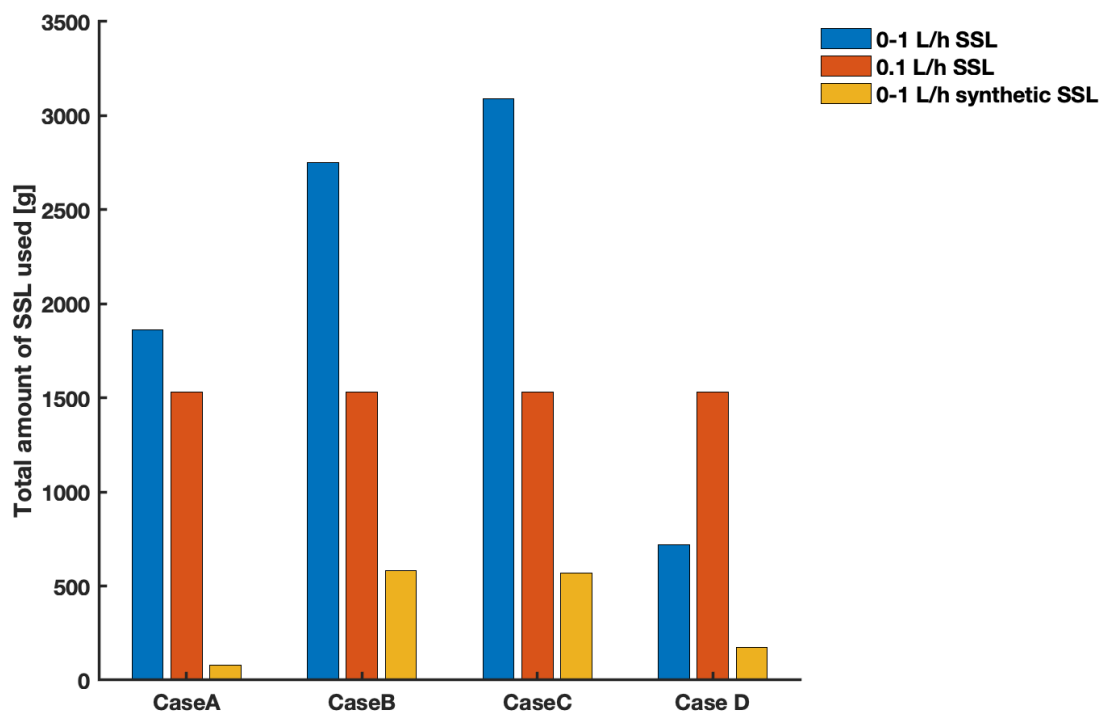


Figure E.5: The plot shows the final amount of SSL used, predicted after 80 hours for the different cases presented in Equation (3.7) to (3.10). The plot shows the results obtained using 0-1 L/h SSL (blue bars), 0.1 L/h SSL (orange bars) and 0-1 L/h synthetic SSL (yellow bars). Results are obtained using the previous version of RiboGlu parameters.

E.2 Changing constraints of RiboMan parameter estimation

The parameters estimated for modeling biomass growth of RiboMan, sugar consumption and product formation using updated constraints are presented in Table E.2.

Table E.2: Parameters estimated for RiboMan strain model with synthetic SSL as its carbon source based on updated constraints. Estimations were based on experiments performed during the specialization project of the fall 2019. Raw data is attached in Appendix Section A. Description of the parameters is presented in Table 3.3.

Parameter	Value	Lower constraint	Upper constraint
$\mu_{max,1}$	0.1079	0	5
$\mu_{max,2}$	1.0000	0	1
$\mu_{max,3}$	0.0008	0	5
$K_{s,1}$	3.3629	0	1000
$K_{s,2}$	800.0000	800	1000
$K_{s,3}$	0.0000	0	1000
$Y_{xs,1}$	-0.2815	-1	0
$Y_{xs,2}$	-0.0832	-1	0
$Y_{xs,3}$	-0.1371	-1	0
Y_{px}	0.8232	0	1

Figure E.6 shows the model simulations of the RiboMan model with the estimated parameters based on new constraints, compared to the experimental data obtained.

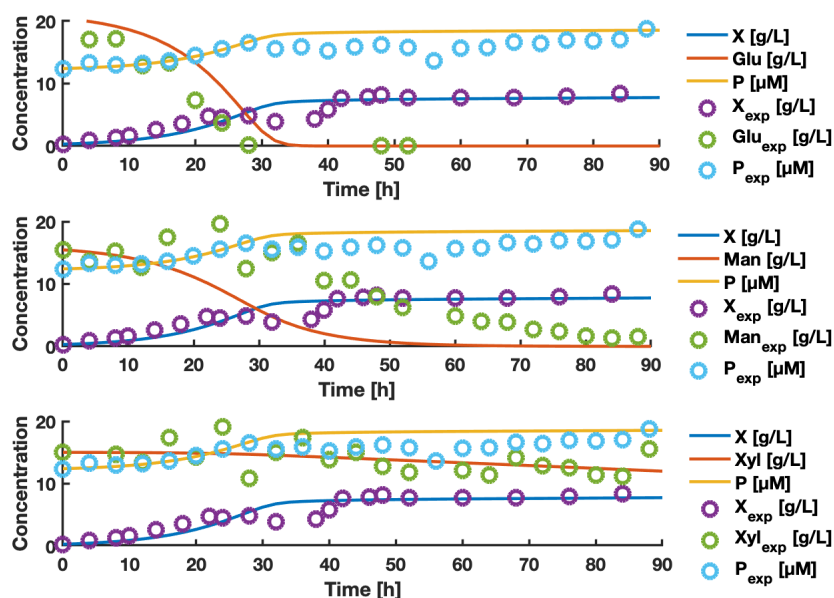


Figure E.6: RiboMan strain model simulations with synthetic SSL as its carbon source based on updated constraints. Circles represents experimental data, while solid lines represents the data fitted using estimated parameters. X, Glu, Man, and Xyl represents biomass, glucose, mannose and xylose concentrations respectively in g/L, P represents product concentration of riboflavin in μ M.

Appendix F MPC results using synthetic SSL

This section shows the MPC results obtained for Case A-D using synthetic SSL and a variable feed stream. In all the cases, the OCP had the time horizon, number of control intervals and number of collocation points outlined in Table 3.7. The constraints used are presented in Table 3.5 and 3.4.

F.1 Case A: Synthetic SSL with flow rate of 0-1 L/h

Figure F.1, F.2 and F.3 shows the inputs, states and riboflavin results respectively obtained from MPC simulations using the objective function of Case A (Equation (3.7)) with a varying synthetic SSL flow rate in the range 0-1 L/h.

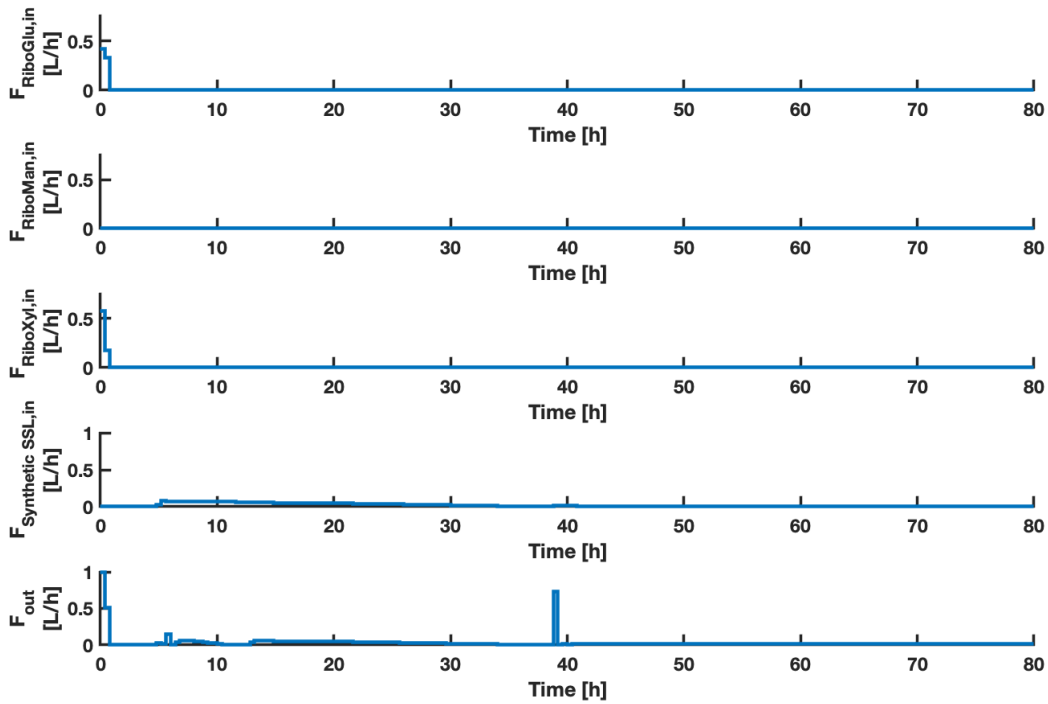


Figure F.1: The plots shows the inputs $F_{RiboGlu,in}$, $F_{RiboMan,in}$, $F_{RiboXyl,in}$, $F_{Synthetic\ SSL,in}$ and F_{out} as a function of time. the MPC inputs were calculated using the objective function of Case A (described in Equation (3.7)). The $F_{Synthetic\ SSL,in}$ had a lower constraint of 0 and an upper constraint of 1 L/h.

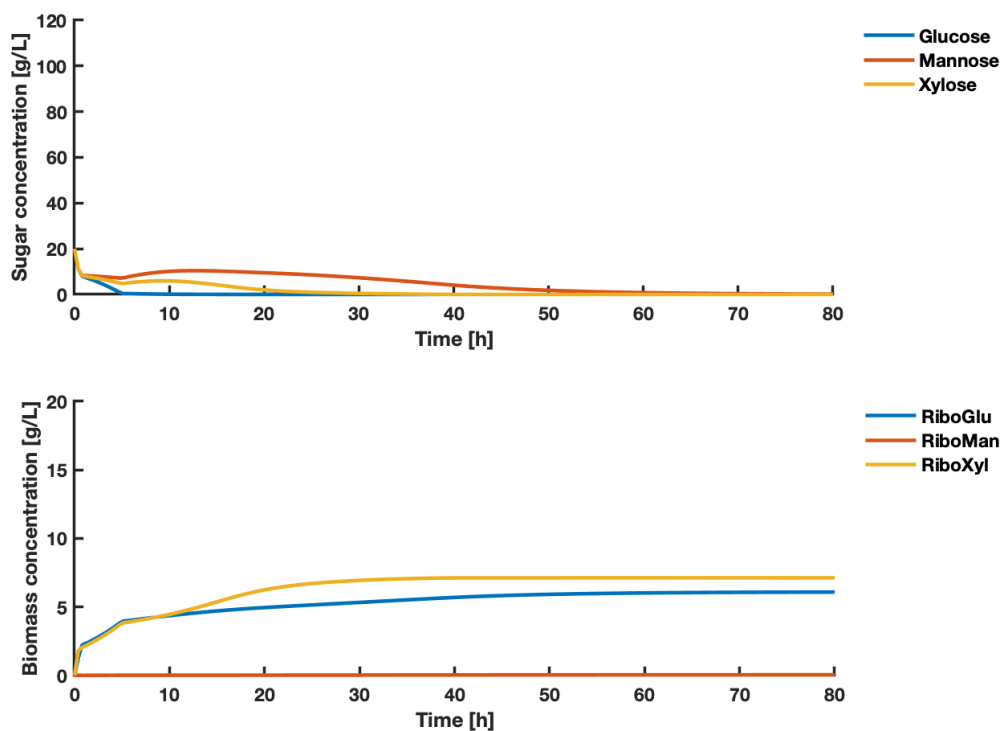


Figure F.2: The upper plot shows the concentrations of the states glucose, mannose, xylose as a function of time. The lower plot shows the concentrations of states RiboGlu, RiboMan and RiboXyl as a function of time. The states are a result of the inputs shown in Figure F.1. MPC states were simulated using the objective function of Case A (described in Equation (3.7)). The $F_{\text{Synthetic SSL},in}$ had a lower constraint of 0 and an upper constraint of 1 L/h.

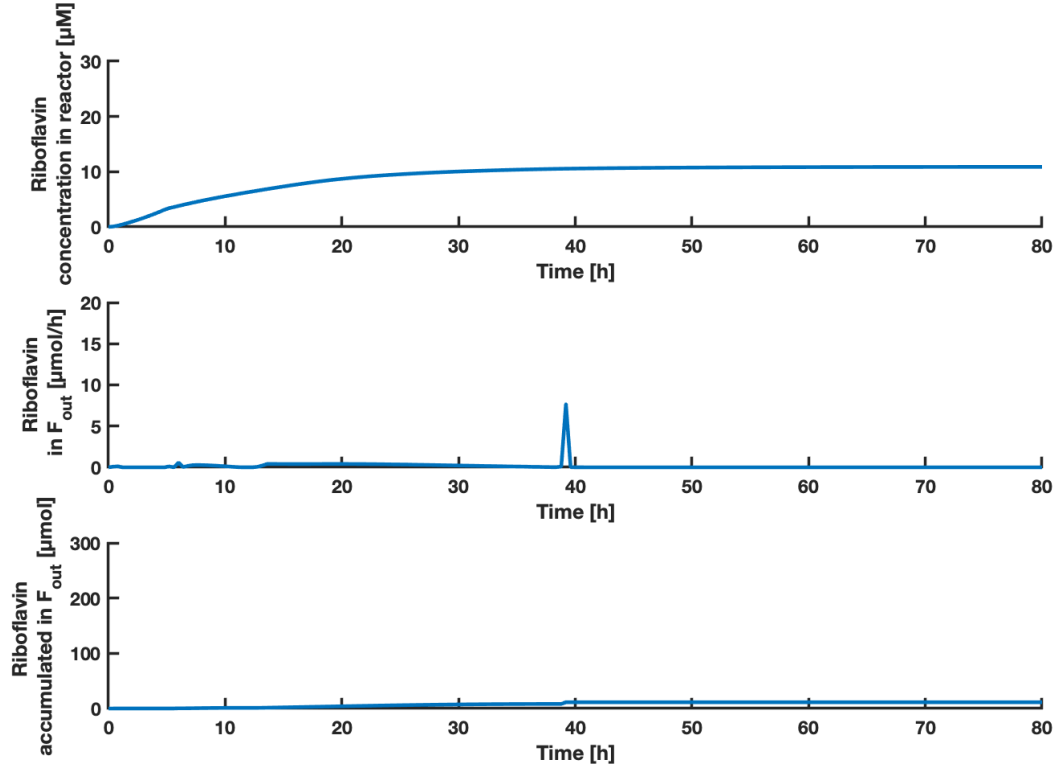


Figure F.3: The upper plot shows the concentration of riboflavin as a function of time. The middle plot shows the amount of riboflavin in the F_{out} stream as a function of time. The lower plot shows the accumulated amount of riboflavin in the F_{out} stream as a function of time. The predicted states of riboflavin concentration in the reactor are a result of the inputs shown in Figure F.1. MPC states were simulated using the objective function of Case A (described in Equation (3.7)). The $F_{Synthetic\ SSL,in}$ had a lower constraint of 0 and an upper constraint of 1 L/h.

For Case A with a synthetic SSL stream of 0-1 L/h, the MPC predicted accumulated amounts of biomass, riboflavin and associated yields as shown in Table F.1.

Table F.1: The table shows the accumulated amounts of RiboGlu, RiboMan and RiboXyl strains, with associated biomass yield, X . The accumulated amount of the product riboflavin P , and the associated yield is shown. The values were calculated based on simulation results for Case A using 0-1 L/h synthetic SSL.

RiboGlu [g]	RiboMan [g]	RiboXyl [g]	X yield [g/g syn SSL]	P [μmol]	P yield [μg/g syn SSL]
7.746	0.05450	9.324	0.2105	11.41	52.77

F.2 Case B: Synthetic SSL with flow rate of 0-1 L/h

Figure F.4, F.5 and F.6 shows the inputs, states and riboflavin results respectively obtained from MPC simulations using the objective function of Case B (Equation (3.8)) with a varying synthetic SSL flow rate in the range 0-1 L/h.

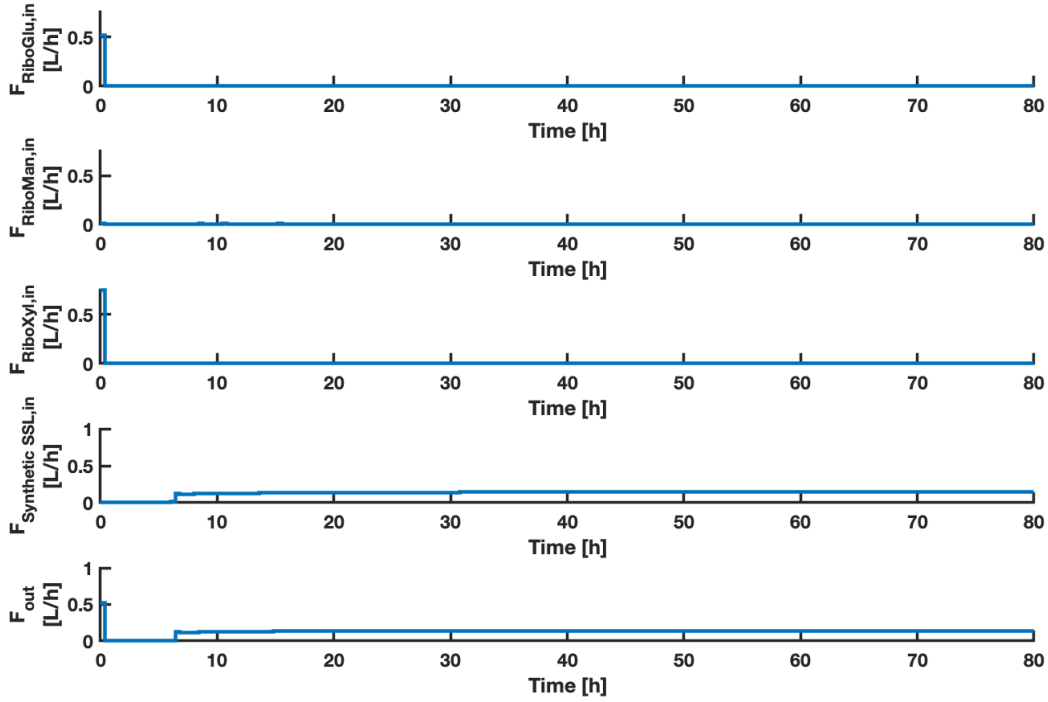


Figure F.4: The plots shows the inputs $F_{RiboGlu,in}$, $F_{RiboMan,in}$, $F_{RiboXyl,in}$, $F_{Synthetic\ SSL,in}$ and F_{out} as a function of time. the MPC inputs were calculated using the objective function of Case B (described in Equation (3.8)). The $F_{Synthetic\ SSL,in}$ had a lower constraint of 0 and an upper constraint of 1 L/h.

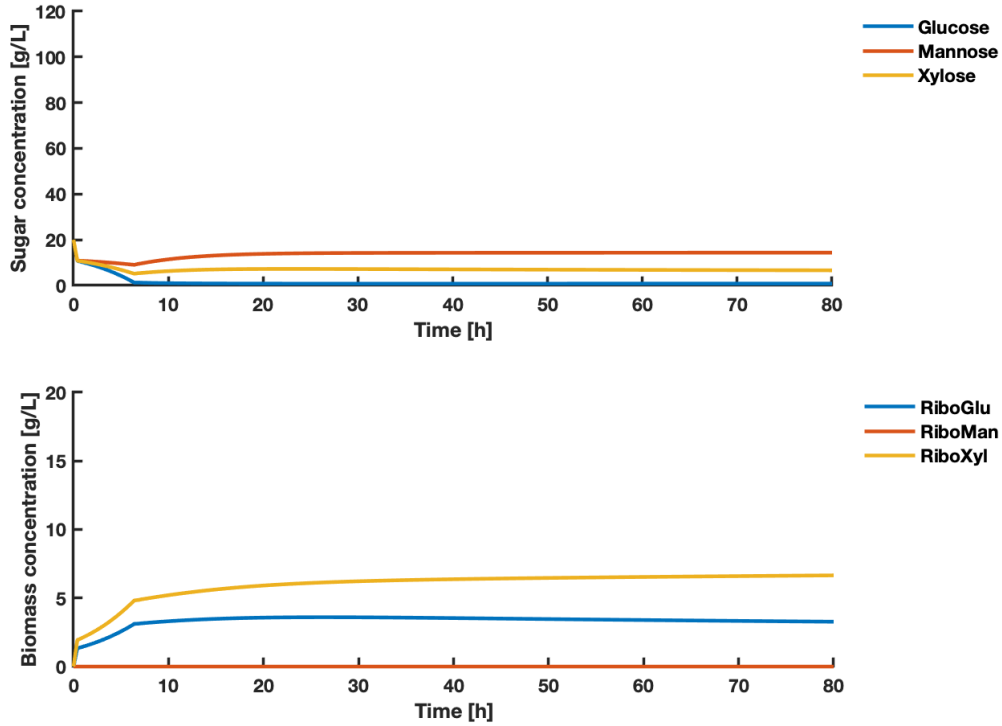


Figure F.5: The upper plot shows the concentrations of the states glucose, mannose, xylose as a function of time. The lower plot shows the concentrations of states RiboGlu, RiboMan and RiboXyl as a function of time. The states are a result of the inputs shown in Figure F.4. MPC states were simulated using the objective function of Case B (described in Equation (3.8)). The $F_{SSL,in}$ had a lower constraint of 0 and an upper constraint of 1 L/h.

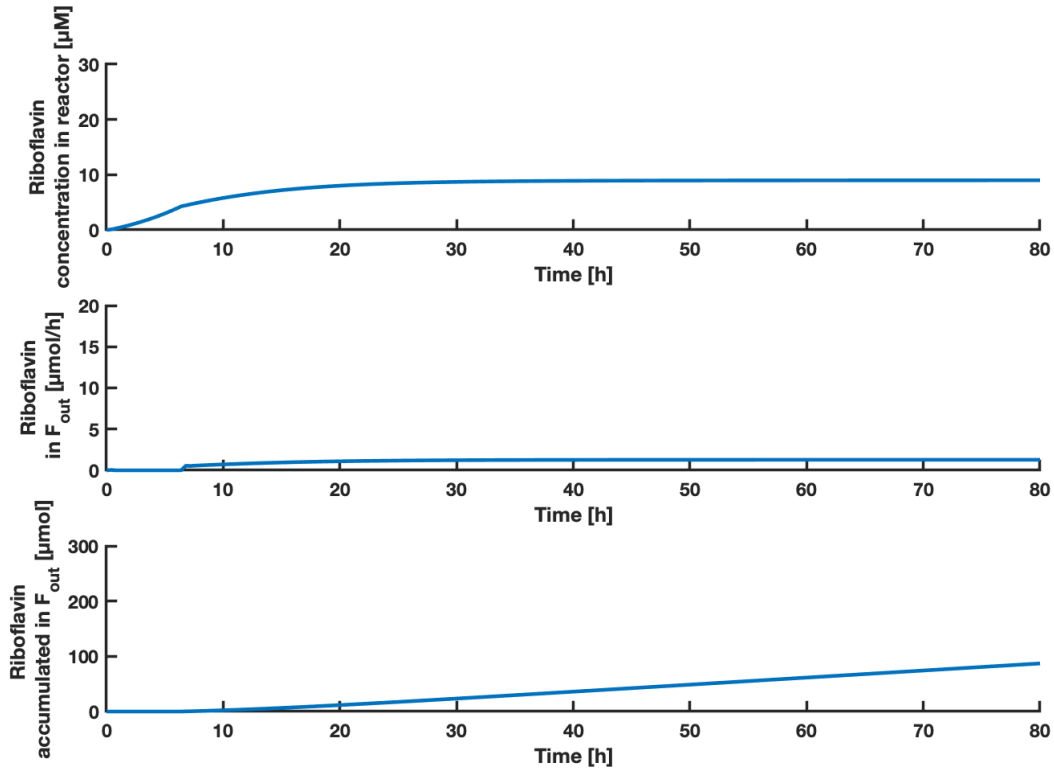


Figure F.6: The upper plot shows the concentration of riboflavin as a function of time. The middle plot shows the amount of riboflavin in the F_{out} stream as a function of time. The lower plot shows the accumulated amount of riboflavin in the F_{out} stream as a function of time. The predicted states of riboflavin concentration in the reactor are a result of the inputs shown in Figure F.4. MPC states were simulated using the objective function of Case B (described in Equation (3.8)). The $F_{Synthetic\ SSL,in}$ had a lower constraint of 0 and an upper constraint of 1 L/h.

For Case B with a synthetic SSL stream of 0-1 L/h, the MPC predicted accumulated amounts of biomass, riboflavin and associated yields as shown in Table F.2.

Table F.2: The table shows the accumulated amounts of RiboGlu, RiboMan and RiboXyl strains, with associated biomass yield, X . The accumulated amount of the product riboflavin P , and the associated yield is shown. The values were calculated based on simulation results for Case B using 0-1 L/h synthetic SSL.

RiboGlu [g]	RiboMan [g]	RiboXyl [g]	X yield [g/g syn SSL]	P [μmol]	P yield [μg/g syn SSL]
35.68	0.00004	64.67	0.1629	87.07	53.20

F.3 Case C: Synthetic SSL with flow rate of 0-1 L/h

Figure F.7, F.8 and F.9 shows the inputs, states and riboflavin results respectively obtained from MPC simulations using the objective function of Case C (Equation (3.9)) with a varying synthetic SSL flow rate in the range 0-1 L/h.

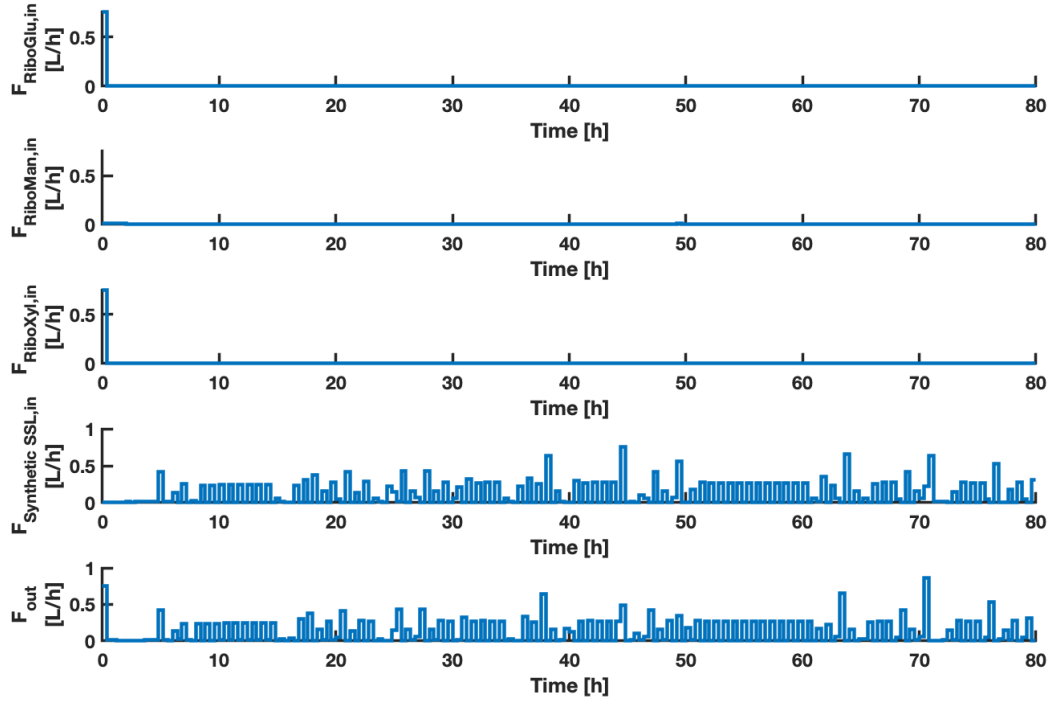


Figure F.7: The plots shows the inputs $F_{RiboGlu,in}$, $F_{RiboMan,in}$, $F_{RiboXyl,in}$, $F_{Synthetic\ SSL,in}$ and F_{out} as a function of time. the MPC inputs were calculated using the objective function of Case C (described in Equation (3.9)). The $F_{Synthetic\ SSL,in}$ had a lower constraint of 0 and an upper constraint of 1 L/h.

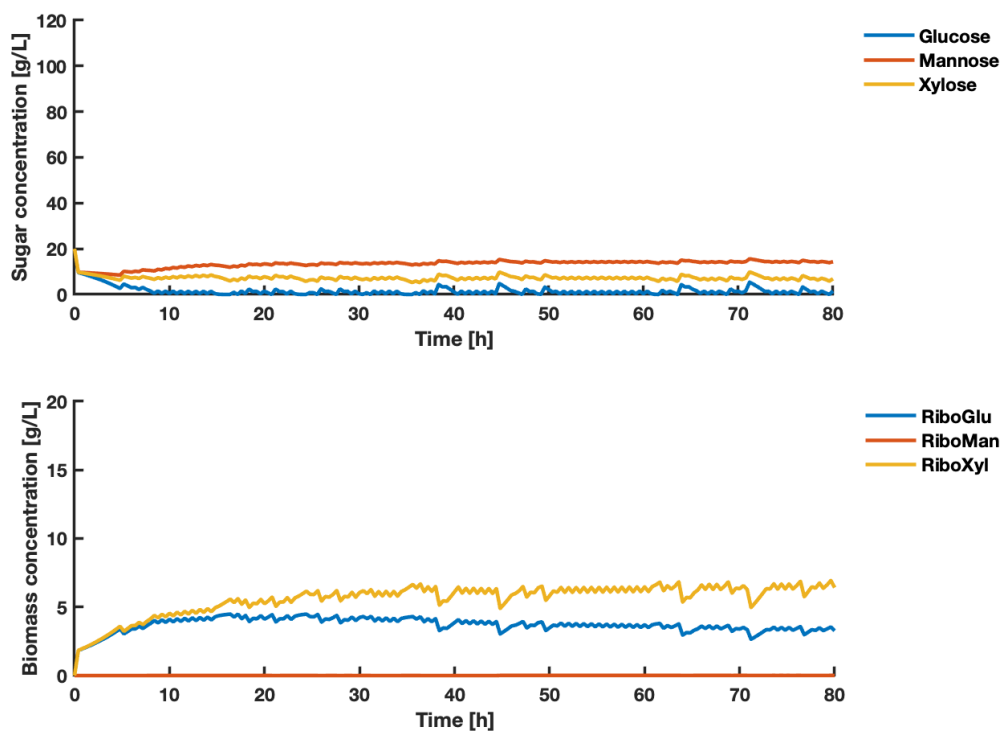


Figure F.8: The upper plot shows the concentrations of the states glucose, mannose, xylose as a function of time. The lower plot shows the concentrations of states RiboGlu, RiboMan and RiboXyl as a function of time. The states are a result of the inputs shown in Figure F.7. MPC states were simulated using the objective function of Case C (described in Equation (3.9)). The $F_{\text{Synthetic SSL},in}$ had a lower constraint of 0 and an upper constraint of 1 L/h.

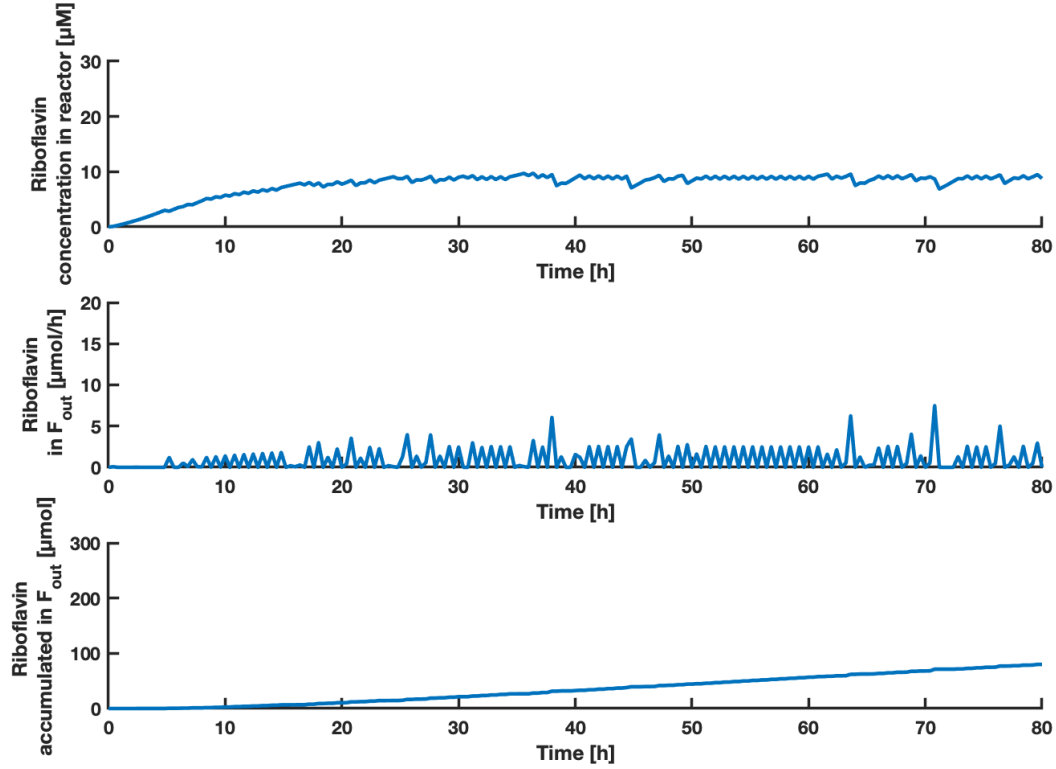


Figure F.9: The upper plot shows the concentration of riboflavin as a function of time. The middle plot shows the amount of riboflavin in the F_{out} stream as a function of time. The lower plot shows the accumulated amount of riboflavin in the F_{out} stream as a function of time. The predicted states of riboflavin concentration in the reactor are a result of the inputs shown in Figure F.7. MPC states were simulated using the objective function of Case C (described in Equation (3.9)). The $F_{Synthetic\ SSL,in}$ had a lower constraint of 0 and an upper constraint of 1 L/h.

For Case C with a synthetic SSL stream of 0-1 L/h, the MPC predicted accumulated amounts of biomass, riboflavin and associated yields as shown in Table F.3.

Table F.3: The table shows the accumulated amounts of RiboGlu, RiboMan and RiboXyl strains, with associated biomass yield, X . The accumulated amount of the product riboflavin P , and the associated yield is shown. The values were calculated based on simulation results for Case C using 0-1 L/h synthetic SSL.

RiboGlu [g]	RiboMan [g]	RiboXyl [g]	X yield [g/g syn SSL]	P [μ mol]	P yield [μ g/g syn SSL]
36.90	0.04930	57.03	0.1670	79.93	53.45

F.4 Case D: Synthetic SSL with flow rate of 0-1 L/h

Figure F.10, F.11 and F.12 shows the inputs, states and riboflavin results respectively obtained from MPC simulations using the objective function of Case D (Equation (3.10)) with a varying synthetic SSL flow rate in the range 0-1 L/h.

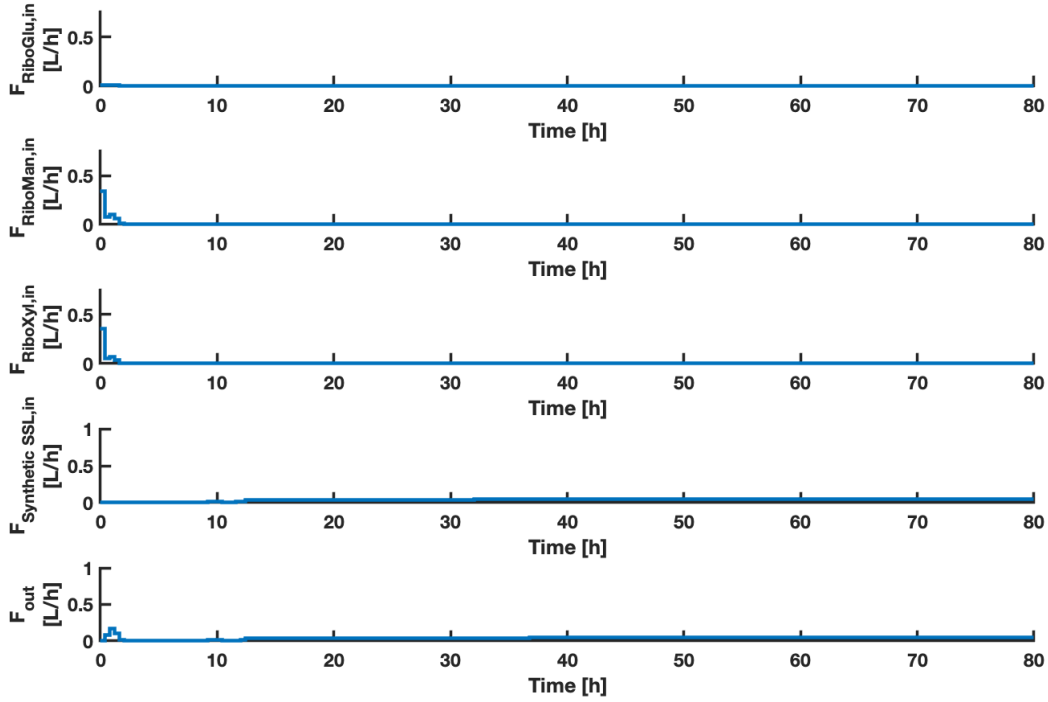


Figure F.10: The plots shows the inputs $F_{RiboGlu,in}$, $F_{RiboMan,in}$, $F_{RiboXyl,in}$, $F_{SSL,in}$ and F_{out} as a function of time. the MPC inputs were calculated using the objective function of Case D (described in Equation (3.10)). The $F_{SSL,in}$ had a lower constraint of 0 and an upper constraint of 1 L/h.

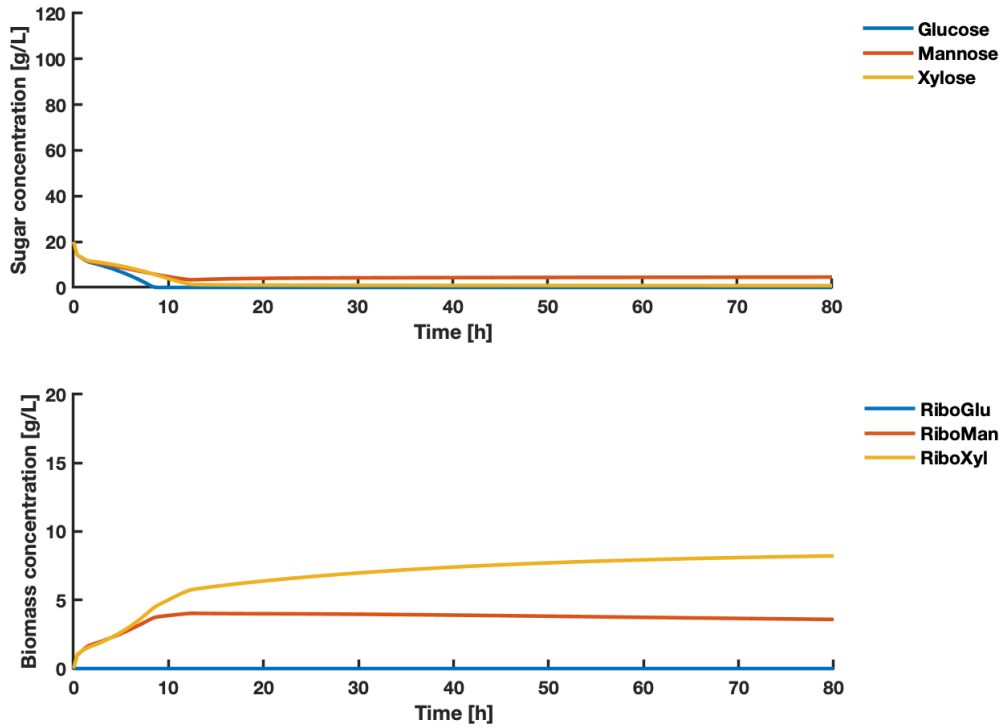


Figure F.11: The upper plot shows the concentrations of the states glucose, mannose, xylose as a function of time. The lower plot shows the concentrations of states RiboGlu, RiboMan and RiboXyl as a function of time. The states are a result of the inputs shown in Figure F.10. MPC states were simulated using the objective function of Case D (described in Equation (3.10)). The $F_{SSL,in}$ had a lower constraint of 0 and an upper constraint of 1 L/h.

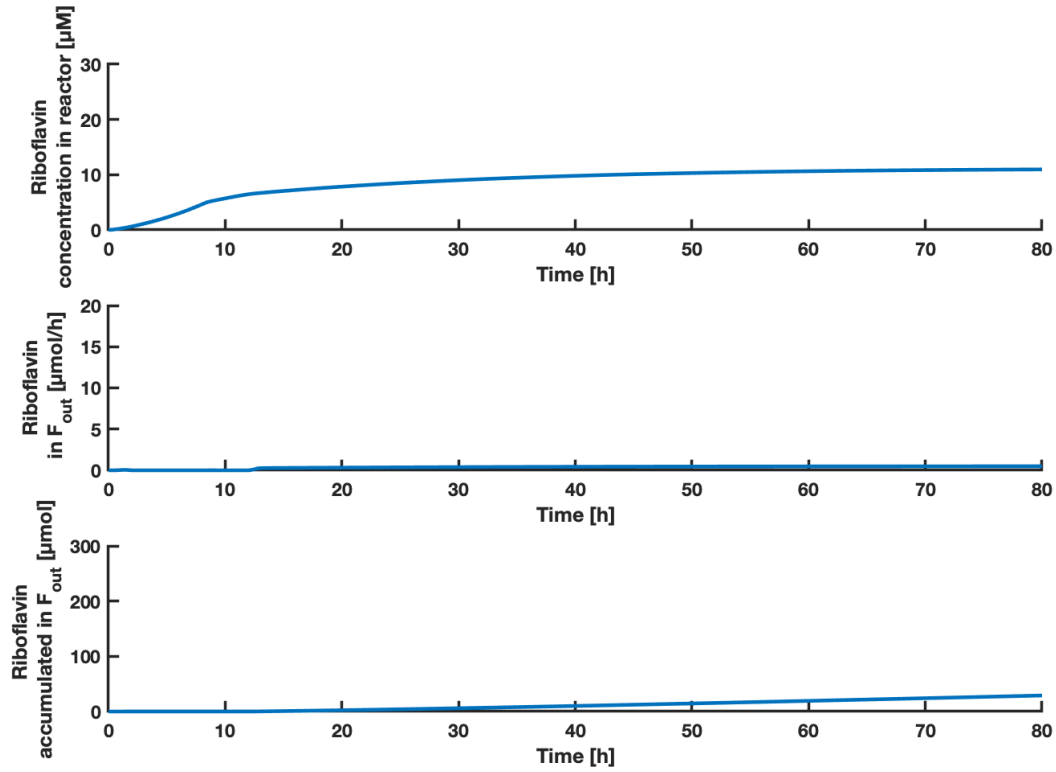


Figure F.12: The upper plot shows the concentration of riboflavin as a function of time. The middle plot shows the amount of riboflavin in the F_{out} stream as a function of time. The lower plot shows the accumulated amount of riboflavin in the F_{out} stream as a function of time. The predicted states of riboflavin concentration in the reactor are a result of the inputs shown in Figure F.10. MPC states were simulated using the objective function of Case D (described in Equation (3.10)). The $F_{Synthetic\ SSL,in}$ had a lower constraint of 0 and an upper constraint of 1 L/h.

For Case D with a synthetic SSL stream of 0-1 L/h, the MPC predicted accumulated amounts of biomass, riboflavin and associated yields as shown in Table F.4.

Table F.4: The table shows the accumulated amounts of RiboGlu, RiboMan and RiboXyl strains, with associated biomass yield, X . The accumulated amount of the product riboflavin P , and the associated yield is shown. The values were calculated based on simulation results for Case D using 0-1 L/h synthetic SSL.

RiboGlu [g]	RiboMan [g]	RiboXyl [g]	X yield [g/g syn SSL]	P [μmol]	P yield [μg/g syn SSL]
0.0005	11.60	22.31	0.1900	29.03	61.23

Appendix G MPC simulations of simplified system after 80 hours

This section presents the MPC simulation results from the simplified system described in Figure 3.2 after 80 hours. The OCP properties used are presented in Table 3.7, and the constraints are presented in Table 3.9 and 3.8. Synthetic SSL was used as carbon source (composition is described in Table 3.6). Figure G.1 to G.3 shows the results obtained.

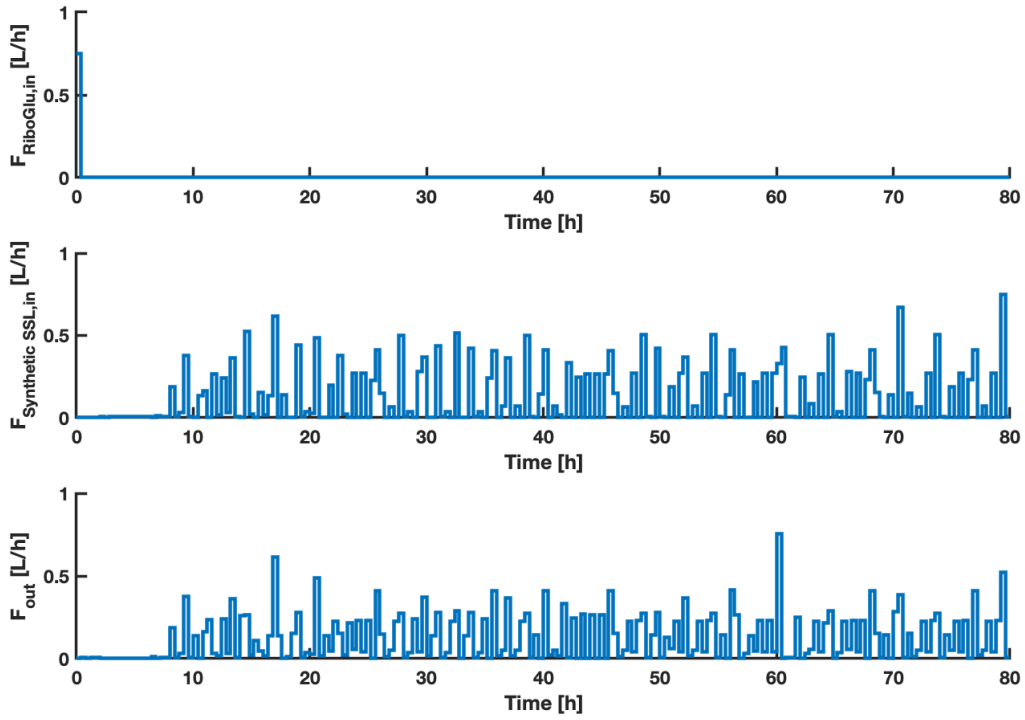


Figure G.1: The plots shows the suggested inputs $F_{RiboGlu,in}$, $F_{Synthetic SSL,in}$ and F_{out} as a function of time. The MPC inputs were calculated using the objective function described in Equation (3.11). The $F_{Synthetic SSL,in}$ had a lower constraint of 0 and an upper constraint of 1 L/h.

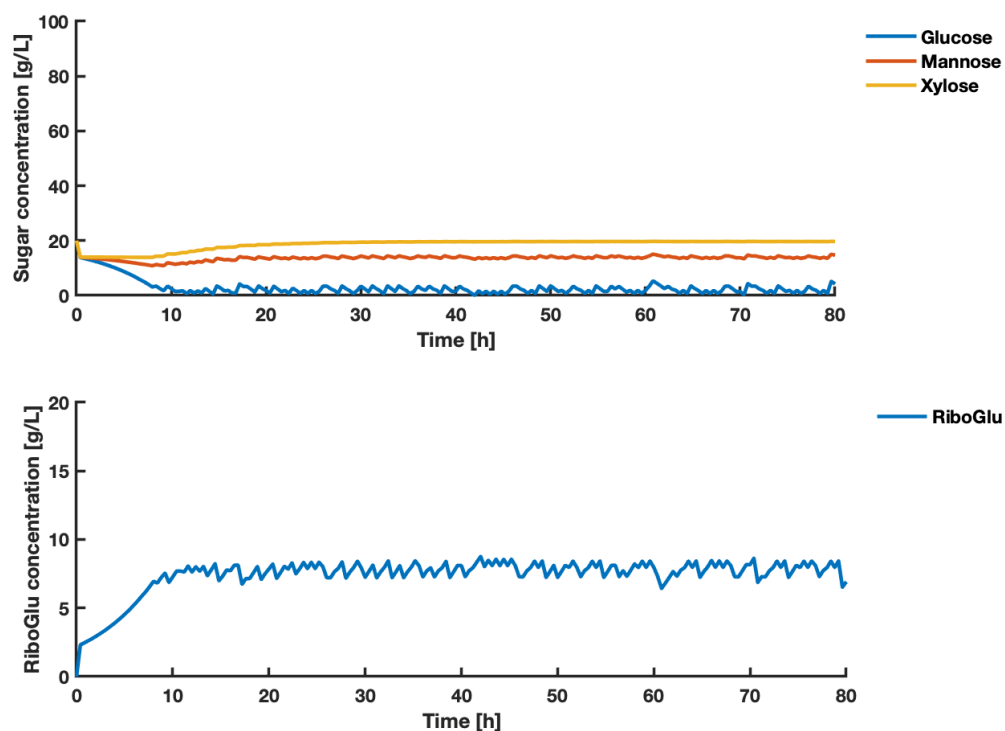


Figure G.2: The upper plot shows the suggested concentrations of the states glucose, mannose, xylose as a function of time. The lower plot shows the concentration of state RiboGlu as a function of time. The states are a result of the inputs shown in Figure 4.38. MPC states were calculated using the objective function described in Equation (3.11). The $F_{\text{Synthetic SSL},in}$ had a lower constraint of 0 and an upper constraint of 1 L/h.

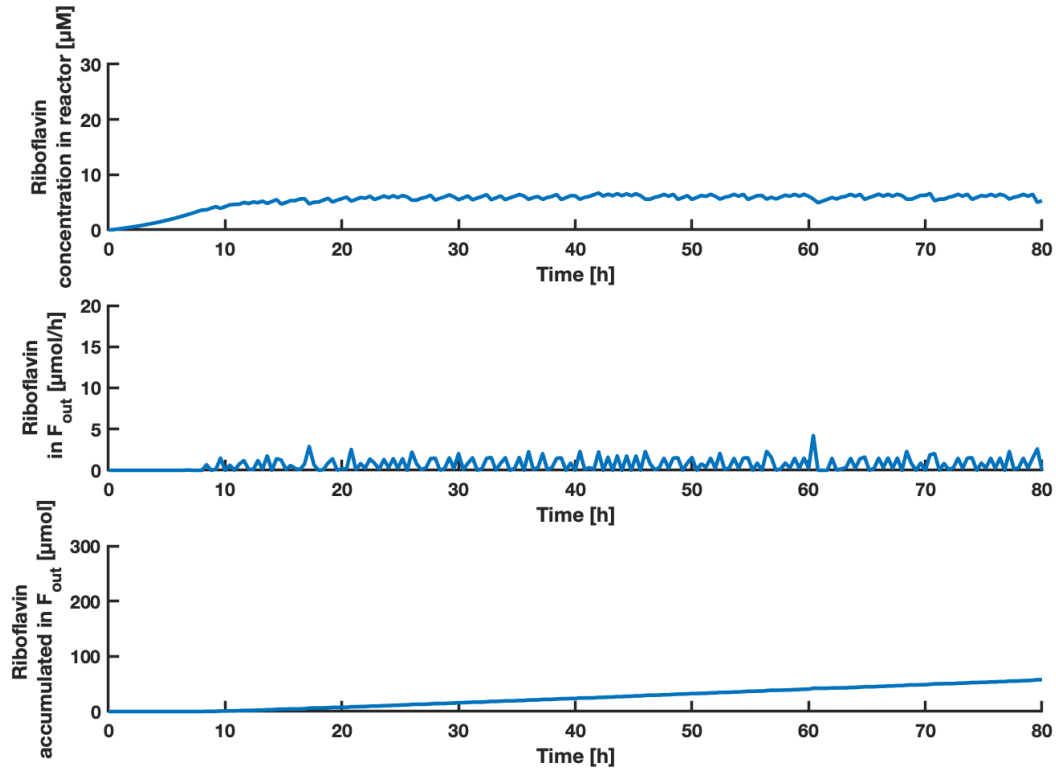


Figure G.3: The upper plot shows the suggested concentration of riboflavin as a function of time. The middle plot shows the amount of riboflavin in the F_{out} stream as a function of time. The lower plot shows the accumulated amount of riboflavin in the F_{out} stream as a function of time. The predicted states of riboflavin concentration in the reactor are a result of the inputs shown in Figure 4.38. MPC states were calculated using the objective function described in Equation (3.11). The $F_{Synthetic\ SSL,in}$ had a lower constraint of 0 and an upper constraint of 1 L/h.

For the simplified system with a synthetic SSL stream of 0-1 L/h, the MPC predicted accumulated amounts of biomass, riboflavin and associated yields after 80 hours as shown in Table G.1.

Table G.1: The table shows the accumulated amounts of RiboGlu, RiboMan and RiboXyl strains, with associated biomass yield, X . The accumulated amount of the product riboflavin P , and the associated yield is shown. The values were calculated based on simulation results for simplified system with a synthetic SSL stream of 0-1 L/h after 80 hours

RiboGlu [g]	X yield [g/g syn SSL]	P [μmol]	P yield [μg/g syn SSL]
77.39	0.1288	57.67	36.11

Appendix H Linearized approximation of Case C

From the simulations done with a linearization of Case C, by maximizing biomass in F_{out} , while minimizing sugars from $F_{SSL,in}$, the system was simulated with a variable feed stream of SSL. The MPC simulation results can be graphically described by Figure H.1 to H.3. The figures shows the inputs, states and riboflavin results respectively.

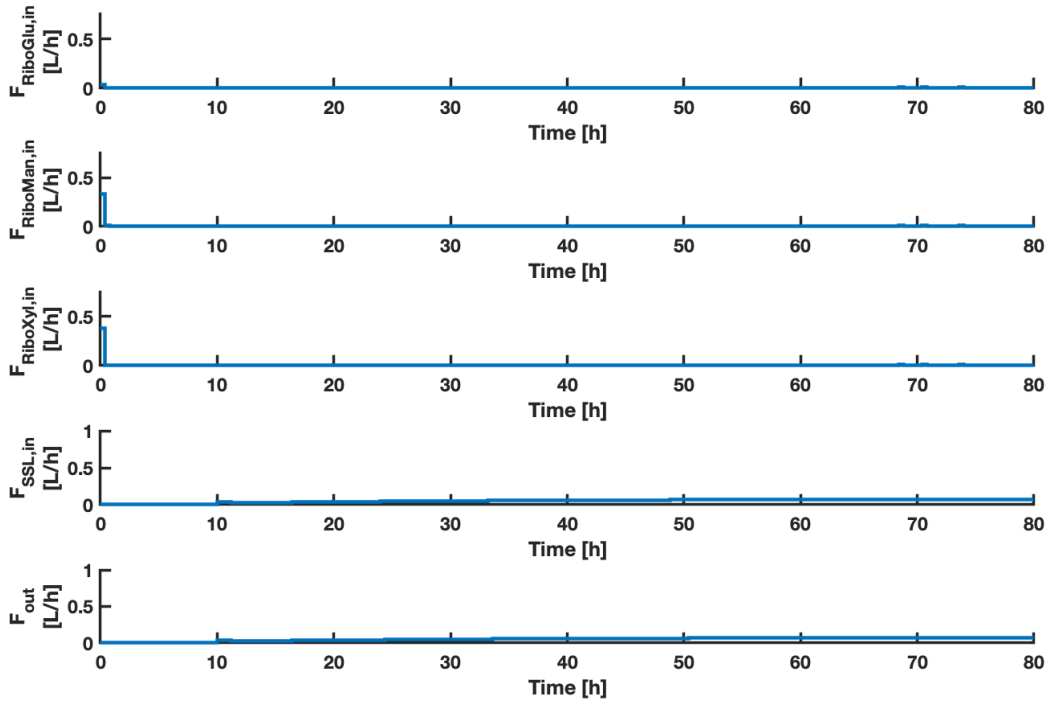


Figure H.1: The plots shows the inputs $F_{RiboGlu,in}$, $F_{RiboMan,in}$, $F_{RiboXyl,in}$, $F_{SSL,in}$ and F_{out} as a function of time. the MPC inputs were calculated using the linearized version of Case C. The $F_{SSL,in}$ had a lower constraint of 0 and an upper constraint of 1 L/h.

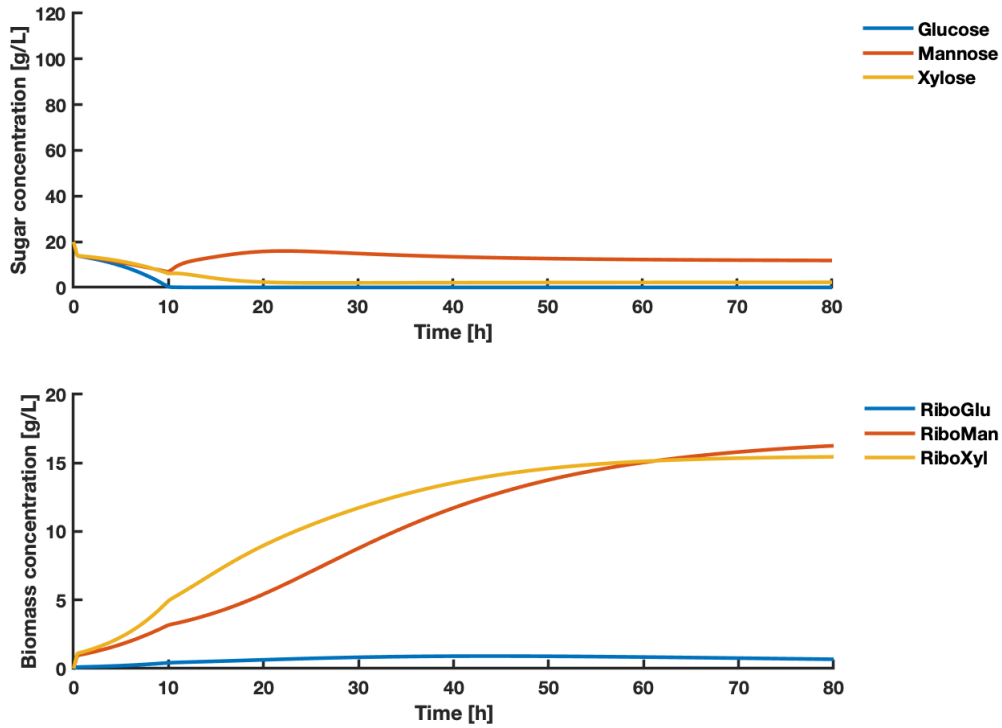


Figure H.2: The upper plot shows the concentrations of the states glucose, mannose, xylose as a function of time. The lower plot shows the concentrations of states RiboGlu, RiboMan and RiboXyl as a function of time. The states are a result of the inputs shown in Figure H.1. MPC states were calculated using the linearized version of Case C. The $F_{SSL,in}$ had a lower constraint of 0 and an upper constraint of 1 L/h.

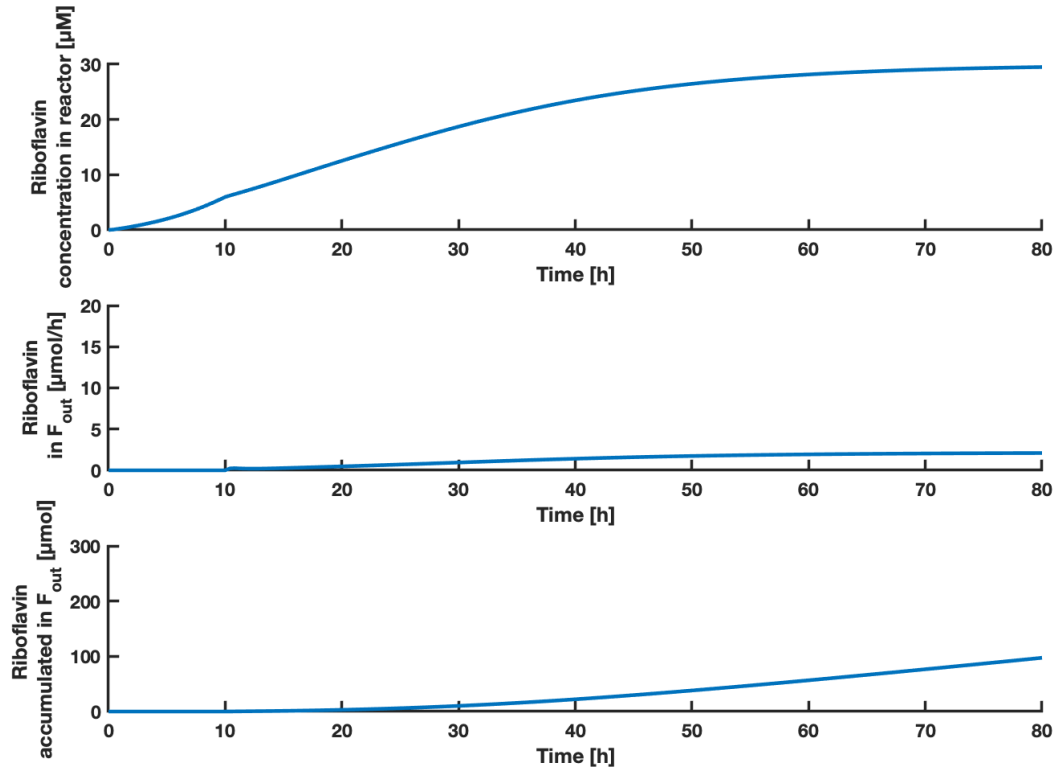


Figure H.3: The upper plot shows the concentration of riboflavin as a function of time. The middle plot shows the amount of riboflavin in the F_{out} stream as a function of time. The lower plot shows the accumulated amount of riboflavin in the F_{out} stream as a function of time. The predicted states of riboflavin concentration in the reactor are a result of the inputs shown in Figure H.1. MPC states were calculated using the linearized version of Case C. The $F_{SSL,in}$ had a lower constraint of 0 and an upper constraint of 1 L/h.

For the linearized version of Case C with a SSL stream of 0-1 L/h, the MPC predicted accumulated amounts of biomass, riboflavin and associated yields as shown in Table H.1.

Table H.1: The table shows the accumulated amounts of RiboGlu, RiboMan and RiboXyl strains, with associated biomass yield, X . The accumulated amount of the product riboflavin P , and the associated yield is shown. The values were calculated based on simulation results for the linearized version of Case C using 0-1 L/h SSL.

RiboGlu [g]	RiboMan [g]	RiboXyl [g]	X yield [g/g SSL]	P [μmol]	P yield [μg/g SSL]
3.221	50.48	54.72	0.1405	97.30	47.44

